



9th INTERNATIONAL KIMBERLITE CONFERENCE

10 - 15 August 2008 • Frankfurt • Germany



GEMOC Extended Abstracts

ARC NATIONAL KEY CENTRE
GEOCHEMICAL EVOLUTION AND
METALLOGENY OF CONTINENTS

School of Earth Sciences
Macquarie University
NSW 2109 Australia

<http://www.es.mq.edu.au/GEMOC/>


MACQUARIE
UNIVERSITY ~ SYDNEY

Micro-inclusions in monocrystalline octahedral diamonds from Diavik, Slave Craton: Clues to diamond genesis.	1
D.P. Araújo, W.L. Griffin, S.Y. O'Reilly	
Carbonatitic to silicic melt inclusions in lherzolite xenoliths from Lac deGras, Slave Craton – Melt differentiation and mantle metasomatism.	4
D.P. Araújo, W.L.Griffin, S.Y. O'Reilly	
Kimberlitic sources of super-deep diamonds in the Juina area, Mato Grosso State, Brazil.	7
P. Andreatza, F.V. Kaminsky, S.M. Sablukov, E.A. Belousova, M. Tremblay, W.L. Griffin	
Combined U-Pb and Lu-Hf analysis of megacrystic zircons from the Kalyandurg-4 kimberlite pipe, S. India: Implications for the emplacement age and Hf isotopic composition of the cratonic mantle.	10
E.V.S.S.K. Babu, W.L. Griffin, A. Mukherjee, S.Y. O'Reilly, E.A. Belousova	
Eclogite xenoliths from the kimberlites of the Eastern Dharwar Craton, South India: Material representing ancient crust of the Western Dharwar Craton?	13
E.V.S.S.K. Babu, W.L. Griffin, S. Panda, S.Y. O'Reilly, Y.J. Bhaskar Rao	
Peridotitic garnet geochemistry: key to the understanding of lithospheric structures and kimberlites diamond potential in Southern Congo.	16
J.M. Batumike, S.Y. O'Reilly, W.L. Griffin	
Age of FS66 Kimberlite beneath Murray Basin, South Australia: Laser ablation ICP-MS dating of kimberlitic zircon, perovskite, and rutile.	19
S.A. Cooper, E.A. Belousova, W.L. Griffin, B.J. Morris	
Isotopic studies of minerals and their host kimberlites from Australia and southern Africa.	22
S.A. Cooper, Y.A. Kostitsyn, E.A. Belousova, W.L. Griffin	
Geology and exploration history of kimberlite and related rocks in South Australia.	24
S.A. Cooper, B.J. Morris	
The kimberlites and related rocks of the Kuruman Kimberlite Province, Kaapvaal Craton, South Africa.	27
C.L. Donnelly, S.Y. O'Reilly, W.L. Griffin	
An evidence for the composition of the Ordovician upper mantle beneath West Sangilen (Southeast Tuva, Russia)	30
A. Gibsher, V. Malkovets, Y. Litasov, W. Griffin, S. O'Reilly	
Petrology and geochemistry of eclogitic sulfides: a new insight on the origin of mantle eclogites?	33
Y. Greau, W.L. Griffin, O. Alard, S.Y. O'Reilly	
Diamonds and carbonatites in the deep lithosphere: Evidence of genetic links.	36
W.L. Griffin, D. Araujo, S.Y. O'Reilly, S. Rege, E. van Achterbergh	
Contrasting lithospheric mantle across the suture between the Eastern and Western Dharwar Cratons, central India.	39
W.L. Griffin, A.F. Kobussen, E.V.S.S.K. Babu, S.Y. O'Reilly, R. Norris, P. Sengupta	

Super-deep diamonds from kimberlites in the Juina area, Mato Grosso State, Brazil.	42
F.V. Kaminsky, G.K. Khachatryan, P. Andreazza, D. Araujo, W.L. Griffin	
The scale and scope of Cretaceous refertilisation of the Kaapvaal lithospheric mantle, Kaapvaal Craton, South Africa.	45
A.F. Kobussen, W.L. Griffin, S.Y. O'Reilly	
Diamondiferous microxenoliths and xenocrysts from the Nyurbinskaya kimberlite pipe, Yakutia.	48
V. Malkovets, D. Zedgenizov, W. Griffin, A. Dak, S. O'Reilly, N. Pokhilenko, S. Mityukhin	
Evolved carbonatitic kimberlite from the Batain Nappes, eastern Oman continental margin.	51
S. Nasir, S. Al-Khribash, H. Rollinson, A. Al-Harthy, A. Al-Sayigh, A. Al-Lazki, E. Belousova, F. Kaminsky, T. Theye, H.-J. Massonne, S. Al-Busaidi	
Late Jurassic-Early Cretaceous kimberlite, carbonatite and ultramafic lamprophyric sill and dyke swarms from the Bomethra area, northeastern Oman.	54
S. Nasir, S. Al-Khribash, H. Rollinson, A. Al-Harthy, A. Al-Sayigh, A. Al-Lazki, E. Belousova, F. Kaminsky, T. Theye, H.-J. Massonne, S. Al-Busaidi	
Archean lithospheric mantle: its formation, its composition and today's refertilised remains.	57
S.Y. O'Reilly, W.L. Griffin, M. Zhang, G. Begg	
In-situ isotope ratio measurement: a decade of development of applications for mantle peridotites and kimberlites.	60
N.J. Pearson, W.L. Griffin, S.Y. O'Reilly	
Trace-element geochemistry of diamond.	63
S. Rege, W.L. Griffin, N.J. Pearson, S.Y. O'Reilly, S.E. Jackson, D. Zedgenizov, G. Kurat	
Natural silicon carbide from different geological settings: polytypes, trace elements, inclusions.	66
A.A. Shiryayev, W.L. Griffin, E. Stoyanov, H. Kagi	
Trace elements and oxygen isotopes in garnets from diamondiferous xenoliths, Nurbinskaya pipe, Yakutia: Implications for diamond genesis	69
Z.V. Spetsius, W.L. Griffin, L. A. Taylor, S.Y. O'Reilly, S.I. Mityukhin, J.W. Valley and M. Spicuzza	
Diamond-forming fluids and kimberlites: The trace element perspective.	72
Y. Weiss, W. L. Griffin, J. W. Harris, O. Navon	
Diamond forming fluids from Kankan, Guinea: major and trace element study.	75
Y. Weiss, R. Kessel, W.L. Griffin, I. Kiflawi, D.R. Bell, J.W. Harris, O. Navon	
Carbonatitic to hydrous-silicic growth medium of diamonds from Internatsionalnaya kimberlite pipe (Yakutia).	78
D.A. Zedgenizov, D. Araujo, A.L. Ragozin, V.S. Shatsky, H.Kagi, W.L. Griffin	

Micro-inclusions in monocrystalline octahedral diamonds from Diavik, Slave Craton: Clues to diamond genesis

D.P. Araújo, W.L. Griffin, S.Y. O'Reilly

GEMOC, Dept. Earth & Planetary Sciences, Macquarie Univ., NSW 2109, Australia

Some gem-quality octahedral diamonds from Diavik Mine, Slave Craton, have abundant shallow planar trigons over part or all their surfaces or above macle and fracture lines (Fig.1). Microscope observation of the etched surfaces revealed the occurrence of micro-inclusions ($< 0.5 \mu\text{m}$) concentrated in layers $\sim 10\text{-}15 \mu\text{m}$ beneath the surface. Areas with higher concentration of micro-inclusions are separated by curvilinear boundaries from smaller areas where they are absent. The micro-inclusions are rounded with small single fractures extending from them, producing a tadpole-like shape. The micro-fractures can be both crystallographically (111) and randomly oriented (Fig.1). Shadows of trigons can be seen under non-etched surfaces, suggesting that diamond growth on those faces continued after etching. Micro-inclusions are also seen along fractures and macle lines associated with trigons.

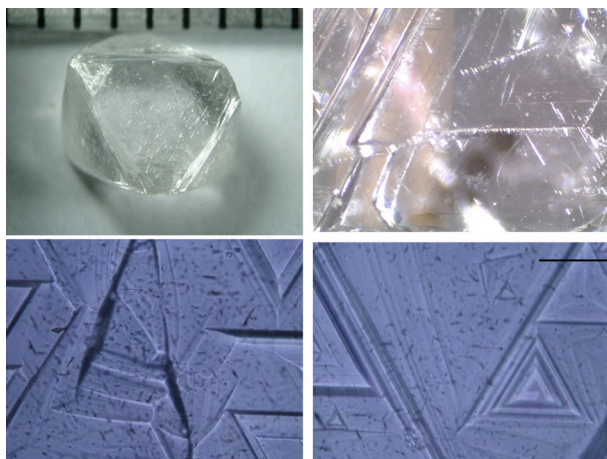


Fig.1 Sharp octahedral diamond from Diavik with abundant trigons (top left). Trigons aligned over fractures (top right, bar is 1mm) and microscopic view of micro-inclusions (40x objective; focused on micro-inclusions).

Four diamonds measured by FTIR are Ia to IaAB (up to 20% of B centers) with 220 to 770 ppm Nitrogen. Time-resolved LA-ICP-MS analyses (100 μm spot size) were done on etched and non-etched surfaces. In one diamond (DVK109), ablation of the etched surfaces shows an increase in trace-element contents coinciding with the sub-surface inclusion-rich layers. The time-resolved signals for several analyses across single surfaces show that the thickness of the micro-inclusion layers is variable and does not exceed 40 μm . In Fig. 2, the change in counts/s for Ba during an analysis (130 seconds, to ca 65 μm depth) shows the layer of micro-inclusions between ~ 10 to 40 μm depth. Absolute concentrations change according to the analysis location, reflecting the abundance of micro-inclusions. Analyses of non-etched surfaces do not show such trace element-enriched layers.

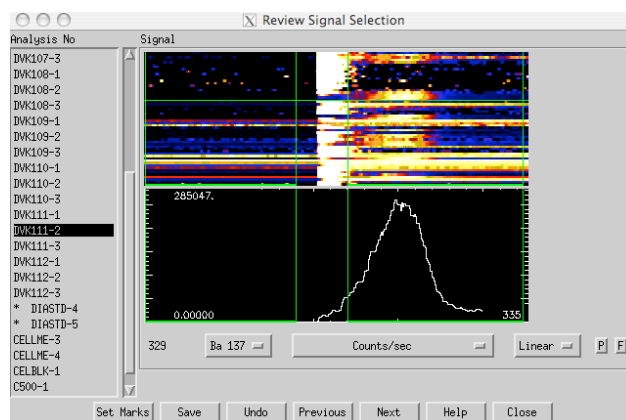


Fig. 2 – Time-resolved linear signal for Ba (counts/s) during ablation (130 seconds, $\sim 65 \mu\text{m}$ deep; GLITTER software Window).

The micro-inclusions have high Ba, K, LREE (Table 1), $\text{Ba}/\text{La}_{(\text{CN})}$ and $\text{Ba}/\text{Lu}_{(\text{CN})} \gg 1$ and a positive $\text{Sr}_{(\text{CN})}$ anomaly relative to Sm compared to the composition of diamond beneath non-etched surfaces. The chondrite-normalised trace-element patterns of the micro-inclusions are comparable to the coats of coated diamonds from the same kimberlite (Griffin et al. this conference, Abst-102). The trace-element levels are intermediate between the levels seen in the diamond

coats and the diamond beneath the non-etched surfaces for elements such as LREE, Ba, Th, Nb and Sr, but are similar to the non-etched surfaces for HREE and most HFSE. Although the absolute trace element contents of the microinclusion-rich layers are lower than the coats, the CN pattern is similar, reflecting the lower abundance of micro-inclusions.

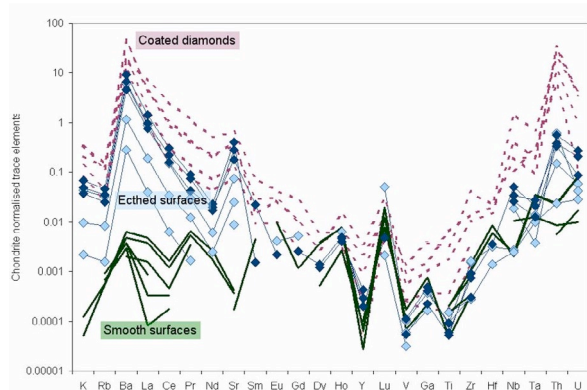


Fig.3 – Chondrite-normalised trace element patterns of etched (rhombic) and non-etched surfaces (solid lines) of octahedral diamonds (this work) and of coated diamonds (dashed lines; Griffin et al. Abst-102).

Table 1 – Range of composition (ppm) and 1 sigma error (average) of layers of micro-inclusions in diamonds DVK109 and DVK111 (6 analyses).

	Min	Max	1σ (ave)
K	1.9	58	1.8
Rb	0.006	0.2	0.004
Ba	1.0	32	0.7
La	0.01	0.5	0.004
Ce	0.006	0.30	0.002
Pr	0.0002	0.012	0.0002
Nd	<0.00104	0.017	0.001
Sr	0.1	4.9	0.03
Sm	<0.00056	0.005	0.0005
Eu	<0.00016	0.0004	0.0001
Gd	<0.00069	0.002	0.0004
Dy	<0.00035	0.0005	0.0003
Ho	<0.00009	0.0005	0.0001
Y	<0.00019	0.0010	0.0002
Lu	<0.00006	0.0019	0.0001
V	<0.0020	0.010	0.001
Ga	<0.0022	0.007	0.001
Ti	<0.0112	0.10	0.01
Zr	0.002	0.01	0.0006
Hf	<0.00023	0.0006	0.0002
Nb	0.0009	0.02	0.0005
Ta	0.0001	0.0007	0.0002
Th	0.00101	0.03	0.0004
U	0.0004	0.003	0.0001

The oxidation of diamond surfaces to produce etching features can take place in the mantle, during diamond growth, or during ascent in the kimberlite magma. Trigons are formed on primary octahedral surfaces and are related to defects, microcracks and impurity clusters, which will determine their morphology and distribution in the diamond surface. Point-bottomed trigons originate at the emergence points of dislocation lines, which commonly occur as bunches emerging from the center of the diamond mostly towards the central portion of the faces, as revealed by X-ray diffraction (Frank and Lang 1965, Khokhryakov and Palynov 2006). As a result point-bottomed trigons related to outcropping bunches are much less abundant near the edge of the surfaces. Flat-bottomed trigons, on the other hand, are related to microcracks and impurity clusters. Etching experiments on diamond plates imaged by X-ray diffraction (Khokhryakov and Palynov 2006) showed that point-bottomed trigons, related to dislocation lines, persisted after repeated etching and flat-bottomed trigons eventually disappeared. We suggest that the formation of abundant flat-bottomed trigons on the Diavik diamonds is related to defects due to the occurrence of the sub-surface layer of micro-inclusions. Coated diamonds from Diavik have similar etching patterns, although trigons are even more abundant.

SHRIMP $^{13}\text{C}/^{12}\text{C}$ *in-situ* analyses (in prep.) on a diamond plate (DVK109) show around 3 per mil difference between the micro-inclusion layers at the rims (lower $^{13}\text{C}/^{12}\text{C}$) and a point 100 μm further towards the center.

High growth rate contributes to fibrous growth and incorporation of impurities. During diamond growth these high rates reflects increasing carbon supersaturation of the system, which can be achieved by lowering the temperature and/or by increasing the chemical potential difference between solid and solvent phases (Sunagawa 1984). The presence of a diamond seed for diamond growth may also play a role in the mechanism of growth, as seen in diamond synthesis. Arima et al. (2002) reported nucleation and growth of diamonds in the carbonatitic system $\text{CaMg}(\text{CO}_3)_2\text{-Si}$ (7.7 GPa; 1500-1800°C) and observed nucleation of octahedral diamonds and also fibrous diamonds grown over seeds. In the absence of Si, no nucleation was produced. The first diamonds formed at starting composition $0.79\text{CaMg}(\text{CO}_3)_2+0.21\text{Si}$.

The fluids forming coated diamonds from Diavik are related to carbonatitic/kimberlitic melts (Griffin et al. Abst-102). The chemical resemblance of the “tadpole” micro-inclusions to the fluids trapped in Diavik diamond coats, and the distribution of micro-inclusions in layers suggest that such fluids also have been present during the growth of monocrystalline diamonds. Changes in growth mechanism due to temperature and/or oxygen fugacity variation can influence the incorporation of micro-inclusions through rapid growth (Sunagawa 1984). However, the distinct

trace-element patterns and $^{13}\text{C}/^{12}\text{C}$ ratios of the micro-inclusion layers suggest that the layers reflect the influx of new fluids into the growth environment. The distinctly different trace-element pattern of the diamond in the center and outermost rim of the four diamonds studied here suggests that these parts of the diamond grew from a fluid quite different from the one trapped in the microinclusions, and in the coats on coated diamonds. The occurrence of the microinclusions as layers within these diamonds suggests that these two different types of fluid coexisted within the local metasomatic environment in which the octahedral diamonds grew.

References

- Griffin, W.L., Araujo, D.P., O'Reilly, S.Y., Rege, S., van Acherbergh, E., 2008. Diamonds and carbonatites in the deep lithosphere: Evidence of genetic links. 9th International Kimberlite Conference, Extended Abstracts 102.
- Sunagawa, I., 1984. Morphology of natural and synthetic diamond crystals. In: Sunagawa I (ed) Material Science of the Earth's Interior, vol. Terra Scientific Publishing Company (TERRAPUB), Tokyo, pp 303-330
- Khokhryakov, A.F., Palyanov, Y.N., 2006. Revealing of dislocations in diamond crystals by the selective etching method. *Journal of Crystal Growth* 293, 469-474.

Carbonatitic to silicic melt inclusions in lherzolite xenoliths from Lac de Gras, Slave Craton – Melt differentiation and mantle metasomatism

D.P. Araújo, W.L.Griffin, S.Y. O'Reilly

GEMOC, Dept. Earth & Planetary Sciences, Macquarie Univ., NSW 2109, Australia

Globules (1 to 4 mm), patches and veinlets of quenched silicate and carbonate melts occur in Cr-diopside in megacrystalline lherzolite xenoliths (1000°C, 5GPa; Griffin et al. 1999) from the A154N kimberlite, Slave Craton, Canada. They belong to the suite of samples previously investigated by van Achterbergh et al. (2004). The clinopyroxene xenocrysts are intensively fractured and veined by the same material composing the globules and patches. They show a large range of textural and chemical variation (Figure 1) from carbonatite (C) to calcitic-silicate (CS) and calcite-bearing silicate (CbS). Calcite is the only carbonate and varies from 3 to 97% (modal).

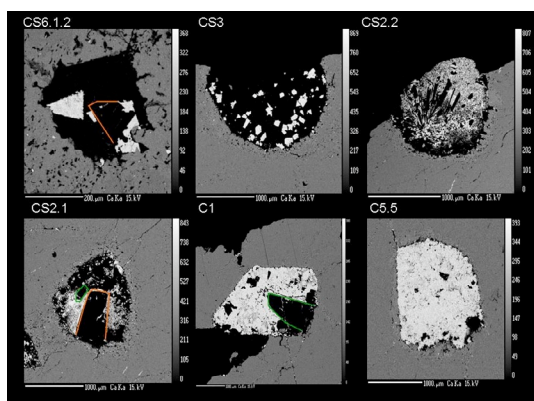


Figure 1 – SEM Ca images of calcite-silicate (CS) and carbonatite (C) globules. Black regions outside the globules in CS3, CS2.1 and C1 are the edge of the sections. Olivine occurs in CS2.1 (radial texture), CS2.1 and C1 (green outline). Phlogopite occurs in CS6.1.2 and CS2.1 (orange outline) and as an accessory phase in all other occurrences. Silicate matrix dominates CS6.1.2, CS3 and is unmixed in the upper part of CS2.1.

Major- and trace element contents of the phenocrysts and matrices in eighteen globules and the host clinopyroxene have been analysed using EMP and LA-ICPMS. The Cr-diopside is intensively metasomatised around the globules and veins. The globules contain phenocrysts of olivine ($f_{0.89-0.92}$), phlogopite (low to high Al-K, probably interlayered phlogopite-chlorite), and calcite ($Ca\# >0.97$) in matrices ranging in composition (EMP) from carbonatitic (calcitic) to Fe-Mg-silicic (1wt% Al_2O_3 , 0.3wt% K_2O , 0.3wt% Na_2O). Phlogopite and calcite phenocrysts are accessory to major constituent phases and olivine abundance does not exceed 25%.

Carbonatitic and silicic matrices are the dominant components of most globules, or may occur as segregated portions within single globules. Matrices with mixed compositions between carbonatitic and silicic end-members can have up to 18% CaO. Quenched textures include elongated olivine phenocrysts with radial texture (Figure 1) and segregated Fe-Mg-Si-phases within a carbonatitic matrix with ring, microlith and colliform microstructures. Sulphide and chromite are rare.

Calcite phenocrysts in carbonatitic and silicic globules have overall high REE ($\Sigma REE = 1250$ ppm), Ba (up to 3200ppm) and Sr (up to 5500 ppm) contents and flat chondrite-normalised (CN) REE patterns.. Calcite in the interstitial matrix ranges from compositions similar to calcite phenocrysts to lower REE contents, but comparable Ba and Sr, giving high Ba/La (CN) and a strong positive Sr anomaly. This compositional range is also found in carbonatite matrix where calcite phenocrysts are absent.

The silicic, Ca-silicic and carbonatitic matrices are enriched in LREE and have similar chondrite-normalised patterns, with some exceptions such as variable Ba/La and Sr/Nd ratios (Figure 2).

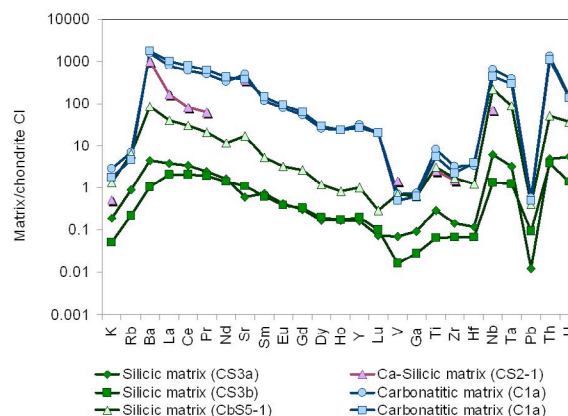


Figure 2 – Chondrite-normalised trace-element distribution of silicic, Ca-silicic and carbonatitic matrices.

All globules, patches and veinlets are surrounded by reaction zones in which the host diopside shows a marked increase in trace element contents and higher LREE/HREE, Nb/Ta and Th/Pb (Figure 3). The CN trace-element distribution of the metasomatised cpx around carbonatite and calcite-silicate globules is very similar and the highest



enrichment is found in cpx rimming calcite-bearing silicate.

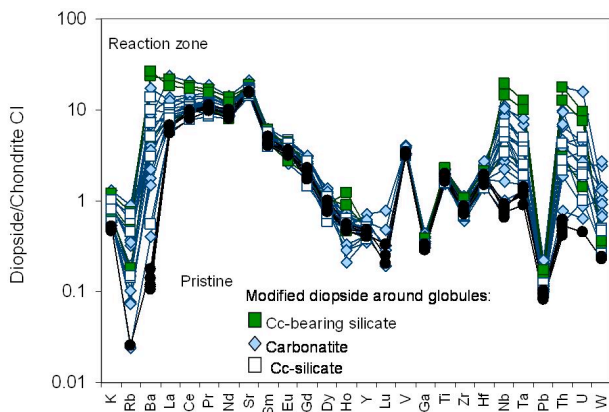


Figure 3 – Chondrite-normalised trace-element patterns of diopside rimming the globules compared to the pristine composition outside the reaction zone.

Carbonate-silicic melt inclusions described by van Achertberg et al. (2004) were interpreted as frozen melt inclusions with kimberlitic composition which were trapped by the host clinopyroxene shortly prior to the xenoliths incorporation in the ascending kimberlite. Similar quenched textures and unmixed silicic and carbonatitic matrices are likewise interpreted as disequilibrium textures.

The composition of the matrices and the bulk compositions of selected globules (calculated from modal composition) cover most of the range between phlogopite and calcite compositions in the ternary plot $\text{SiO}_2\text{-MgO-CaO}$ (Figure 4) where carbonatitic (>97% calcite) and calcite-bearing silicate (<3% calcite) globules are end-members.

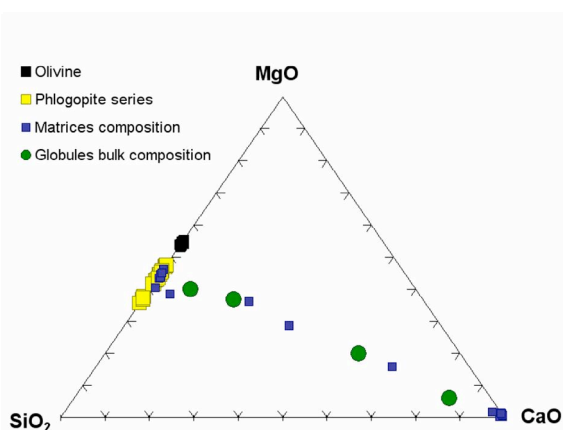


Figure 4 – $\text{SiO}_2\text{-MgO-CaO}$ (Wt%) composition of the matrices, olivine, phlogopite series and bulk compositions of C1, CS3, CS6.2.1 and CS6.1.4.

Our results are similar to the composition of the Diavik and Jericho kimberlites in the ternary plot $\text{SiO}_2\text{-MgO-CaO}$ (Figure 5). The Diavik kimberlite is a volcanoclastic phase (Graham et al. 1999) and coincides with the macrocrystic kimberlite from

Jericho (Price et al. 2005). The Jericho aphanitic kimberlite, which is interpreted by the authors as closest composition to the parental kimberlite magma, lies along the compositional line defined by the globules. The saline to carbonatitic fluid inclusions (FI) in coated diamonds from Diavik cluster about this line.

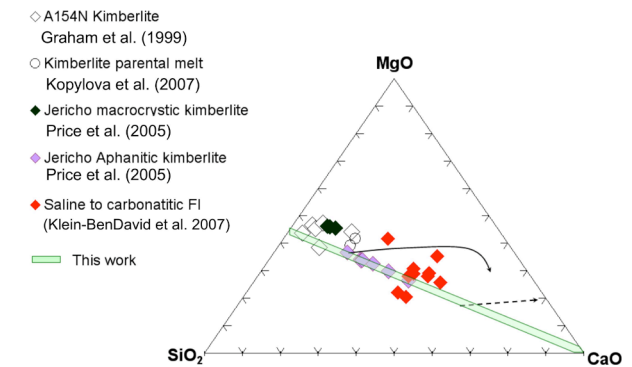


Figure 5 – Ternary plot $\text{SiO}_2\text{-MgO-CaO}$ with composition of Diavik and Jericho kimberlites and fluid inclusions in Diavik coated diamonds. Also shown are kimberlitic to carbonatitic melts in equilibrium with carbonated peridotite (solid arrow; Dalton and Presnall 1998a, 1998b, Gudfinsson and Presnall 2005) and carbonated eclogite (dashed arrow; Brey and Yaxley 2004). In figure legend – put dot after “al”, and fix Klein-BenDavid

The compositions of melts in equilibrium with metasomatised diopside around the globules has been calculated using partition coefficients between clinopyroxene and kimberlitic (Fujimaki et al. 1984 and Keshav et al. 2005) and carbonatitic melts (Adam and Green et al. 1992, Sweeney et al. 1995, Klemme et al. 1995, Blundy et al. 2000). The calculated fluids have overall similar compositions (Figure 6), but the influence of PT conditions and starting materials used in each experiment are yet to be discussed.

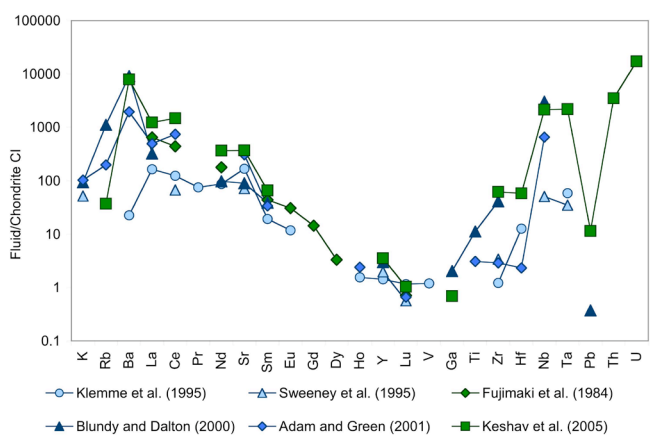


Figure 6 – Composition of the fluids (CN) in equilibrium with the metasomatised cpx using $K_d(\text{cpx}/\text{melt})$ from the literature (see text).

The trace element patterns of the Diavik and Jericho kimberlites have lower alkalis, LREE and Ba, relative to the HREE, than the calculated fluids (Figure 7).

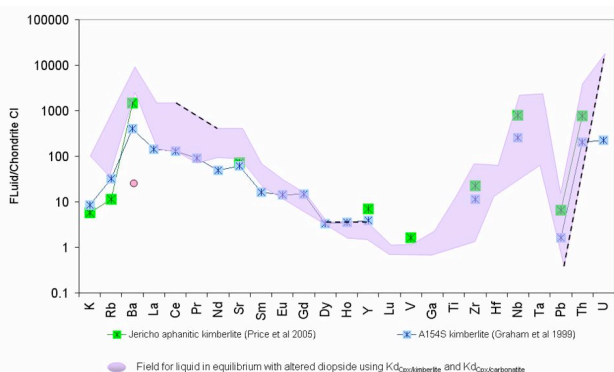


Figure 7 – Composition (CN) of Jericho and Diavik kimberlites compared to the range of fluids in equilibrium with the metasomatised diopside (see text). Circle fluid using $Kd(Ba)$ from Kempe et al. (1995). Dashed line – no Kd data.

Both the major element compositions of the globules and the metasomatic overprint in the host diopside suggest parental melts with kimberlitic to carbonatitic compositions, evolving fluids with fractionated compositions. Kimberlitic to carbonatitic melts in equilibrium with carbonated peridotite (Dalton and Presnall 1998a, 1998b; Gudfinnsson and Presnall 2005) are produced experimentally with decreasing pressure (8 to 6 GPa) and temperature (at 6 GPa), as indicated by the solid arrow in Figure 5. Similar results are found for melts in equilibrium with carbonated eclogite (Brey and Yaxley 2004), but the compositions of the melts are more calcitic (dashed arrow, Figure 4).

The compositional range of the globules from carbonatitic to silicic was produced before the entrapment of the melt inclusions, possibly by fractionation of calcite, olivine, phlogopite and interaction with the host rock. Further fractionation of carbonates and silicates from evolved fluids would drive them to end-member compositions. Additionally, fluid immiscibility could contribute to separation of carbonatitic and silicic melts. Immiscibility of carbonatitic and silicic melts in equilibrium with carbonated eclogite (6 GPa; 1300°C) has been observed in experiments by Hammouda (2003).

References

Adam J., Green, T., 2001. Experimentally determined partition coefficients for minor and trace elements in peridotite mineral and carbonatitic melt, and their relevance to natural carbonatites. *European Journal of Mineralogy* 13, 815-827.

Blundy, J., Dalton, J., 2000. Experimental comparison of trace element partitioning between clinopyroxene and melt in carbonate and silicate systems, and implications for mantle metasomatism. *Contribution to Mineralogy and Petrology* 139, 356-371.

Dalton, J.A., Presnall, D.C., 1998a. Carbonatitic melts along the solidus of model lherzolite in the system CaO-MgO-

Al_2O_3 - SiO_2 - CO_2 from 3 to 7 GPa. *Contributions to Mineralogy and Petrology* 131, 123-135.

Dalton, J.A., Presnall, D.C., 1998b. The continuum of primary carbonatitic-kimberlitic melt compositions in equilibrium with lherzolite; data from the system CaO-MgO- Al_2O_3 - SiO_2 - CO_2 at 6 GPa. *Journal of Petrology* 39, 1953-1964.

Fujimaki H., Tatsumoto M., Aoki K-I., 1984. Partition coefficients of Hf, Zr, and REE between phenocrysts and groundmasses. *Journal of Geophysical Research* 89, 662-672.

Graham I., Burgess, J.L., Bryan, D., Ravenscroft, P.J., Thomas, E.M., Doyle, B.J., Hopkins, R., Armstrong, K.A., 1999. Exploration history and geology of the Diavik Kimberlites, Lac de Gras, Northwest Territories, Canada. *Proceedings of the 7th International Kimberlite Conference*, Vol. 1, 262-279.

Griffin, W.L., Doyle, B.J., Ryan, C.G., Pearson, N.J., O'Reilly, S.Y., Davies, R., Kivi, K., van Acherterbergh, E., Natapov, L.M., 1999. Layered mantle lithosphere in the Lac de Gras area, Slave Craton; composition, structure and origin. *Journal of Petrology* 40, 705-727.

Gudfinnsson, G.H., Presnall, D.C., 2005. Continuous gradations among primary carbonatitic, kimberlitic, melilititic, basaltic, picritic, and komatiitic melts in equilibrium with garnet lherzolite at 3-8 GPa. *Journal of Petrology* 46, 1645-1659.

Hammouda, T., 2003. High-pressure melting of carbonated eclogite and experimental constraints on carbon recycling and storage in the mantle. *Earth and Planetary Science Letters* 214, 357-368.

Keshav, S., Corgne, A., Gudfinnsson, G.H., Bizimis, M., McDonough, W.F., Fei, Y., 2005. Kimberlite petrogenesis; insights from clinopyroxene-melt partitioning experiments at 6 GPa in the CaO-MgO- Al_2O_3 - SiO_2 - CO_2 system. *Geochimica et Cosmochimica Acta* 69, 2829-2845.

Klein-BenDavid, O., Izraeli, E.S., Hauri, E., Navon, O., 2007. Fluid inclusions in diamonds from the Diavik mine, Canada and the evolution of diamond-forming fluids. *Geochimica et Cosmochimica Acta* 71, 723-744.

Klemme, S., van der Laan, S.R., Foley, S.F., Guenther, D., 1995. Experimentally determined trace and minor element partitioning between clinopyroxene and carbonatite melt under upper mantle conditions. *Earth and Planetary Science Letters* 133, 439-448.

Kopylova, M.G., Matveev, S., Raudsepp, M., 2007. Searching for parental kimberlite melt. *Geochimica et Cosmochimica Acta* 71, 3616-3629.

McDonough, W.F., Sun, S-S., 1995. The composition of the Earth. *Chemical Geology* 120(34):223-53.

Price, S.E., Russell, J.K., Kopylova, M.G., 2000. Primitive magma from the Jericho Pipe, N.W.T., Canada; constraints on primary kimberlite melt chemistry. *Journal of Petrology* 41, 789-808.

Sweeney, R.J., Prozesky, V., Przybylowicz, W., 1995. Selected trace and minor element partitioning between peridotite minerals and carbonatite melts at 18-46 kb pressure. *Geochimica et Cosmochimica Acta* 59, 3671-3683.

van Acherterbergh, E., Griffin, W.L., Ryan, C.G., O'Reilly, S.Y., Pearson, N.J., Kivi, K., Doyle, B.J., 2004. Melt inclusions from the deep Slave lithosphere; implications for the origin and evolution of mantle-derived carbonatite and kimberlite. *Lithos* 76, 461-474.

Yaxley, G.M., Brey, G.P., 2004. Phase relations of carbonate-bearing eclogite assemblages from 2.5 to 5.5 GPa; implications for petrogenesis of carbonatites. *Contributions to Mineralogy and Petrology* 146, 606-619.



Kimberlitic sources of super-deep diamonds in the Juina area, Mato Grosso State, Brazil

Paulo Andrezza¹, Felix V. Kaminsky², Sergei M. Sablukov², Elena A. Belousova³,
Mousseau Tremblay¹, William L. Griffin³

¹Diagem Inc., Montreal, Quebec, Canada

²KM Diamond Exploration Ltd., West Vancouver, Canada

³GEMOC Key Centre, Dept. of Earth and Planetary Sciences, Macquarie University, Sydney, Australia

The Juina diamond field, in the 1970-80s, was producing up to 5-6 million carats per year from rich placer deposits, but no economic primary deposits had been found in the area. De Beers, from the mid-seventies to the late eighties, and Rio Tinto, between 1992 and 1997, actively explored the Juina District for kimberlite. Their respective efforts led to the discovery of 26 kimberlite bodies. Among them, was the sub-economic Collier-04 kimberlite pipe. However, the overall low grade of the different kimberlite pipes, the small size of the stones and depressed diamond prices led both companies to withdrawn from the area. In 2006-2007, Diagem Inc. discovered a group of diamondiferous kimberlitic pipes (Pandrea-1 to -7) within the Chapadão Plateau, at the head of a drainage system which has produced most of the alluvial diamonds mined in the Juina area.

Geological setting

The Juina area lies within the Tapajós Province of the Amazonian Craton. The oldest cratonic consolidation recorded in the Amazonian Craton culminated during the Early Proterozoic Transamazonian orogeny (2.25 – 1.9 Ga), with the accretion of the Maroni – Itacaiúnas Province (2.2 – 1.95 Ga) to the north and northeast of a stable Archean nucleus (> 2.3 Ga) (Brito Neves *et al.*, 1990). From Middle to Late Proterozoic, during the Uruçuano orogeny (1.9 – 0.9 Ga), several mobile belts with a NW-SE structural trend accreted to each other in a northeastward direction on the southwestern edge of the central Archean nucleus to form the Amazonian Craton. The studied area lies in the Rio Negro – Juruena Belt which straddles this NW-SE trend approximately 2000 km long and 600 km wide in the western portion of the Amazonian Craton.

Kimberlites were emplaced in the region and across the whole South American Platform in Brazil during the Cretaceous. At least fifteen kimberlite provinces have been recognized throughout Brazil. Most of them appear along three major continental-scale lineaments that were reactivated during the opening of the Atlantic

Ocean in Jurassic and Cretaceous times. One of the lineaments, the NW-SE striking Lineament 125 ° AZ is interpreted to be a continental extension of oceanic fractures in the South Atlantic. It encloses the Juina diamondiferous kimberlite field, among the others.

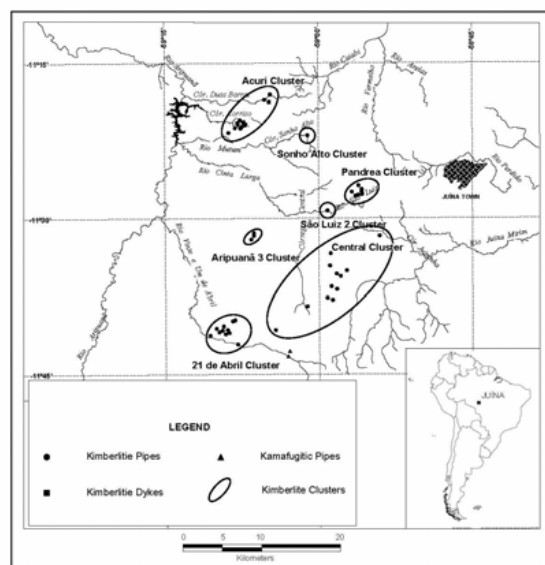


Fig. 1. Juina kimberlite field.

In total, 51 kimberlites are known to date in the Juina area including 47 pipes and 4 dykes. They are grouped in six clusters: Acuri, Sonho Alto, Sao Luis-2, Pandrea, Aripuanã-3, Central and 21 de Avril (Fig. 1). The average size of the known kimberlite pipes is approximately five hectares, but they vary between 0.10 ha and 60 ha. They all are barren or weakly diamondiferous except the Collier-04 pipe, with a surface area of 16.5 ha and estimated resource of 13.9 million tonnes of kimberlite with averaging 0.40 ct/t diamond grade. Almost all kimberlitic clusters within the Juina field (except the Aripuanã-3 cluster) are located at the intersections of NE- and NW-striking lineament corridors.

Pandrea (Chapadão) kimberlites

The kimberlitic volcanoclastic rocks, forming the crater faces of the Pandrea-1 to -7 pipes in the Pandrea (Chapadão) cluster, comprise 20-30-meter visible sequences of ash-fall and/or tuffitic material blanketed by Upper Cretaceous and Tertiary sediments. They form complex, mainly cross-bedded systems in which pyroclastic and epiclastic units are recognizable. Kimberlitic material is represented by tuffs, tuffites and various epiclastic sediments containing chrome spinel, picroilmenite, manganian ilmenite, zircon and diamond. The diamond grade varies from 0.2-1.8 car/m³.

The magmatic component of the rocks, sometimes comprising up to 50 % by volume, is represented by kimberlitic rock fragments and olivine grains fully replaced by serpentine and other secondary minerals, with a grain size of 0.2 to 3 mm (Fig. 2). These pseudomorphs usually have a characteristic 'parquet-like' replacement structure, which is typical of olivine replaced by serpentine

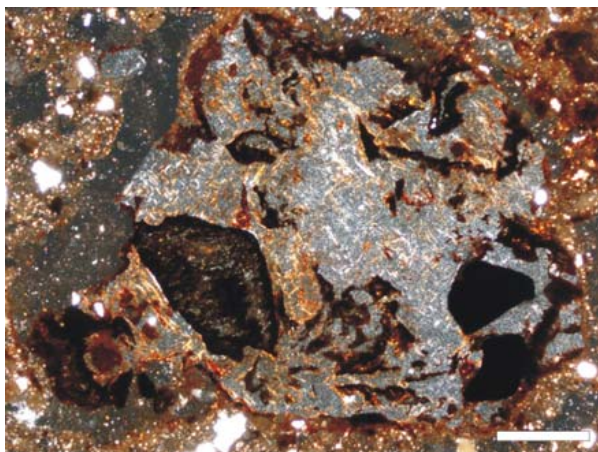


Fig. 2. Kimberlitic lithoclasts with ilmenite inclusions and pseudomorphs after olivine in kimberlitic tuffite, Pandrea-1 pipe. Scale bar is 0.5 mm.

The heavy mineral fraction of the volcanoclastic rocks shows a quite poor spectrum of kimberlite indicator minerals that is dominated by ilmenite, with a minor admixture of chrome spinel. Chrome spinel has 30-61 wt % Cr₂O₃; some of the chrome spinel grains are similar to chromite inclusions in diamond. Picroilmenite contains 6-14 wt % MgO and 0.2-4 wt % Cr₂O₃. Its composition, in Haggerty's diagram, lies within the diamond preservation field. Manganian ilmenite has less up to 3 wt % MgO and 0.38-1.41 wt % MnO (Kaminsky and Belousova, 2008). The ¹⁷⁶Hf/¹⁷⁷Hf ratio in kimberlitic zircons varies from 0.028288-0.28295 with ε_{Hf} = 5.9-8.3, and lies on the average kimberlite trend between depleted mantle and CHUR.

Kimberlitic volcanoclastic rocks belong to the mature weathering crust, where they were very intensely altered, and the magmatic component is almost

completely replaced by clay minerals. Besides, the rocks are severely contaminated by terrigenous material, primarily by quartz sand. Therefore their geochemical composition does not represent the initial composition of the kimberlitic rocks; they are very enriched in silica (55-67 wt.% SiO₂) and alumina (20-27 wt.% Al₂O₃). The highest Ti and Fe contents (up to 3.12 wt.% TiO₂ and up to 11.98 wt.% Fe_{tot}) are characteristic of kimberlites. Some trace elements show distribution characteristics similar to kimberlites (e.g., 36-160 ppm Nb and 360-660 ppm Zr).

Zircon age and Hf isotopes in zircons

U-Pb dating of zircons was performed using a New Wave/Merchantek UP213 laser ablation system (λ = 213 nm) attached to an Agilent 7500cs quadrupole ICP-MS. The mean zircon ²⁰⁶Pb/²³⁸U ages for zircon grains from the three pipes are almost identical, and within the analytical uncertainties:

- Pandrea-1 – 93.5 ± 0.7 Ma (n = 12; 95 % conf.; MSWD = 0.81; probability 0.63);
- Pandrea-6 – 93.7 ± 0.7 Ma (n = 10; 95 % conf.; MSWD = 0.51; probability 0.87);
- Pandrea-7 – 93.7 ± 0.7 Ma (n = 14; 95 % conf.; MSWD = 1.16; probability 0.30).

This allows us to consider the data from the three pipes together and calculate the average mean zircon ²⁰⁶Pb/²³⁸U age for all Pandrea pipes comprising the new Chapadão cluster (Fig. 3).

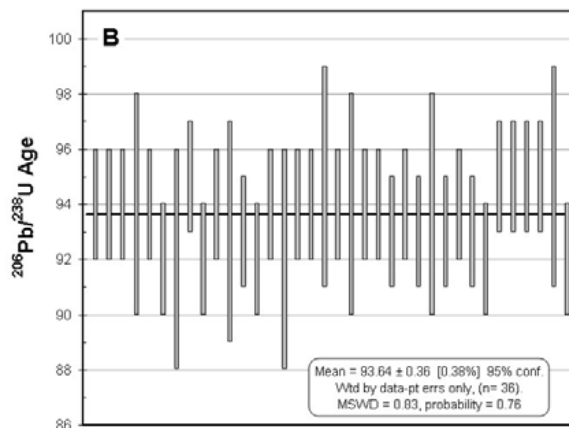


Fig. 3. Weighted mean average diagram for Juina zircon grains showing data-point errors.

For these analyses, the mean is 93.6 ± 0.4 Ma; with a 95 % confidence, MSWD = 0.83, and probability 0.76. This age can be considered as the age of the Pandrea kimberlitic pipes comprising the Chapadão cluster in the Juina area.

The results of Hf-isotope analyses are plotted in Fig. 4. One can see that both the initial ¹⁷⁶Hf/¹⁷⁷Hf values and ε_{Hf} are located between the values expected for a chondritic reservoir (CHUR), and those expected for zircons crystallized from magmas with a depleted-mantle source. The Hf isotopic composition of the Juina zircons well

corresponds to the average kimberlitic trend, according to the data of Griffin *et al.* (2000).

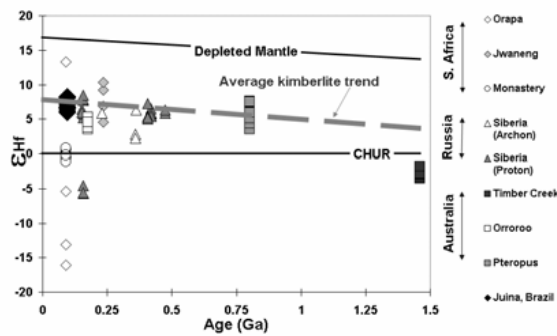


Fig. 4. ϵ_{Hf} of zircons from different localities, plotted against the intrusion age of the host kimberlites (after Griffin *et al.*, 2000).

Discussion

The major geological difference between the earlier known, barren and weakly-diamondiferous kimberlites in the Juina area and the new ones is in their ages: the Pandrea kimberlites appear to be 93.6 ± 0.4 Ma old, approximately 14 Ma older than the kimberlite ages in the Central cluster of the Juina area (80.1 Ma and 79.2 Ma; Davis, 1977). That age represents a time of magmatic reactivation related to the formation of southern part of Atlantic Ocean. The Pandrea kimberlites are Cenomanian/Turonian, more ancient than the sedimentary Cretaceous Parecis Formation. Basal conglomerates of the Parecis Formation contain diamonds (in some areas in sub-economic concentrations); this proves that the major sources of diamonds in this area are older.

The newly found Pandrea kimberlites in the Juina area, hosting super-deep diamonds that originated in the lower mantle and transition zone (Kaminsky *et al.*, 2008) presumably originated at similar depths, and hence may be considered as the deepest known kimberlites. The mechanism of the origin of kimberlitic magma at such depth (up to 660 km and, possibly, deeper) is yet to be explained. There are some features of mineral inclusions in Juina diamonds (Harte *et al.*, 1999; Kaminsky *et al.*, 2001, 2008), such as a higher iron index in ilmenite, chrome spinel and 'olivine' than in the same phases occurring as 'usual' upper-mantle inclusions in diamond, which may reflect a process of core/mantle convection. On the other hand, some evidence may point to a possibility of super-deep subduction processes initiating partial melting of zones in the lower mantle with subsequent ascent of proto-kimberlitic magma. This evidence comprises inclusions of carbonates and hydrous minerals in diamonds. A nanocrystalline hydrous aluminium silicate phase (AlSiO_3OH , phase 'Egg') in association with stishovite was found in one of the Juina diamonds (Wirth *et al.*, 2007). This phase is stable at pressures at least up to 1625 °C and 17 GPa (Sano *et al.*, 2004), and it may be a possible water-bearing mineral in Al-rich sediments

or hydrous basalts, subducted to the depth of the transition zone or below. In other Juina diamonds, several syngenetic carbonate inclusions 20-50 μm in size were found *in situ* in association with Ca-walstromite and 'olivine' (Brenker *et al.*, 2007). The origin of these lower-mantle carbonates is most likely related to CO_2 -enriched crustal or lithospheric material that has been transported to great depths via subduction processes, associated with destructive plate margins.

References

- Brenker, F.E., Vollmer, C., Vincze, L., Vekemans, B., Szymanski, A., Janssens, K., Szaloki, I., Nasdala, L., Kaminsky, F., 2007. Carbonates from the lower part of transition zone or even the lower mantle: Earth and Planetary Science Letters, 260, 1-9.
- Brito Neves, B.B., Teixeira, W., Tassinari, C.C.G., Kawashita, K., 1990. A contribution to the subdivision of the Precambrian in South America. Revista Brasileira de Geociências, 20, 267-276.
- Davis, G.L., 1977: The age and uranium contents of zircons from kimberlites and associated rocks. In: Geophysical Laboratory, Carnegie Institute, Washington Yearbook, 76, 631-635.
- Griffin, W.L., Pearson, N.J., Belousova, E.A., Jackson, S.R., Van Aichtenberg, E., O'Reilly, S.Y., Shee, S.R., 2000. The Hf isotope composition of cratonic mantle: LAM-MC-ICPMS analysis of zircon megacrysts in kimberlites. Geochimica et Cosmochimica Acta, 64, 133-147.
- Harte, B., Harris, J.W., Hutchison, M.T., Watt, G.R., Wilding, M.C., 1999. Lower mantle mineral associations in diamonds from Sao Luiz, Brazil. In: Fei, Y., Bertka, C.M. and Mysen, B.O. (Eds), Mantle Petrology: Field Observations and High Pressure Experimentation, Geochemical Society Special Publication, 6, 125-153.
- Kaminsky, F.V., Belousova, E., 2008. Manganian ilmenite as kimberlite/diamond indicator mineral. Geologia i Geofizika (Russian Geology and Geophysics) (submitted).
- Kaminsky, F.V., Zakharchenko, O.D., Davies, R., Griffin, W.L., Khachatryan-Blinova, G.K., Shiryaev, A.A., 2001. Super-deep diamonds from the Juina area, Mato Grosso State, Brazil. Contributions to Mineralogy and Petrology, 140, 734-753.
- Kaminsky, F.V., Khachatryan, G.K., Andreazza, P., Araujo, D., Griffin, W.L., 2008. Super-deep diamonds from kimberlites in the Juina area, Mato Grosso State, Brazil. 9th International Kimberlite Conference Extended Abstract No. 9IKC-A-00005.
- Sano, A., Ohtani, E., Kubo, T., Funakoshi, K., 2004. In-situ X-ray observation of decomposition of hydrous aluminium silicate $\text{AlSiO}_3(\text{OH})$ and aluminium oxide hydroxide $\delta\text{-AlOOH}$ at high pressure and temperature. Journal of Physics and Chemistry of Solids, 65, 1547-1554.
- Wirth, R., Vollmer, C., Brenker, F., Matsyuk, S., Kaminsky, F., 2007. Nanocrystalline hydrous aluminium silicate in super-deep diamonds from Juina (Mato Grosso State, Brazil): Earth and Planetary Science Letters, 259, 384-399.

Combined U-Pb and Lu-Hf analysis of megacrystic zircons from the Kalyandurg-4 kimberlite pipe, S. India: Implications for the emplacement age and Hf isotopic composition of the cratonic mantle

E.V.S.S.K. Babu^{1,2}, W.L. Griffin¹, Abhijeet Mukherjee³, S.Y. O'Reilly¹ and E.A. Belousova¹

¹ARC National Key Centre GEMOC, Macquarie University, NSW 2109, Australia,

²National Geophysical Research Institute, Uppal Road, Hyderabad-500007, India,

³NMDC Ltd., Khanij Bhavan, Masab Tank, Hyderabad-500028, India

Introduction

The occurrence of zircon in most igneous, sedimentary and metamorphic rocks is not unique. However, the occurrence of the zircon megacrysts ranging upto cm-size grains hosted by kimberlite is considered enigmatic (Griffin et al. 2000, Page et al. 2007 and reference cited therein). Since zircon is one of the most refractory minerals, it preserves a robust record of trace elemental abundances, oxygen, U-Pb, Lu-Hf isotopic compositions unique to its geological history from genesis to post-formational changes (Hanchar and Hoskin, 2003, Valley, 2003). Texturally, the kimberlite-borne mantle-derived megacrystic zircons display unique characters in terms of appearance compared to their crustal varieties. They are colorless and glassy for external appearance (see Page et al. 2007 for a recent review). The published data further suggests that in most occurrences, U-Pb geochronology of these zircons record the emplacement of the kimberlite host (see Griffin et al. 2000 for an exhaustive data set). As parental melts of the kimberlites originate from the sub-continental lithospheric mantle, the Hf isotopic composition of the zircon megacrysts, if any would help in tracing out the Hf isotopic composition of this major isotopic reservoir of the Earth.

Here we report a combined U-Pb and Lu-Hf isotopic study on the megacrystic zircon xenocrysts from the Kalyandurg-4 kimberlite (KL-4) of the Eastern Dharwar Craton, S. India. The aim is to decipher the hitherto unknown emplacement age of the Kalyandurg kimberlite cluster and constrain the Hf isotopic composition of the subcrustal mantle at the time of emplacement. The Kalyandurg kimberlite cluster is the western-most of the kimberlite clusters in the Eastern Dharwar Craton, South India intruding the ca. 2.5 Ga Closepet Granite Complex (Figure 1). This zone forms part of the Neoproterozoic accretionary

complex between the Eastern and Western Dharwar Cratonic blocks.

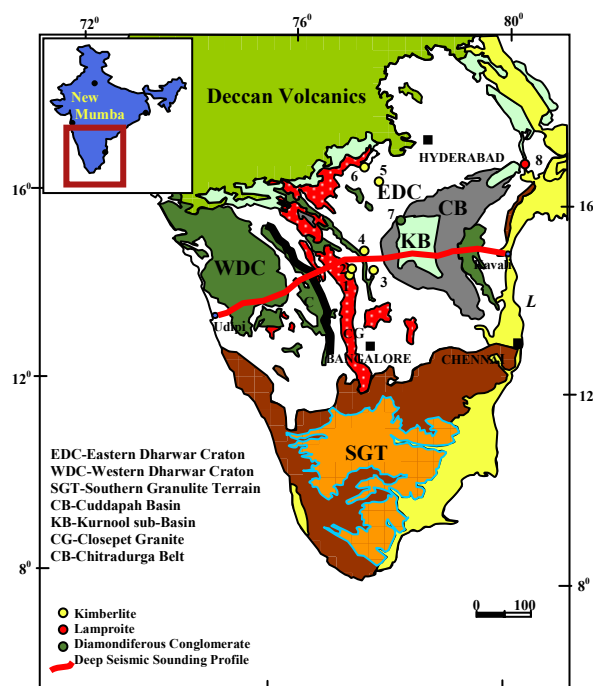


Figure 1. Location map of the Dharwar Craton Kimberlites and Lamproites in the southern India. 1. Kalyandurg, 2. Brahmanapalli, 3. Chigicherla, 4. Wajrakarur, 5. Riachur, 6. Mahaboobnagar, 7. R. Kota, 8. Krishna Lamproite

Materials, Methods and Results

10 fragments of megacrystic zircons were separated from the kimberlite matrix and were subjected to EPMA, LAM-ICPMS and LAM-MC-ICPMS analysis for the determination of major, trace elemental abundances and U-Pb and Lu-Hf isotopic determinations respectively following the methods described in Belousova et al. 2002 and Griffin et al. (2004). The analysed zircon fragments range in size from 1 to 2.3 mm in longer dimension. The grains are colorless, glassy and do not show any zoning in

Cathodoluminescence (CL) and Back Scattered Electron (BSE) imaging (Figure 2).

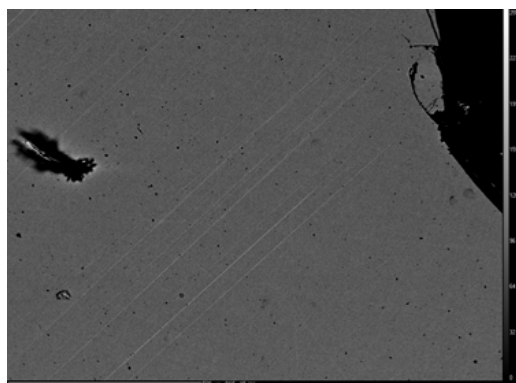


Figure 2. CL image of a KL-4 zircon fragment.

LAM-ICPMS Trace element compositions of KL-4 zircons show very low U (1-3 ppm) and Th (4-8 ppm) and REE concentrations are typical of other worldwide kimberlitic zircon occurrences. U-Pb data determined by LAM-ICPMS gave two sets of concordant ages 1097 ± 5.7 Ma (MSWD=0.92) and 1154 ± 5.1 (MSWD=0.105) for the analysed KL-4 kimberlite zircons (Figure 3). Both the age estimates fall within the limits established for the other kimberlite clusters of the Dharwar Craton in S. India. (see Anil Kumar, 2007).

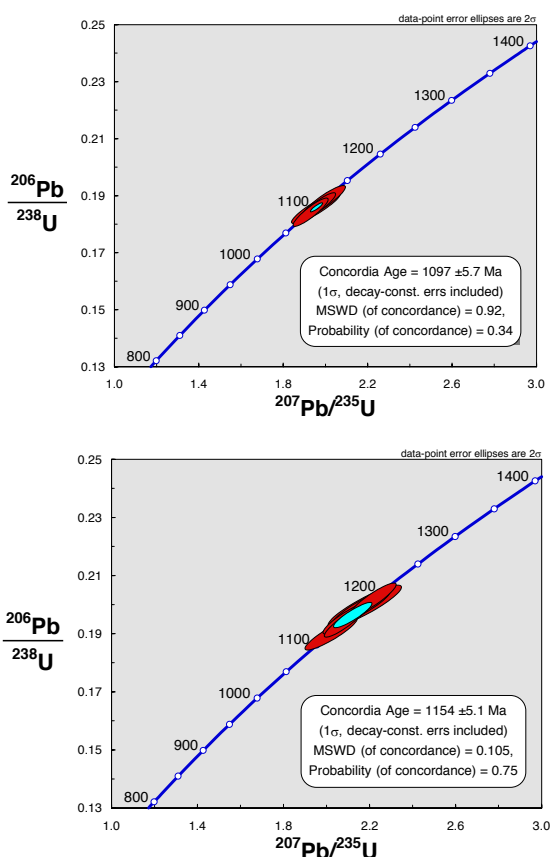


Figure 3. U-Pb Concordia diagram for the KL-4 zircons.

ϵ_{Hf} values fall in a range from 3.88 ± 0.60 to 6.78 ± 0.56 and Hf T_{DM} (Ga) model ages range from 1.33 to 1.45 Ga. The $^{176}\text{Hf}/^{177}\text{Hf}_i$ ratios of the Kalyandurg zircons range from 0.282163 to 0.282254, falling between values expected for a chondritic reservoir and those of from magmas with a depleted-mantle (DM) source (Figure 4).

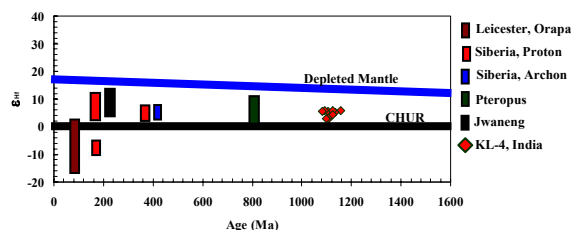


Figure 4. ϵ_{Hf} of the analysed zircons from KL-4 plotted against intrusion age of the host kimberlite. Comparisons shown with the other localities (data from Griffin et al. 2000)

This pattern is characteristic of most kimberlitic zircons with ages of 0.1-2.5 Ga worldwide; it probably represents either the long-term Hf-isotopic composition of the cratonic lithospheric mantle, or a very consistent pattern of interaction between the (low-Lu/Hf) lithospheric mantle and melts derived from the DM source.

Conclusions

1. KL-4 pipe intrusion age derived from the U-Pb data of zircons suggests that it is contemporary to the other ~ 1.1 Ga kimberlite intrusions within the Dharwar Craton.
2. Hf isotopic data of the megacrystic KL-4 zircons show similarities with the other world occurrences suggesting a long-term Hf-isotopic composition of the cratonic lithospheric mantle, or a very consistent pattern of interaction between the (low-Lu/Hf) lithospheric mantle and melts derived from the DM source.

References

- Anil Kumar, Heaman, L.M. and Manikyamba, C. 2007. Mesoproterozoic kimberlites in south India: A possible link to ~ 1.1 Ga global magmatism. *Precambrian Research*. Volume 154, pp. 192–204.
- Belousova E. A., Griffin W. L., O'Reilly S. Y. and Fisher N. I. 2002. Igneous zircon: trace element composition as an indicator of source rock type. *Contributions to Mineralogy and Petrology*. 143, 602–622.
- Griffin, W. L., Pearson, N.J., Belousova, E., Jackson, S.E., van Acherbergh, E, O'Reilly, S. and Shee, S.R. 2000. The Hf isotope composition of cratonic mantle: LAM-MC-ICPMS analysis of zircon megacrysts in kimberlites. *Geochimica et Cosmochimica Acta*, Volume 64, No. 1, pp. 133–147.

Griffin, W. L., Belousova, E., Shee, S.R., Pearson, N.J. and O'Reilly, S. 2004. Archean crustal evolution in the northern Yilgarn Craton: U-Pb and Hf isotope evidence from detrital zircons. *Precambrian Research*, Volume 131, pp. 231–282.

Hanchar J. M. and Hoskin P. W. O. 2003. Zircon—Reviews in *Mineralogy and Geochemistry*, vol. 53, Mineralogical Society of America/Geochemical Society, p. 500.

Page, Z. F., Bin Fu, Noriko T. Kita, John Fournelle, Michael J. Spicuzza, Daniel J. Schulze, Fanus Viljoen,

Miguel A.S. Basei, John W. Valley. 2007. Zircons from kimberlite: New insights from oxygen isotopes, trace elements, and Ti in zircon thermometry. *Geochimica et Cosmochimica Acta* 71, pp. 3887–3903.

Valley J. W. 2003. Oxygen isotopes in zircon. In *Zircon*, *Rev. Mineral. Geochem.* Vol. 53 (eds. J. M. Hanchar and P. W. O. Hoskin). Mineralogical Society of America/Geochemical Society, pp. 343–385.

Eclogite Xenoliths from the kimberlites of the Eastern Dharwar Craton, South India: material representing ancient crust of the Western Dharwar Craton?

E.V.S.S.K. Babu^{1,2,*}, W.L. Griffin¹, S. Panda², S.Y. O'Reilly¹, Y.J. Bhaskar Rao²

¹ARC National Key Centre GEMOC, Macquarie University, NSW 2109, Australia

²National Geophysical Research Institute, Uppal Road, Hyderabad-500007, India

*e-mail: evsskbabu@yahoo.co.in

Introduction

Eclogites, *sensu stricto* are bimineralic rocks of pyrope and omphacite equilibrated under upper-mantle temperature and pressures. However, they could represent a range of protoliths such as picritic basalts crystallized in magma chambers within the mantle, subducted ocean floor or delaminated lower crustal material. Such heterogeneity from a suite of eclogite xenoliths brought by explosive kimberlite volcanism can often be identified through their constituent mineralogy and compositions.

Here we present a set of new mineralogical, thermobarometric and geochemical data on kimberlite-borne eclogitic xenoliths from the Eastern Dharwar Craton (EDC), south India to speculate on their possible protoliths and their geodynamic significance in the light of an ongoing debate on the crustal and lithospheric architecture of the Dharwar Craton (Figure 1). Based on the lithological variations, nature of volcano-sedimentary sequences, magmatic character, geochronological data, metamorphic grade and geophysical properties the Dharwar Craton is divided into distinct Eastern and Western domains (Refs. Chadwick et al. 2000; Chadwick et al. 2007; Jayananda et al. 2000; Gupta et al. 2003 and references cited therein). Current tectonic models visualize a Neoproterozoic oblique convergence of the WDC and EDC. Implicit is that the older WDC crust underlies a tectonic stack of west-verging EDC (Chadwick et al. 2007). A prominent zone of mylonites straddles the eastern margin of the Chitradurga schist belt in the WDC and the ca 2.5 Ga Closepet granite complex is proximal to this mylonite zone. The eastern margin of this accretion zone also localised several clusters of ~ 1.1 Ga kimberlite pipes (Anil Kumar et al. 2007). These kimberlites entrained diverse eclogite xenolith suits representing a variety of protoliths. This work assumes significance in tracing the xenoliths to protoliths and find possible genetic linkages with the co-spatial TTG gneisses of the terrain.

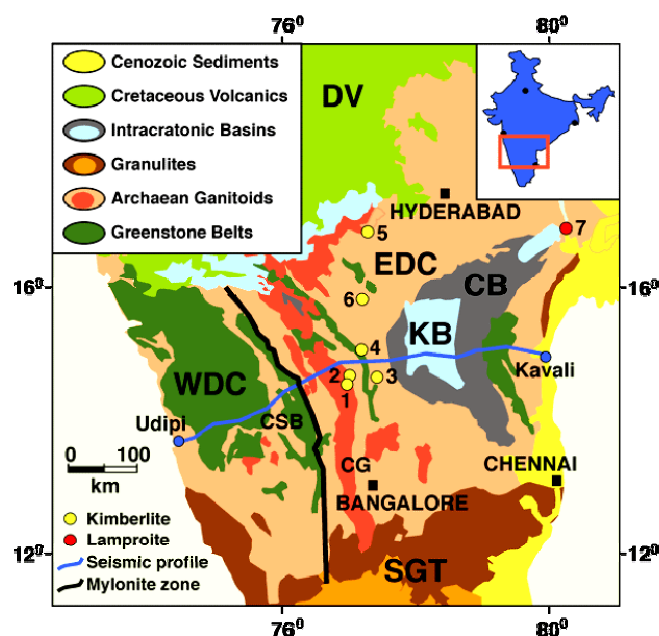


Figure 1. Location of the major kimberlite and lamproite clusters of the Dharwar craton, south India. 1. Kalyandurg, 2. Brahmanapally, 3. Chigicherla, 4. Wajrakarur, 5. Mahaboobnagar, 6. Raichur, 7. Krishna Lamproite field. EDC-Eastern Dharwar Craton, WDC-Western Dharwar Craton, CSB-Chitradurga Schist Belt, DV-Deccan Volcanics, SGT-Southern Granulite Terrain, CG-Closepet Granite.

Materials and Methods

The eclogite types include bimineralic and kyanite-coesite-rutile-bearing varieties with the former restricted to the Wajrakarur cluster. Some of the kyanite-coesite bearing eclogites (Figure 2) show alteration zones with traces of celadonite, hyalophane and barite suggesting extensive Ba metasomatism.

A new class of prehnite-bearing eclogites was also identified suggesting post kimberlite emplacement low-temperature alteration of the eclogite xenolith. Some of the eclogite xenoliths also have both intracrystalline primary base metal sulphides as well as secondary sulphide veins.

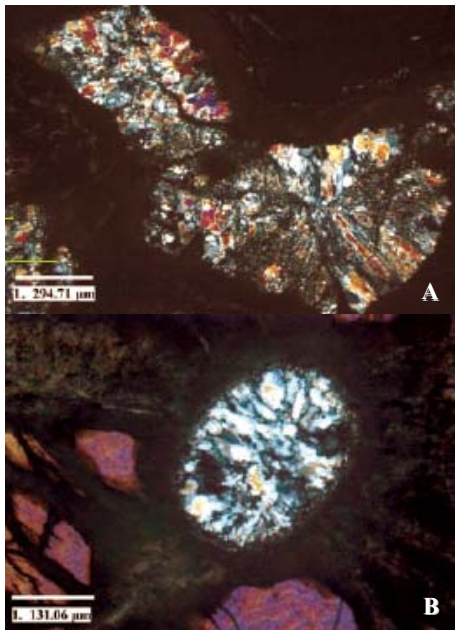


Figure 2. A. Coesite-bearing and B. Kyanite-coesite-bearing eclogite xenoliths.

Thermobarometry

Temperature estimates based on the conventional thermometry using the garnet and clinopyroxene were projected on to the xenolith geotherms of different kimberlite clusters. Kalyandurg xenoliths fall on a typical Archaean geotherm with a 35 mW/m^2 and those from the Wajrakarur represent a 40 mW/m^2 Proterozoic geotherm.

The eclogite xenoliths from the Wajrakarur kimberlite cluster shows P-Ts ranging from 750-1225°C and 29-61 kbar with a wide depth distribution (Figure 3). Whereas, the xenoliths from the Kalyandurg cluster are restricted to a narrow range of 1020-1185°C and 56-61 kbar corresponding to a single layer corresponding to a depth of 176-191 km (figure 3).

Although eclogites from the Kalyandurg cluster show marked distribution of mineralogical variations, their depth distribution is confined to a 10-20 km layer between 176-191 km. This feature is similar to that seen in many SCLM sections (see Griffin and O'Reilly, 2007) The studies on garnet xenocrysts from these clusters (see 9IKC-A-00103 by Griffin et al. in this abstract volume) further puts constraints on the nature of Indian Sub continental lithospheric mantle (SCLM) at this depth at $\sim 1.1 \text{ Ga}$. The presence of eclogite layers in the SCLM also show correspondence with the pyropic garnet trace element signatures at the corresponding depths.

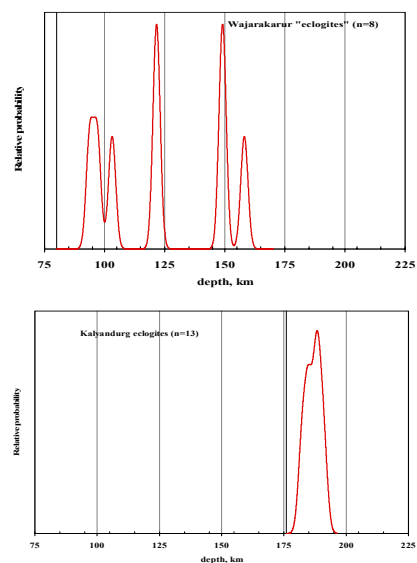


Figure 3. Relative probability vs. depth distribution for eclogite xenoliths from the Wajrakarur and Kalyandurg Kimberlite clusters. The depth distribution was arrived after projecting the estimated pressures and temperatures from conventional thermobarometry on to the xenolith geotherm.

Major and Trace element geochemistry

35 petrographically distinct eclogites were analysed for mineral and bulk chemical compositions. They are characterized by low MgO (5.3-12.15 wt. %), high Al_2O_3 (14.75-26.22 %) and CaO (11.14 to 28.12 %). High MgO eclogites were observed from only the Wajrakarur cluster. Whereas, the eclogites from the Kalyandurg cluster show lower bulk MgO contents.

Among the trace element abundances the most enriched elements are Ba (309-9270 ppm) and Sr (2220-15823 ppm) with minor enrichment of Rb (0.7-145 ppm). Most of the biminerally eclogites show flat REE patterns. In contrast, kyanite-bearing types show pronounced +ve Eu anomalies with LREE-enriched and HREE depleted patterns; these anomalies are also seen in the cpx and gnt. High field strength element abundances vary with the abundance of accessory rutile. The major and trace element compositions such as low MgO, high Al_2O_3 and CaO, presence of Eu anomalies in bulk rock analyses and individual minerals suggest altered crustal protoliths.

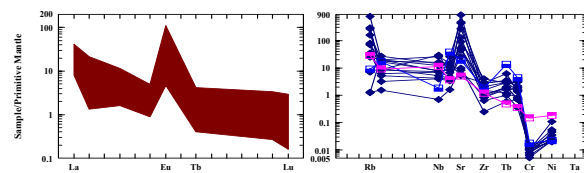


Figure 4. Bulk REE and trace element distributions of kyanite eclogite xenoliths from the Kalyandurg.

Conclusions

- (1) Eclogite xenoliths from the S. Indian kimberlite pipes could represent a variety of protoliths.
- (2) Wajrakarur and Kalyandurg clusters entrain kimberlites from distinct horizons of the Subcontinental Lithospheric Mantle sections.
- (3) High Mg# biminerally deeper eclogites could possibly represent picritic trapped melts. Whereas, the low Mg# kyanite-coesite eclogites represent crustally derived protoliths or picritic sources severely altered by crustal components.
- (4) The crustal component observed in the eclogite xenoliths could possibly be derived from the WDC.
- (5) The eclogite xenoliths show extensive Barroisite metasomatism with the presence of baryte and rarely celsian.
- (6) Prehnite eclogites further suggests post-entrapment alteration.

Jayananda, M., Moyen, J-F., Martin, H., Peucat, J-J., Auvray, B. and Mahabaleshwar, B. (2000) Late Archaean (2550-2520 Ma) juvenile magmatism in the Eastern Dharwar Craton, southern India : constraints from geochronology, Nd-Sr isotopes and whole rock geochemistry. *Precambrian Research*. V. 99. pp. 225-254.

References

- Anil Kumar, Heaman, L.M. and Manikyamba, C. 2007. Mesoproterozoic kimberlites in south India: A possible link to ~1.1 Ga global magmatism. *Precambrian Research*. Volume 154, pp. 192–204.
- Chadwick, B., Vasudev, V.N. and Hegde, G.V. (2000) The Dharwar craton, southern India, interpreted as the result of Late Archaean oblique convergence. *Precambrian Research*. V. 99, pp. 91–111.
- Chadwick, B., Vasudev, V.N., Hegde, G.V. and Nutman, A.P. Structure and SHRIMP U/Pb Zircon ages of granites adjacent to the Chitradurga Schist Belt: Implications for Neoproterozoic convergence in the Dharwar Craton, Southern India. *Journal of the Geological Society of India*. v. 69. pp. 5-24.
- Griffin, W.L. and O'Reilly, S.Y., 2007. Cratonic lithospheric mantle: Is anything subducted? *Episodes*. V. 30, pp. 43-53.
- Griffin, W.L., Kobussen, A. F., Babu, E.V.S.S.K., O'Reilly, S.Y., Norris, R. and Sengupta, P. 2008. Contrasting lithospheric mantle across the suture between the Eastern and Western Dharwar Cratons, central India. *Proceedings of the 9th International Kimberlite conference*. Extended Abstract No. 9IKC-A-00103, Frankfurt, Germany. 10-15 August, 2008.
- Gupta, S., Rai, S.S., Praksam, K.S., Srinagesh, D., Bansal, B.K., Chadha, R.K. Priestley, K. and Gaur, V.K. (2003) The nature of the crust in southern India: Implications for Precambrian crustal evolution, *Geophysical Research Letters*, V. 30. No. 8, 1419, doi:10.1029/2002GL016770.



Peridotitic garnet geochemistry: key to the understanding of lithospheric structures and kimberlites diamond potential in Southern Congo

J.M. Batumike^{1,2}, S.Y.O'Reilly¹ and W.L. Griffin¹

¹ARC National Key Centre for Geochemical Evolution and Metallogeny of Continents, Department of Earth and Planetary Sciences, Macquarie University, Sydney, NSW 2109, Australia

²Département de Géologie, Université de Lubumbashi, Route Kasapa, BP 1825, Lubumbashi, D.R. Congo

Kimberlites occur in the southern part of the Democratic Republic of the Congo (Fig. 1) in the Kasai Province (eg. Mbuji Mayi, Luebo) and the Kundelungu Plateau (Katanga Province). The Mbuji Mayi kimberlites are Cretaceous (Demafiffé et al., 1983). U-Pb dating of perovskites indicates that Kundelungu kimberlites intruded at 32 Ma (Batumike et al., 2008).

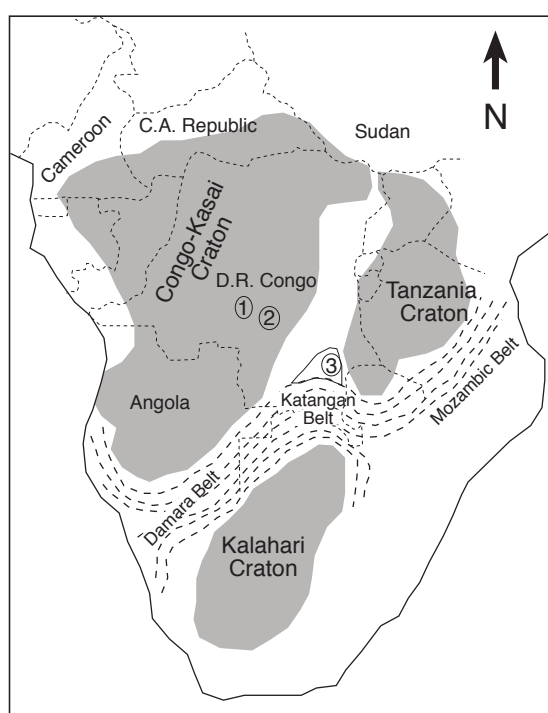


Fig.1. Location of study areas: 1, Luebo; 2, Mbuji Mayi; 3, Kundelungu Plateau

The Mbuji Mayi and Luebo kimberlitic fields are located inside the Congo Craton. The Kundelungu kimberlites intruded the Neoproterozoic Katangan Belt and the off-craton basement beneath the region is predominantly Paleoproterozoic (Batumike et al., 2007). This study uses major- and trace-element compositions of peridotitic garnets in order to map the chemical heterogeneity of the subcontinental lithospheric mantle and to assess the diamond potential of the kimberlites.

Kundelungu Plateau

The peridotitic garnets in the Kundelungu kimberlites are mainly lherzolitic with very few harzburgitic and wehrlitic garnets.

The garnets show two different populations in terms of Y, Ti and Ni contents (Fig. 2). These two populations define different geotherms. The conductive geotherm defined by the population with high Y/Ti is quite low, in general between 35 and 37.5 mW/m² at depths <ca 130 km; the other group defines a geotherm closer to a 40 mW/m² model, mainly at depths >130 km (Fig. 3). This pattern suggests that the initially low conductive geotherm in the region has been perturbed by high-T melts which induced the metasomatism (high Ti/Y) observed in the garnets.

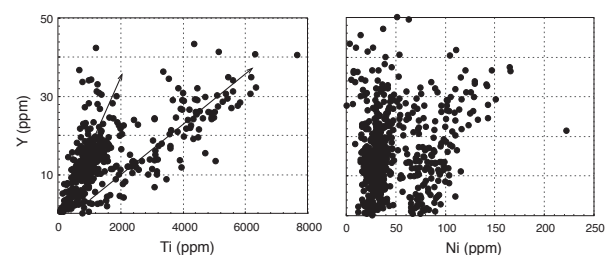


Fig. 2. Y-Ti-Ni relationships in Kundelungu garnet concentrates, showing two different clusters separated by a Ni (T) gap.

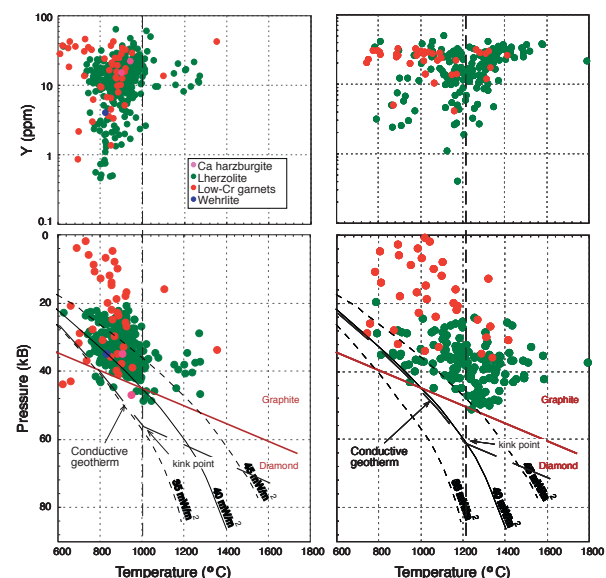


Fig. 3. Geotherms (lower panels) and distribution of Y with Temperature (Ni) in Kundelungu, for (a) low-T and (b) high-Ti/Y garnets. The envelope of maximum P at each T defines the Garnet Geotherm (Ryan et al., 1996).



The garnets characteristic of the higher geotherm are also characterised by a low calculated XMg in coexisting olivine (after Gaul et al., 2000), typical of peridotites metasomatised by asthenosphere-derived melts (Fig. 4).

The lithosphere-asthenosphere boundary represents a zone where there is interaction between a depleted lithosphere and fertile asthenosphere. The depth of this zone is estimated by the lower depth limit of low-Y garnets. In the Kundelungu Plateau the lithosphere-asthenosphere boundary depth is estimated at 175 km (Fig. 4), but detailed data from the region show that the lithosphere is slightly thicker in the eastern than the western part of the plateau. The lithospheric section shows the presence of a thin layer of harzburgites within the diamond stability field (Fig. 4).

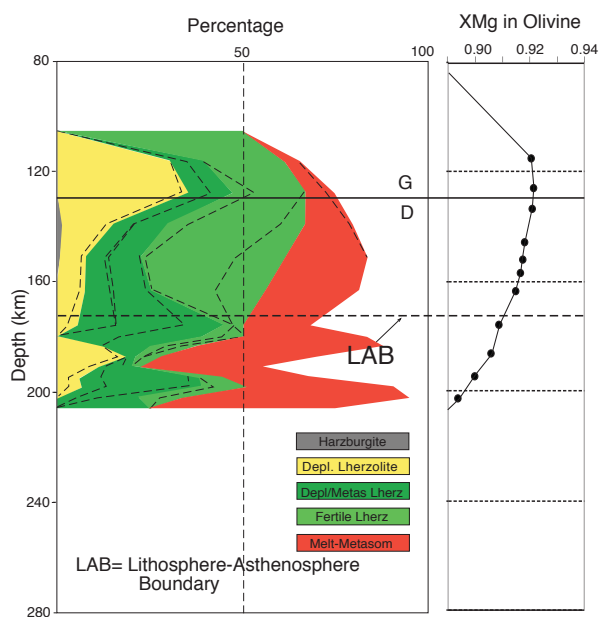


Fig. 4. Chemical tomography section of the lithosphere beneath the Kundelungu Plateau and distribution of XMg in olivine coexisting with garnets.

Mbuji Mayi Region

The mantle beneath the Mbuji Mayi kimberlite field, which includes the Mbuji Mayi and Tshibwe clusters, is characterised by predominantly harzburgitic and lherzolititic garnets but there are also low-Cr garnets, wehrlitic and low-Ca harzburgitic garnets. The conductive geotherm is ~ 35 mW/m², which is quite low and typical of cratonic settings. The estimated lithospheric thickness is 210 km (Fig. 5).

The lithospheric section of this region is characterised by the presence of two harzburgitic layers within the diamond stability field (Fig. 5). Melt-related metasomatism and phlogopite metasomatism were the main processes that have affected the lithosphere; melt-related metasomatism becomes progressively more important below ca 180 km depth.

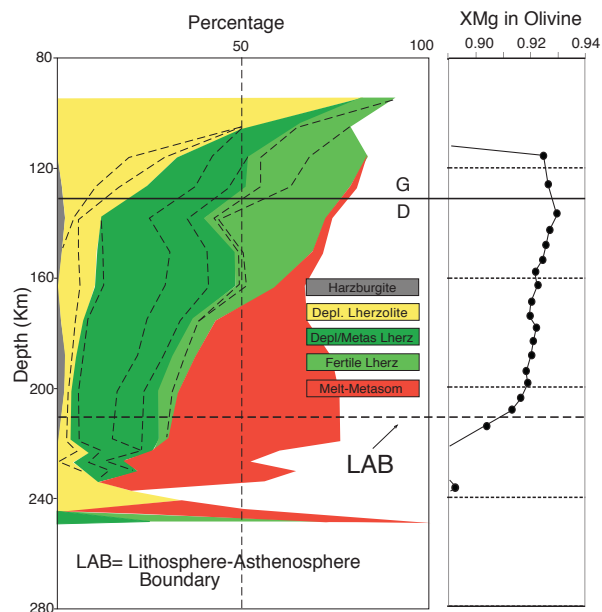


Fig. 5. Chemical tomography section of the lithosphere in Mbuji Mayi region and distribution of XMg (calculated) in olivine coexisting with garnets.

Luebo Region

The Luebo garnet population consists of lherzolititic, Ca- and low-Ca harzburgitic, and low-Cr garnets. The conductive geotherm derived from the garnets is ~ 35 mW/m², which is low and typical of cool cratonic lithosphere.

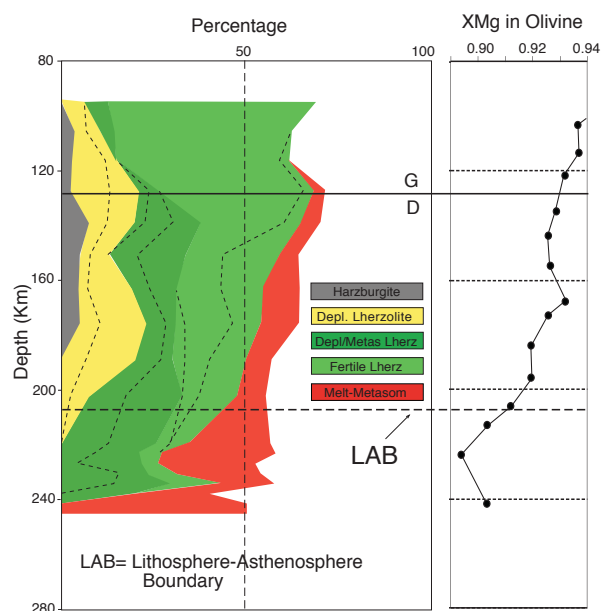


Fig. 6. Chemical tomography section of the lithosphere in Luebo region and distribution of XMg in olivine

The Luebo garnets are characterised by a near-absence of low-Y garnets above 1100 °C, which corresponds also to a drop of XMg in coexisting olivine to <91%. This temperature corresponds to a depth for the lithosphere-asthenosphere boundary of about 205 km (Fig. 6), which is similar to the LAB estimates for the

Mbuji Mayi region. Garnet compositions indicate melt-related and phlogopite-related metasomatism as shown by anomalous enrichment in elements such as Ti, Y and Zr in some garnets. There is a relatively high abundance of harzburgitic garnets within the diamond stability field in the lithosphere beneath the region.

Diamond potential

The low conductive geotherm in Kundelungu is similar to that of cratonic regions where diamonds are found. The garnets from Kundelungu Plateau are mostly lherzolitic in composition. The rare harzburgitic garnets are restricted to the Talala pipe, where Verhoogen (1938) found also the highest grade in diamond (~6.3 carats per 1000t) for the whole Kundelungu area. There are also some lherzolitic garnets with composition similar to diamond inclusions (Fig. 7a). The absence of diamond in Kundelungu may be due to the thermal perturbation and metasomatism by hot asthenospheric melts.

The garnet populations from Luebo and Mbuji Mayi are characterised by abundant garnets with sinusoidal REE patterns, which are similar to patterns observed in diamond inclusions. The sinusoidal REE patterns are shown in Fig. 7 by high Nd/Y. The relationships between Nd, Y and temperature (Ni) indicate the presence of garnets with diamond-inclusion affinities within the diamond stability field (Fig. 7b). The relative proportion of such garnets is similar in the Luebo and Mbuji Mayi districts, and much higher than in the Kundelungu kimberlites as also shown by the greater abundance of harzburgitic rocks within diamond stability field in these two regions compared to that in Kundelungu. This is consistent with what is known about diamond potential in these areas.

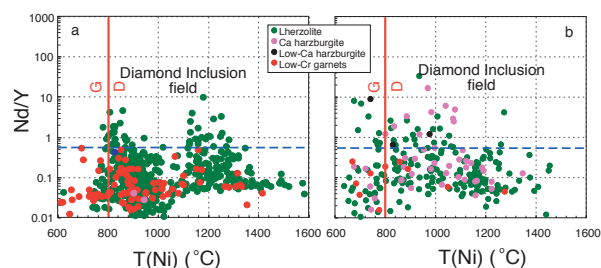


Fig. 7. Nd/Y vs T in garnets from the Kundelungu kimberlites (a) and the Luebo region (b). Vertical lines (G/D) show the T of intersection between the geotherm and the diamond stability field (G: Graphite, D: Diamond); garnets with high Nd/Y and $T > G/D$ may coexist with diamond. Since the high-T Kundelungu garnets are strongly metasomatised, the Luebo field clearly has the higher diamond potential.

Conclusions

The Kundelungu, Mbuji Mayi and Luebo regions are characterised by a low conductive geotherm, but the deeper parts of the Kundelungu section have been thermally disturbed. The lithosphere beneath the Kundelungu Plateau is also relatively thin compared to that beneath Mbuji Mayi and Luebo. This is compatible

with the location of these regions, Kundelungu being located off-craton whereas Mbuji Mayi and Luebo are within the craton. The 32 Ma kimberlite magmatism in the Kundelungu Plateau is correlated with the initial stage of the opening of the East African Rift, and the disturbance of the initially low conductive geotherm may reflect the upwelling of melts related to the opening of the rift. Both Mbuji Mayi and Luebo have garnet compositions indicating melt-metasomatism processes but not to the same extent as observed in Kundelungu Plateau. Mbuji Mayi and Luebo have higher diamond potential than Kundelungu. The low diamond potential of Kundelungu could be attributed to the melt metasomatism that affected the lithosphere in this region.

Acknowledgements

We thank De Beers for access to mineral-chemistry data from both Kundelungu and Mbuji Mayi, and Gravity Diamonds for samples and data from Luebo. This work was supported by an ARC Discovery and Linkage grants (SYOR and WLG), and an iMURS and IPRS (JMB); and used instrumentation funded by ARC LIEF and DEST systemic Infrastructure Grants, Macquarie University and Industry.

References

- Batumike, J.M., O'Reilly, S.Y., Griffin, W.L., Belousova, E.A. 2007. U-Pb and Hf-isotope analyses of zircon from the Kundelungu kimberlites, D. R. of the Congo: Implications for crustal evolution. *Precambrian Research* 156, 195-225
- Batumike, J.M., Griffin, W.L., Belousova, E.A., Pearson, N.J., O'Reilly, S.Y., Shee, S. R. 2008. LAM-ICPMS U-Pb dating of kimberlitic perovskite: Eocene-Oligocene kimberlites from the Kundelungu Plateau, D.R. Congo. *Earth and Planetary Science Letters* 267, 609-619.
- Demaiffe, D., Fieremans, M., Fieremans, C., 1991. The kimberlites of Central Africa: A review. In: Kampunzu, A.B. and Lubala, R.T. (Editors.), *Magmatism in extensional structural setting: The Phanerozoic Africa plate*. Springer-Verlag, Berlin, 538-557.
- Gaul, O.F., Griffin, W.L., O'Reilly, S.Y., Pearson, N.J., 2000. Mapping olivine composition in the lithospheric mantle: *Earth and Planetary Science Letters* 182, 223-235
- Malkovets, V.G., Griffin, W.L., O'Reilly, S.Y., Wood, B.J., 2007. Diamond, subcalcic garnet, and mantle metasomatism: Kimberlite sampling patterns define the link: *Geology* 35, 339-342.
- Ryan, C.G., Griffin, W.L., Pearson, N.J., 1996. Garnet geotherms: Pressure-temperature data from Cr-pyropite garnet xenocrysts in volcanic rocks: *Journal of Geophysical Research* 101, 5611-5626.
- Verhoogen, J., 1938. Les pipes de kimberlite du Katanga: *Annales du Service des Mines, Com. Spéc. Katanga* 9, 1-49.



Age of FS66 Kimberlite Beneath Murray Basin, South Australia: Laser Ablation ICP-MS Dating of Kimberlitic Zircon, Perovskite, and Rutile

Steven A. Cooper^{1,2}, Elena A. Belousova¹, W.L. Griffin¹, & Brian J. Morris³

¹GEMOC ARC National Key Centre, Macquarie University, NSW, 2109, Australia

²Orogenic Exploration Pty Ltd, Burwood, Vic, 3125, Australia

³South Australia Geological Survey, PIRSA, Adelaide, SA, 5000, Australia

Grains of zircon, perovskite and rutile (0.3-1.0mm in size) have been recovered from a deeply buried kimberlite in South Australia. U-Pb ages of these grains have been determined using *in situ* LAM-ICPMS techniques at GEMOC, Macquarie University, Sydney. The kimberlitic pipe, designated FS66, is located 10.6 kilometres NNW of the town of Blanchetown along the Murray River, beneath 214 metres of Tertiary Murray Basin sediments. Another similar intrusion, designated FS3, is located nearby (Fig. 1). While described as breccia kimberlite (Lewis, 1985), the recovery of sample was limited to only very fine drill chips, with most minerals replaced by secondary carbonate and clays.

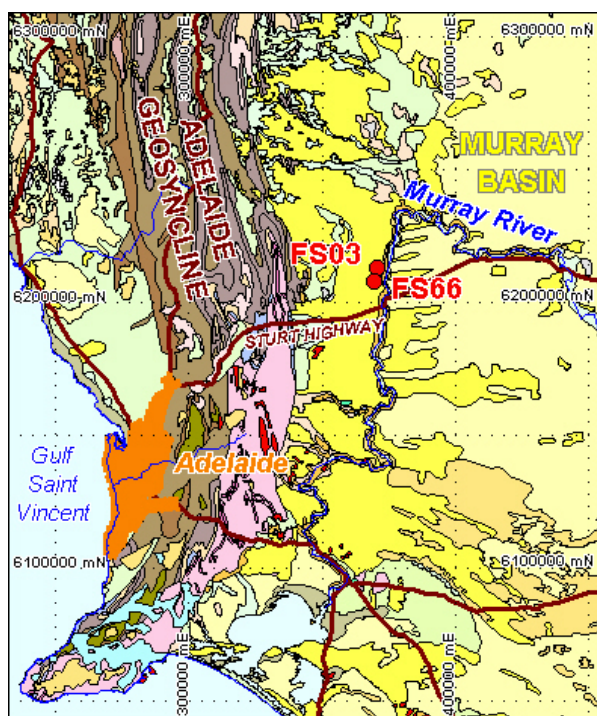


Figure 1. Location map of FS66 and FS03 kimberlitic pipes.

This is the first reported dating of zircon, perovskite and rutile from the same kimberlitic body. All analyses were performed using the laser ablation ICP-MS technique. The validity of using a zircon standard

for the perovskite analysis, and the accuracy of the methodology have been demonstrated by Batumike *et al.*, (2007). Here we show that an analogous methodology can also be applied to rutile. All zircon and perovskite grains produced similar ²⁰⁶Pb/²³⁸U ages within analytical uncertainty (Fig. 2). The weighted mean age of the FS66 zircon age is 179±2 Ma (n=10, Fig. 3). The perovskites contain significant initial Pb, and the scatter in the data suggests that there is some heterogeneity in the isotopic composition of the initial Pb. On the inverse-Concordia plot (Fig. 4) the mean lower intercept age is 181±16 Ma (n=74). We accept the more precise zircon age as the emplacement age of the kimberlite. A single kimberlitic Nb, Cr-rich rutile gave a weighted mean Concordia age of 197±6 Ma (5 analyses) suggesting that it is a mantle-derived xenocryst (Fig. 5). The kimberlite has a strong positive-polarity magnetic anomaly, which is consistent with the normal (positive) paleomagnetic polarity for the period 180-179 Ma (Jones *et al.*, 2001) matching the zircon age.

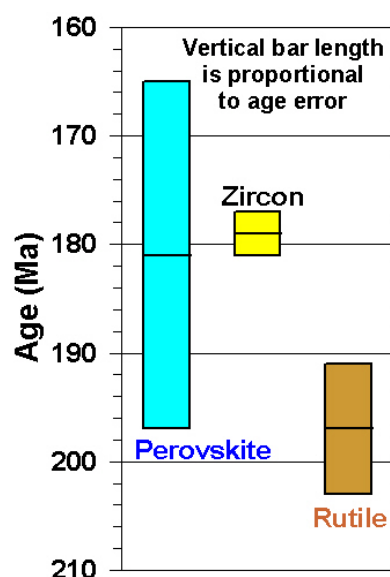


Figure 2. Ages of perovskite, zircon, and rutile from FS66 measured by LAM-ICPMS.

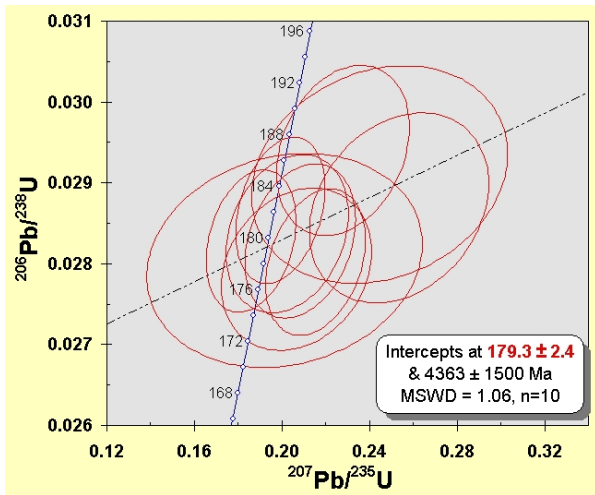


Figure 3. Concordia plot for FS66 zircons.

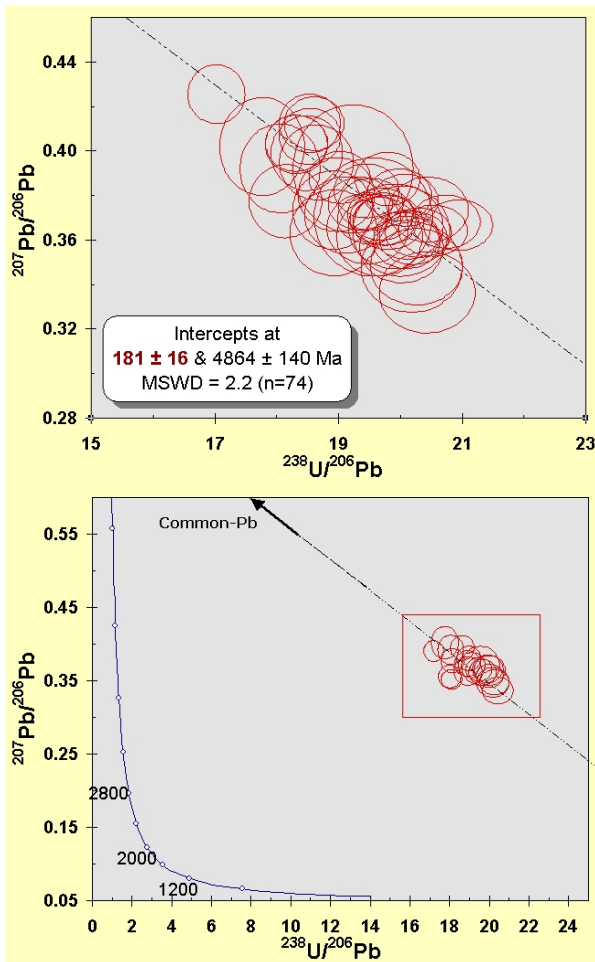


Figure 4. Inverse-Concordia plot for FS66 perovskites, all analyses (n=80). The intercepts of the regression line diagram provide both an estimate of the $^{207}\text{Pb}/^{206}\text{Pb}$ of the initial-Pb component (upper intercept) and the inferred crystallisation age (lower intercept).

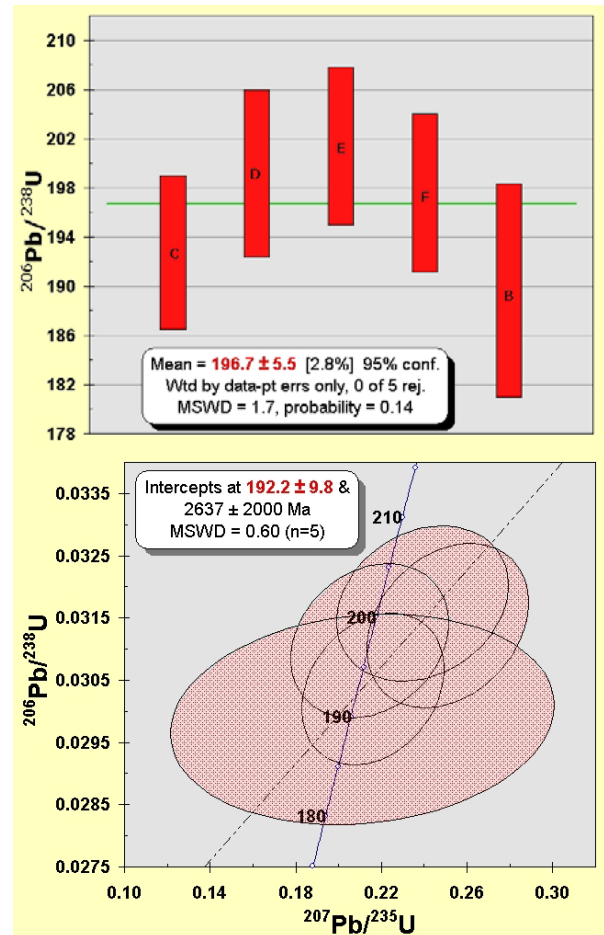


Figure 5. Weighted mean $^{206}\text{Pb}/^{238}\text{U}$ age and Concordia plot for FS66 rutile.

Gaul (1993) determined a minimum temperature of 1100°C at the base of the lithosphere based on garnets from FS66 and FS3, and concluded that the lithospheric mantle volume sampled by the intrusions was not in the diamond stability field; this is consistent with the lack of microdiamonds in the drill samples (Lewis, 1985). Additional trace element work on recovered pyropes and chromites now improves this local lithospheric section. The maximum temperature of the rutile calculated from the Zr thermometer (Zack *et al.*, 2004) is 1150°C. This is slightly higher than the 900-1100°C and 20-30 kb range suggested for the stability of Cr-Nb-rutile formed by the reaction of peridotite with metasomatic fluids (Haggerty, 1983). The dated rutile grain has a fine lamellar intergrowth pattern of ilmenite (Fig. 6) and is distinguished from rutile in MARID xenoliths by high Cr values. The large phenocrysts of perovskite suggest an evolved kimberlitic intrusion. Perovskite REE patterns show strong LREE enrichment (Fig. 7).

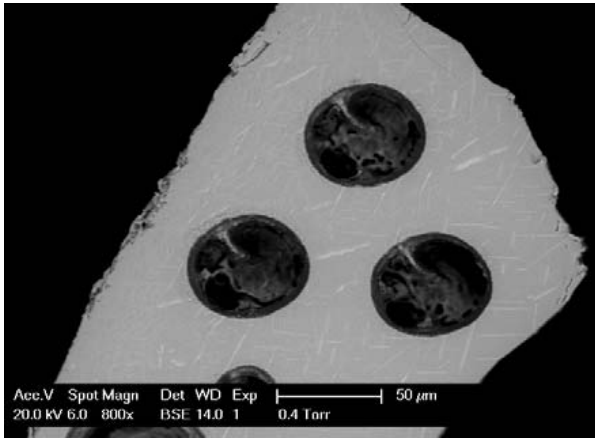


Figure 6. Backscatter image of rutile grain showing fine lamellar intergrowth and laser ablation spots used for dating,

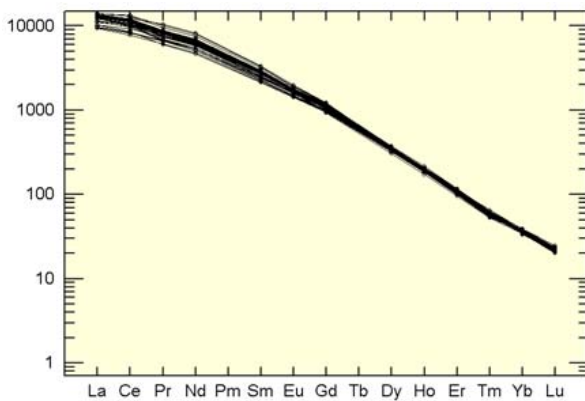


Figure 7. Chondrite-normalised REE plot for FS66 perovskites.

Trace element studies (Yao, 1999; Belousova *et al.*, 2002) of the chromites and zircons indicate that they are kimberlitic in nature, but no whole rock analyses are available to confirm the lithology. Sr and Nd isotopes in the perovskite, and Lu-Hf isotopes in the zircons and rutile constrain the composition and origin of the lithospheric mantle, and the sources of the kimberlitic intrusion. The initial $^{87}\text{Sr}/^{86}\text{Sr}$ ratios are 0.70417 ± 0.00004 (2sd) and $^{143}\text{Nd}/^{144}\text{Nd}$ ratios are 0.51274 ± 0.00007 (2sd) for perovskite. The isotopic data for FS66 perovskite plot in the depleted quadrant on a Nd-Sr isotope diagram, and are close to those of many Jurassic-Cretaceous kimberlites.

References

- Batumike, J.M., Griffin, W.L., Belousova, E.A., Pearson, N.J., O'Reilly, S.Y., & Shee, S.R., 2008. LAM-ICPMS U-Pb dating of kimberlitic perovskite: Eocene-Oligocene kimberlites from the Kundelungu Plateau, D.R. Congo. *Earth & Planetary Science Letters* 267, 609-619.
- Belousova, E.A., Griffin, W.L., O'Reilly, S.Y., & Fisher, N.I., 2002. Igneous zircon: trace element composition as

- an indicator of source rock type. *Contributions to Mineralogy and Petrology* 143, 602-622.
- Gaul, O.F., 1999. Composition of the Lithospheric Mantle beneath Australia. Unpublished PhD thesis, Macquarie University, Sydney.
- Haggerty, S.E., 1983. The mineral chemistry of new titanates from the Jagersfontein Kimberlite, South Africa: Implications for metasomatism in the upper mantle. *Geochimica et Cosmochimica* 47, 1833-1854.
- Jones, D.L., Duncan, R.A., Briden, J.C., Randall, D.E., & MacNiocaill, C., 2001. Age of the Batoka Basalts, northern Zimbabwe, and the duration of Karoo Large Igneous Province magmatism. *Geochemistry Geophysics Geosystems*, 2. Paper No.2000GC000110.
- Lewis, P., 1985. Final Report on the Murray Basin Tenements, South Australia for the period Ending 6 December 1984, Bungunna EL1033, Kakoonie EL1034, Redcliffe EL1037, Waikerie EL1052 & Narrung EL1053. Unpublished report by CRAE. PRISA Open-file Envelope 3957
- Yao, S., 1999. Chemical Composition of Chromites from Ultramafic Rocks: Application to Mineral Exploration and Petrogenesis. Unpublished PhD thesis, Macquarie University, Sydney.
- Zack, T., Moraes, R., & Kronz, A., 2004. Temperature dependence of Zr in Rutile: empirical calibration of a Rutile Thermometer. *Contributions to Mineralogy and Petrology*, 148. 471-488.



Figure 8. Perovskite from FS66 drillhole, scale (top left) is 0.5mm wide.

Isotopic Studies of Minerals and Their Host Kimberlites from Australia and Southern Africa

Steven A. Cooper^{1,2}, Y.A. Kostitsyn³, Elena A. Belousova¹, & W.L. Griffin¹

¹GEMOC ARC National Key Centre, Macquarie University, NSW, 2109, Australia

²Orogenic Exploration Pty Ltd, Burwood, Vic, 3125, Australia

³Laboratory of Isotopic Geochemistry and Geochronology, GEOKHI RAS, Russia

Isotopic signatures are used to distinguish Group I, Transition, and Group II kimberlites, and provide information on the origin of melts parental to the final intrusion. Kimberlitic rocks are often weathered and altered, making them potentially unsuitable for whole rock isotopic studies. We therefore have explored the alternative use of the isotopic signatures of resistant minerals in kimberlites including zircon, rutile and perovskite. These minerals also have the advantage of being amenable to rapid dating by the *in situ* LA-ICPMS technique (Cooper *et al.*, this conference). The study by Mirnejad *et al.* (2003) shows altered lamproite whole rock samples, and the mineral phases clinopyroxene, apatite, perovskite, and potassic richierite are in isotopic equilibrium for lamproite. The relationship between the isotopic systems in these minerals and host kimberlites is reported in this study.

Lu-Hf isotopes have been determined by in-situ laser ablation MC-ICPMS on previously dated zircon and rutile from a range of kimberlites across South Australia (Cooper *et al.*, this conference; Griffin *et al.*, 2000). Sm-Nd isotopes were determined on whole rock samples from the Timber Creek kimberlites in Northern Territory of Australia, El Alamein, Pitcairn JS (176±10Ma) pipe from South Australia, and the Proterozoic diamondiferous Blacktop 01 kimberlite dyke in the Pilbara region of Western Australia. The diamondiferous Mileura 01 kimberlite dyke has not been dated, but is believed to be of similar emplacement age to the Nabberu kimberlites (1900Ma) located 460 km to the ENE on the Yilgarn Craton. Sm-Nd data for the Nabberu kimberlite were reported by Graham *et al.* (1999). Southern African samples are represented by kimberlites from Orapa, Leicester and Monastery (80Ma).

The preliminary results for Australian samples indicate that whole-rock ϵ_{Nd} (range from -6.3 to 1.4) and zircon ϵ_{Hf} data plot close to the Mantle Array, showing an evolved signature compared to the Depleted Mantle. However, zircons in some kimberlites (Orapa, Leicester) show a large range in Hf-isotope composition compared to the whole-rock Sm-Nd data (Figure 1).

Preliminary Sr and Nd isotopic data for perovskite from South Australian kimberlites show initial $^{87}\text{Sr}/^{86}\text{Sr}$ ratios are 0.70417 ± 0.00004 (2sd) and $^{143}\text{Nd}/^{144}\text{Nd}$ ratios are 0.51274 ± 0.00007 (2sd) for FS66 kimberlite perovskite. For Mt Hope 05 kimberlite the initial $^{87}\text{Sr}/^{86}\text{Sr}$ ratios are 0.70480 ± 0.00004 (2sd) and $^{143}\text{Nd}/^{144}\text{Nd}$ ratios are 0.51254 ± 0.00005 (2sd). This data is shown on Nd-Sr isotope diagrams in Figures 2 and 3.

References

- Graham, S., Lambert, D.D., Shee, S.R., Smith, C.B. and Hamilton, R., 1999. Re-Os and Sm-Nd isotopic Constraints on the Sources of Kimberlites and melnoites, Earahedy Basin, Western Australia. In Proc. VII Int. Kimberlite Conference, Gurney, J.J., Gurney, J.L., Pascoe, M.D., & Richardson, S.H., eds. 280-290.
- Griffin, W. L., Pearson, N. J., Belousova, E. A., Jackson, S. R., van Achterbergh, E., O'Reilly, S. Y., & Shee, S. R., 2000. The Hf isotope composition of cratonic mantle: LAM-MC-ICPMS analysis of zircon megacrysts in kimberlites. *Geochim. Cosmochim. Acta*, 64, 133-147.
- Mitchell, R.H., 1995. Kimberlites, Orangeites, and Related Rocks. Plenum Press.
- Mirnejad, H., Bell, K., & Kjarsgaard, B., 2003. Sr and Nd isotopic geochemistry of Pegmatoid Laproites from Walgidee Hills, West Kimberley, Australia. *Geological Society of America Abstracts with Programs*, 35. 325.

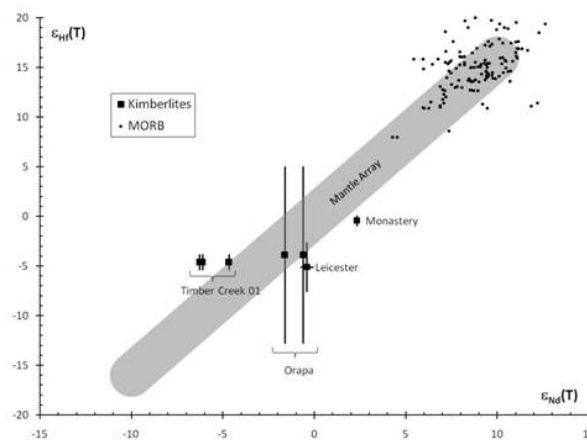


Figure 1. Zircon Hf isotopes and whole rock Nd isotopes for selected kimberlite, compared with MORB.

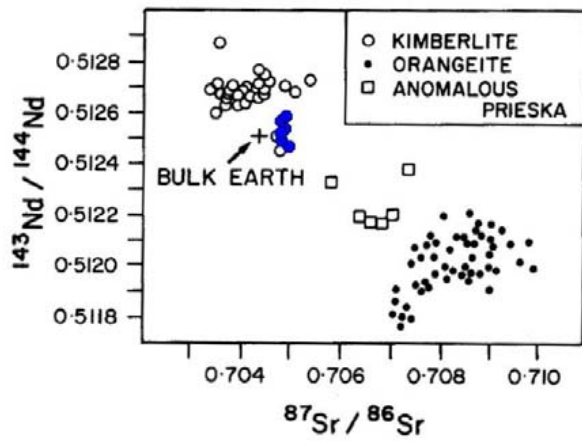


Figure 2. Sr-Nd isotopic ratio figure (from Mitchell, 1995) showing perovskite from Mt Hope 05 kimberlite (blue, n=7).

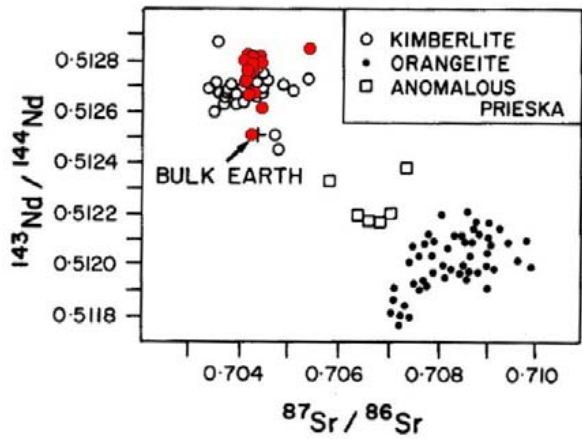


Figure 3. Sr-Nd isotopic ratio figure (from Mitchell, 1995) showing perovskite from FS66 kimberlite (red, n=18).

Geology and Exploration History of Kimberlite and Related Rocks in South Australia

Steven A. Cooper^{1,2} & Brian J. Morris³

¹GEMOC ARC National Key Centre, Macquarie University, NSW, 2109, Australia

²Orogenic Exploration Pty Ltd, Burwood, Vic, 3125, Australia

³South Australia Geological Survey, PIRSA, Adelaide, SA, 5000, Australia

There are currently around 200 kimberlitic occurrences known in South Australia. The kimberlites occur in seven discrete provinces spanning a distance of 400 kilometres across South Australia (Figure 1). By the early 1980s all the known outcropping kimberlitic intrusions had been located while subsequent discoveries have generally been concealed bodies located by aeromagnetic surveys.

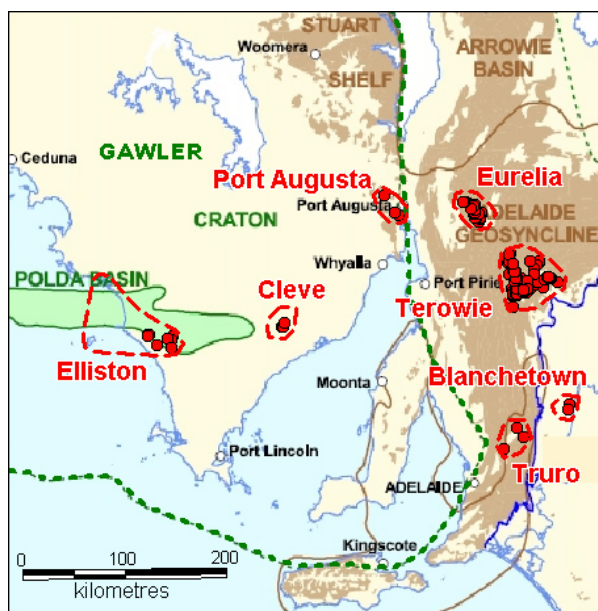


Figure 1. Kimberlitic Provinces in South Australia

ELLISTON PROVINCE

On the western Eyre Peninsula are the nine Mt Hope kimberlites. All were discovered in 1990-1991 by drilling discrete aerial magnetic targets after regional surface loam heavy mineral samples confirmed the presence of indicator grains in the area. Due to complex cover of Upper Jurassic fluvial clayey sandstones and lignite, Tertiary poorly sorted fluvial sands and inter-bedded clays, and extensive Quaternary calcarenites and calcrete, surface indicator patterns are displaced and dispersed away from the kimberlites. The kimberlites are hypabyssal and diatreme facies, porphyritic, possible monticellite?-phlogopite kimberlites. Microprobe studies of chromites from some Mt Hope bodies show strong evidence of mantle metasomatism.

This Province also includes the North Venus Bay (north side Pollda Basin) and Flinders Island kimberlite indicator anomalies. Flinders Island is unique in having large numbers of all types of indicator minerals, including diamonds within the island soil (Cooper, 2002). Source rocks have not yet been located in these two areas.

CLEVE

The eastern Eyre Peninsula contains the three Cleve kimberlite dykes (Wyatt *et al.*, 1991), first drilled in 1986. Stream and loam grid sampling narrowed down the location, with final costean and drilling based on ground magnetics and surface indicator counts. Groundmass perovskite U-Pb was used to obtain an 180 ± 3 Ma date on the Cleve 01 kimberlite (Bristow, unpublished data, in Wyatt *et al.*, 1991).

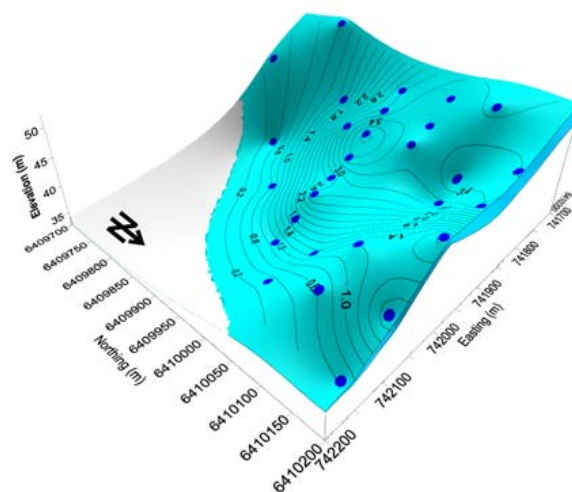


Figure 2. Model of the Sugarloaf Dam kimberlite sill based on drillhole intersections (dark blue circles), with thickness contours overlain. Image is looking southwest.

PORT AUGUSTA

The kimberlites in this area comprise two sills, the El Alamein, and Sugarloaf Dam sills. Recent work has shown the previously separated El Alamein East and West sills are actually the same body and appear to be nearly horizontal. The Sugarloaf Dam sill thickens towards the northwest and is a gentle syncline with fold axis plunging shallowly towards the southeast (Figure 2). Both sills were discovered in 1973 using surface loam sampling at ever-increasing density.



EURELIA PROVINCE

The province comprises a number of kimberlite dykes, with the first 12 discovered described by Scott Smith *et al.* (1984). They are centred around the town of Eurelia, north of Orroroo, in the Adelaide Geosyncline. The diamondiferous Eurelia K07 kimberlite dyke and blow has been the most extensively studied of this province. The petrological descriptions by Scott Smith *et al.* (1984) came from the vertical drillhole DHR3 completed by Stockdale Prospecting during 1981.

The first kimberlitic rock dated in South Australia was from drillhole CD010, northwest from Eurelia (sample 75210434 in Stracke *et al.*, 1979). Further dykes, some diamondiferous, are still being found currently in this area based on detailed high-resolution magnetic surveys. The Eurelia Province also includes dykes of carbonatitic affinity exposed in creek banks in the Walloway Diapir area discovered by Tucker & Collerson (1972).

TEROWIE PROVINCE

Most of the kimberlites were located by De Beers during the period 1969-1972. This Province contains some of the first true kimberlite rocks found in the State, and probably in Australia. Exploration primarily involved the collection of alluvial heavy mineral samples. The Calcutteroo, Mittopitta, Pine Creek and other kimberlites were discovered by heavy mineral sampling, mapping along gullies, then shallow drilling. A large number of recent discoveries has been made by using high-resolution magnetic surveys. Some of these have been confirmed as weakly diamondiferous in the northern part of the province. It is possible the province merges with the Eurelia Province to the north, but currently there is still a 40km gap between the two.

TRURO

Several small pipes are known from this area. They have been discovered by a combination of stream heavy mineral sampling and detailed magnetics.

BLANCHETOWN

By drilling blind magnetic targets in 1982, Rio Tinto discovered two kimberlitic intrusions below about 214 metres of Tertiary Murray Basin sediments.

As part of a project to systematically map and describe all the kimberlites and related rocks in South Australia, heavy mineral samples have been collected from a number of kimberlites in every kimberlitic field within each province. Not all are true kimberlites (see Cooper *et al.*, 2007), and emplacement ages are not continuous across the State. Table 1 provides the first accurate location details for about half the State's kimberlites, some previously published, and many that have never been published.

The rate of discoveries of outcropping kimberlite has effectively dropped to zero in South Australia. Recent discoveries have all been under sediment cover. This trend will continue with the new frontier being the pervasively sediment-covered Gawler Craton. The discovery of diamonds and kimberlite indicator minerals, showing good mantle conditions on Flinders Island, suggests other parts of the Gawler Craton are prospective for diamonds, and not all areas have suffered the same metasomatism as the Mt Hope kimberlites (see Figure 3).

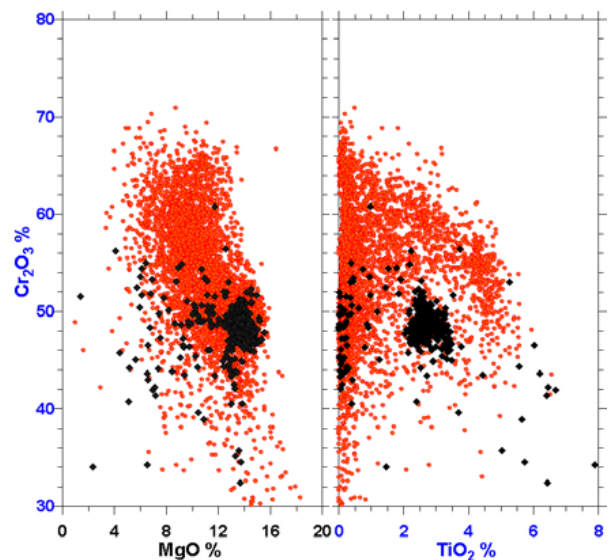


Figure 3. Microprobe analyses of chromite cores from Flinders Island (red, n=4559) and Mt Hope kimberlites (black, n=418) showing stark differences in population chemistry.

References

- Cooper, S.A., 2002. New diamond field discovered in SA. *MESA Journal* 24, 6-9.
- Cooper, S.A., Barron, B.J., & Morris, B.J., 2007. *Petrology of selected Kimberlite and Related Rocks in South Australia – Volume 1*. South Australian Department of Primary Industries & Resources, Report Book 2007/3.
- Scott Smith, B.H., Danchin, R.V., Harris, J.W., & Stracke, K.J. 1984. Kimberlites near Orroroo, South Australia. In: J. Kornprobst (ed.), *Kimberlites and related rocks*. Proceedings of the 3IKC, Vol. 1, Elsevier's Development in Petrology series, no. 11A, p. 121-142.
- Stracke, K.J., Ferguson, J., & Black, L.P., 1979. Structural Setting of Kimberlites in South-Eastern Australia. In Boyd, F.R. & Meyer H.O.A., eds., *Kimberlites, Diatremes and Diamonds*, A.U.G., Washington, 71-91.
- Tucker, D.H., & Collerson, K.D., 1972. Lamprophyric intrusions of probable carbonatitic affinity from South Australia. *Journal of the Geological Society of Australia* 19, 387-391
- Wyatt, B.A., Shee, S.R., Griffin, W.L., Zweistra, P., & Robison, H.R., 1994. The petrology of the Cleve kimberlite, Eyre peninsula, South Australia. In: Meyer, H.O. & Leonardos, O.H. (eds) *Kimberlites, Related Rocks and Mantle Xenoliths*. CPRM Special Publication 1A, 62-79.

Table 1. Kimberlite locations in South Australia. Coordinates are in WSG84 Datum.

Name	Longitude	Latitude	Province	Name	Longitude	Latitude	Province
147a	139.3333761	-33.10289955	Terowie	Mt Hope 03	135.3563276	-33.68241512	Elliston
41c	138.577001	-32.55247979	Eurelia	Mt Hope 04	135.345096	-33.709222	Elliston
6633RS99	138.502979	-32.482167	Eurelia	Mt Hope 05	135.300734	-33.697874	Elliston
An42	139.274532	-33.1883438	Terowie	Mt Hope 06	135.10887	-33.665019	Elliston
An65	139.2684098	-33.1636398	Terowie	Mt Hope 07	135.091452	-33.666395	Elliston
Angaston 01	139.1241498	-34.51279385	Truro	Mt Hope 08	135.097106	-33.677629	Elliston
Calcuteroo 01	139.1998847	-33.11982289	Terowie	Mungibbie 01	138.964993	-33.27643507	Terowie
Calcuteroo 02 East	139.1939805	-33.1312899	Terowie	Mungibbie 02	138.96248	-33.26937	Terowie
Calcuteroo 02 West	139.195045	-33.131248	Terowie	Mungibbie 03	138.960037	-33.263402	Terowie
Calcuteroo 02a	139.19509	-33.1306	Terowie	Mungibbie 04	138.961525	-33.253453	Terowie
Calcuteroo 02b	139.1946464	-33.13099624	Terowie	Mungibbie 05	138.961525	-33.253453	Terowie
Calcuteroo 03	139.1934772	-33.1338799	Terowie	Mungibbie North 01	138.9618	-33.2357	Terowie
Calcuteroo 04a	139.19722	-33.11273	Terowie	Mungibbie North 02	138.9618	-33.236	Terowie
Calcuteroo 05	139.2024833	-33.1311424	Terowie	Pandappa 01	139.186996	-33.167683	Terowie
Calcuteroo 06	139.200228	-33.130823	Terowie	Pandappa 02	139.188491	-33.15282	Terowie
CD10	138.4932691	-32.51319461	Eurelia	Pandappa 02a	139.186123	-33.161736	Terowie
Cleve 01	136.5228415	-33.59453644	Cleve	Pandappa 02b	139.186123	-33.161736	Terowie
Cleve 02	136.526441	-33.58682	Cleve	Pandappa 03	139.188491	-33.15282	Terowie
Cleve 03	136.53833	-33.558263	Cleve	Pandappa 04	139.201826	-33.143754	Terowie
El Alamein East	137.733724	-32.5838873	Pt Augusta	Pine Creek 01	139.272983	-33.187521	Terowie
El Alamein West	137.685583	-32.5666713	Pt Augusta	Pitcairn E1430	139.215642	-32.967166	Terowie
Eurelia K01	138.543858	-32.529034	Eurelia	Pitcairn E1522	139.223599	-32.961528	Terowie
Eurelia K02	138.530165	-32.52092	Eurelia	Pitcairn E1524	139.221259	-32.963617	Terowie
Eurelia K03	138.577127	-32.558836	Eurelia	Pitcairn E1525	139.220408	-32.966004	Terowie
Eurelia K04	138.5367888	-32.50532477	Eurelia	Pitcairn E1526	139.226606	-32.962586	Terowie
Eurelia K05	138.609503	-32.551722	Eurelia	Pitcairn JS	139.2226891	-32.96266857	Terowie
Eurelia K06	138.600452	-32.54298	Eurelia	Stockwell 01	139.05055	-34.434337	Truro
Eurelia K07	138.51812	-32.4907568	Eurelia	Sugarloaf Dam	137.57183	-32.421003	Pt Augusta
Eurelia K08	138.500561	-32.495936	Eurelia	Walloway X	138.578986	-32.628828	Eurelia
Eurelia K09a	138.457337	-32.47007	Eurelia	Waupunyah 01	139.0064	-33.2079	Terowie
Eurelia K09b	138.43612	-32.456405	Eurelia	Waupunyah 02	139.0058	-33.2081	Terowie
Eurelia K10	138.510325	-32.490697	Eurelia	Waupunyah 03	138.9962	-33.21	Terowie
Eurelia K11	138.525414	-32.479652	Eurelia	Waupunyah 04	138.9931	-33.2088	Terowie
Eurelia K12	138.509485	-32.483817	Eurelia	Waupunyah 05	138.9919	-33.21	Terowie
Eurelia K13	138.502664	-32.477538	Eurelia	Waupunyah 06	138.9888	-33.2106	Terowie
Franklyn Pipe	139.03618	-33.148729	Terowie	Wonna (ZK24)	139.0027011	-33.26636078	Terowie
FS03	139.5985849	-34.21327646	Blanchetown	Wonna 01	138.995974	-33.255754	Terowie
FS66	139.5820328	-34.26172697	Blanchetown	Wonna 02	138.995679	-33.249056	Terowie
Hiles Lagoon 01	138.9608	-33.2017	Terowie	Wonna 03	138.99631	-33.248145	Terowie
Hiles Lagoon 02	138.946	-33.2064	Terowie	Wonna 04	138.995637	-33.248236	Terowie
Ian Ross	138.9136	-34.62582	Truro	Wonna 05	138.993999	-33.24465	Terowie
Mittopitta 01	139.008736	-33.248479	Terowie	Wonna 06	138.992774	-33.243613	Terowie
Mittopitta 02	139.006858	-33.254982	Terowie	Wonna 07	138.992354	-33.245103	Terowie
Mittopitta 06	139.0061373	-33.25686612	Terowie	Wonna 08	138.983385	-33.247619	Terowie
Mittopitta Diatrema	139.006752	-33.252567	Terowie	Wonna 09	138.9948	-33.248414	Terowie
Monks Hill	139.336981	-33.103795	Terowie	Wonna 10	138.9938	-33.2464	Terowie
Mt Hope 01	135.1938877	-33.7554577	Elliston	Wonna 13	138.9958	-33.2478	Terowie
Mt Hope 01 Satellite	135.1955375	-33.75223116	Elliston	Wonna 14	138.9968	-33.2472	Terowie
Mt Hope 02	135.343791	-33.785207	Elliston	Wonna 17	138.9905	-33.2436	Terowie

The Kimberlites and Related Rocks of the Kuruman Kimberlite Province, Kaapvaal Craton, South Africa

Cara L. Donnelly¹, Suzanne Y. O'Reilly¹ and William L. Griffin¹

¹GEMOC ARC National Key Centre, Department of Earth and Planetary Sciences, Macquarie University, Sydney, NSW 2109, Australia.

Introduction

The Kuruman kimberlite province comprises of 16 intrusive bodies (Figure 1) and contains some of the oldest known kimberlites (>1.6 Ga). These kimberlites were intruded across the western margin of the Archean Kaapvaal Craton following a major collisional orogeny (ca 1.75 Ga). While most kimberlites intrude through subcontinental lithospheric mantle (SCLM) that has undergone multiple episodes of metasomatism, the Kuruman province may provide a unique opportunity to examine a relatively undisturbed section of the SCLM across an ancient craton margin.

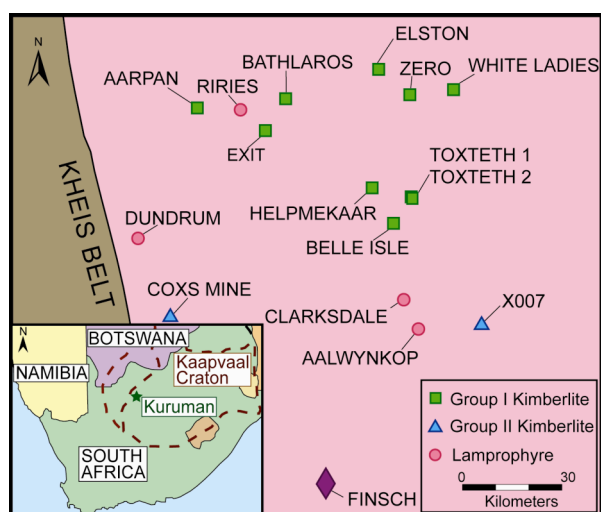


Figure 1. Map showing the location and petrographic classification of the Kuruman kimberlite province.

The Kuruman kimberlites can be subdivided petrographically into five groups: (a) Group I kimberlites (b) evolved, carbonatitic Group I kimberlites, (c) Group II kimberlites, or 'orangeites' (Mitchell, 1995), (d) transitional lamprophyric kimberlites, (e) lamprophyres. Shee et al. (1989) noted that there was a change in the petrographic character of the Kuruman kimberlites from east to west, progressing from typical Group I kimberlites, through evolved Group I kimberlites, to lamprophyres. This study has also found a progression towards more lamprophyric and Group II bodies to the south.

Groundmass Perovskite

Groundmass perovskites occur in samples of the Bathlaros, Elston, Helpmekaar, White Ladies, X007 and Zero kimberlites. The size and the morphology of

the perovskite crystals varies significantly between pipes. In X007 perovskite is rare and occurs as small rounded crystals that are typically 10 to 30 μm in size. In the Bathlaros pipe, perovskite is abundant (up to 10 vol%) and occurs as large brown, semi-opaque cauliflower-shaped grains typically 200 to 400 μm in size. Perovskites from Elston, Helpmekaar and Zero are typically well-preserved euhedral grains on the order of 40 to 70 μm for Helpmekaar and Elston and 20 to 40 μm for the Zero pipe. The White Ladies kimberlite contains rounded, patchy grains that are typically on the order of 30 to 50 μm across. The perovskite grains generally occur as discrete crystals set in a serpentine-calcite matrix and commonly show a necklace microstructure around olivine macrocrysts. Alteration of perovskite is variable and pipe-dependent with grains being resorbed or replaced by later minerals, including rutile, ilmenite, titanite and calcite.

A large proportion of the perovskites display zonation. The most common zonation pattern involves a decrease in rare earth elements (REE) and Th from core to rim (Figure 2a and 2c). Less frequently observed zonation patterns include a reversed trend (Figure 2b) in which the rim is enriched in REE and Th, while a fine-scale, oscillatory zoning occurs rarely (Figure 2d).

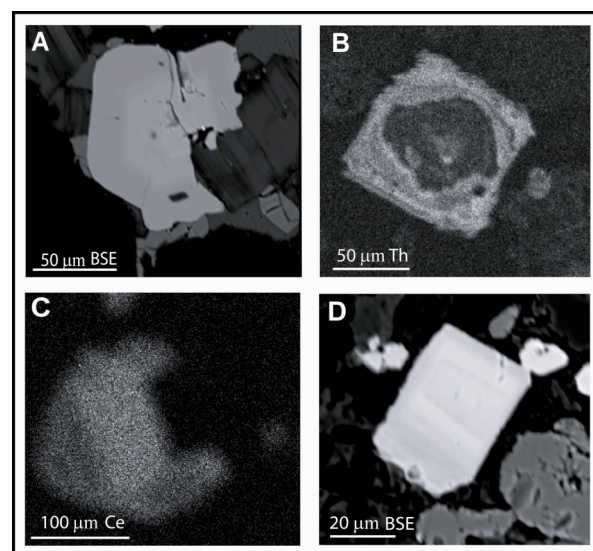


Figure 2. Zonation patterns of REE and Th in Kuruman perovskites.

The perovskites have CaTiO_3 contents that range between 75 mol% (Zero) and 96 mol % (Bathlaros) with an average value of 86 mol% (Figure 3a). The Kuruman perovskites show a large range in REE contents from ≤ 0.11 to 9.68 wt% with an average 5.32 wt% REE_2O_3 and SrO contents of ≤ 0.35 to 1.04 wt%, average 0.48 wt%. The REE contents of perovskites from different pipes are distinct (Figure 3b), with variations of up to 6 mol% between pipes. White Ladies has the lowest REE contents (average of 2.61 wt% REE_2O_3 and 0.41 wt% SrO) and Zero has the highest (average of 8.24 wt % REE_2O_3 and 0.47 wt% SrO). Other elements present in significant amounts include NaO (≤ 0.03 to 1.60 wt%, average 0.57 wt%), FeO_T (≤ 0.07 to 5.34 wt%, average 2.16 wt%) and Nb_2O_5 (0.33 to 5.86 wt%, average 1.54 wt%).

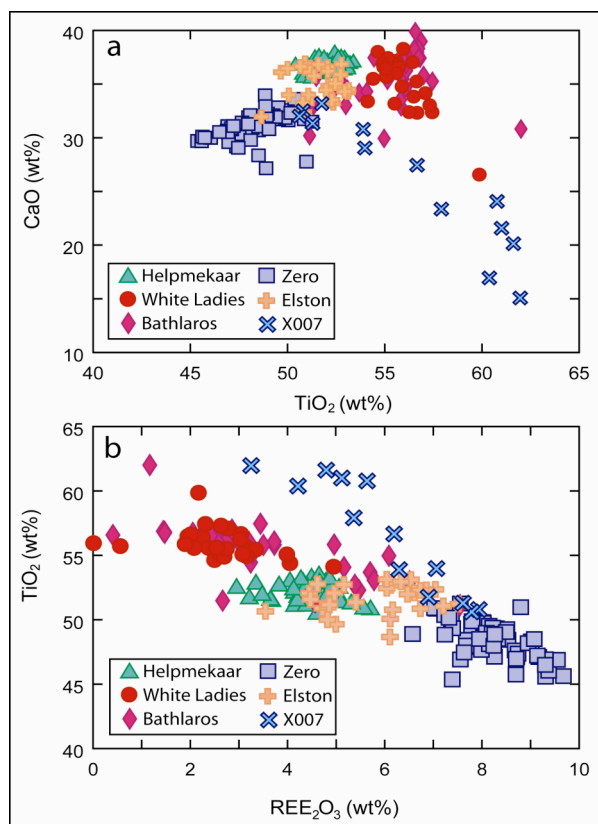


Figure 3. Variations in major- and minor- element contents of Kuruman groundmass perovskites. Where REE_2O_3 includes La_2O_3 , Ce_2O_3 , and Nd_2O_3 .

Chondrite-normalized REE distribution patterns for the Kuruman perovskites are shown in Figure 4. The perovskites are characterized by extreme enrichment in the LREE, with La and Ce values ranging from 4620 to 39300 and 6070 to 97900 ppm, respectively. Within individual kimberlites there is little variation and the REE_N patterns are similar between different kimberlite pipes.

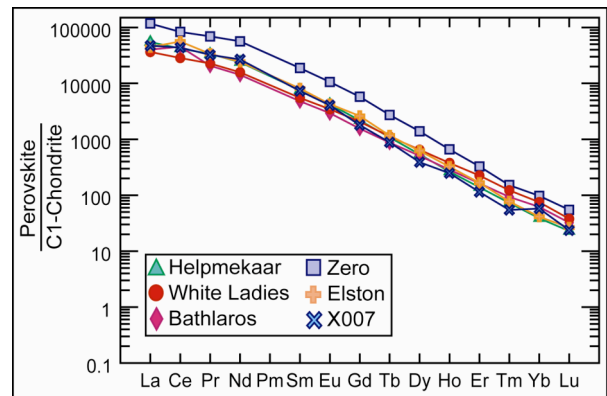


Figure 4. Averaged REE_N concentrations (ppm) of the Kuruman perovskites, normalized after McDonough and Sun (1995).

U-Pb Dating

At present, the age of the Kuruman kimberlite province is poorly constrained. The age for this province is defined by a single mica Rb-Sr isochron age of 1694 ± 42 Ma from the Bathlaros pipe and three errorchron ages of approximately 1606 Ma, 1635 Ma, and 1674 Ma from the Zero, Elston and Riries intrusives, respectively (Shee et al., 1989).

In situ LAM-ICPMS U-Pb dating of perovskite (see Batumike et al., 2008) was conducted to determine the sequence of eruption. The resulting U-Pb data (Figure 5, Table 1) yield eruption ages ranging from 124 ± 16 Ma (X007) to 1607 ± 96 Ma (White Ladies).

Pipe	Age (Ma)	Upper Intercept (Ma)	MSWD
Helpmekaar	1303 ± 190	3052 ± 320	5.9
Zero	1147 ± 240	3213 ± 280	17
Bathlaros	506 ± 71	2692 ± 100	50
White Ladies	1607 ± 96	4531 ± 140	35
Elston	1265 ± 220	3295 ± 320	11
X007	126 ± 16	5059 ± 12	0.35

Table 1. Summary of the obtained U-Pb ages from the Kuruman perovskites.

The U-Pb inverse-Concordia plots reveal a large spread in the data, reflecting large isotopic heterogeneity within individual pipes. Large age errors and MSWDs are obtained for all pipes, excepting X007, and the upper intercept “ages” (reflecting the $^{207}\text{Pb}/^{206}\text{Pb}$ of the initial Pb component) are unrealistically low (Table 1). The measured ages therefore are unrealistic, with the exception of White Ladies and X007. The Kuruman perovskites are atypical in that they have high Th contents and this high radiogenic ^{208}Pb . Except for X007, perovskites from all of the Kuruman kimberlites show large variations in initial lead compositions and multiple spot analyses on single grains also record this heterogeneity (Figure 5c). These abnormal U-Pb systematics of the Kuruman perovskites may have resulted from heterogeneous initial lead compositions, reflecting some form of multi-component mixing before and during the crystallization of the perovskite.

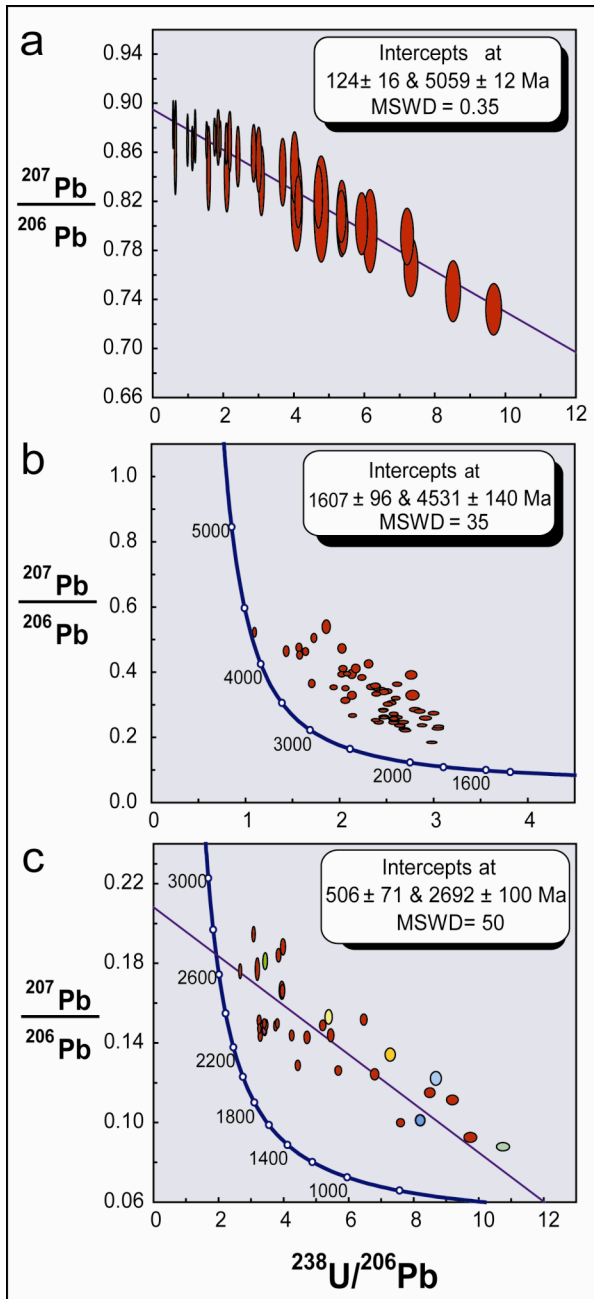


Figure 5. U-Pb inverse-Concordia plots for X007 (Figure 5a), White Ladies (Figure 5b) and Bathlaros (Figure 5c). Coloured data points on Figure 5c correspond to rim (dark) and core (light) analyses on single grains.

Sr and Nd Isotopes

Preliminary *in-situ* LAM-MC-ICPMS analysis of Sr and Nd isotopes in perovskite has shown considerable variation. The $^{87}\text{Sr}/^{86}\text{Sr}$ contents varied between 0.70396 and 0.71011, with the majority of samples having values in the lower end of this range (Figure 6). The Nd contents are more tightly constrained with values of $^{143}\text{Nd}/^{144}\text{Nd}$ between 0.51093 and 0.51164 (excluding the anomalous Zero sample #344; Figure 6). These values are similar, though still slightly enriched, to that of the bulk Earth at the time of kimberlite emplacement.

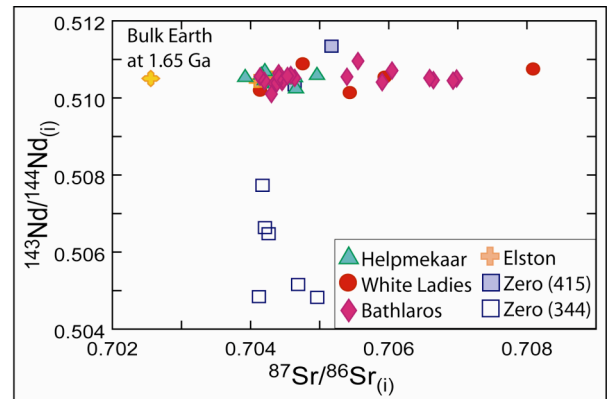


Figure 6. Initial $^{143}\text{Nd}/^{144}\text{Nd}$ and $^{87}\text{Sr}/^{86}\text{Sr}$ contents of perovskite compared with the composition of the bulk earth

Preliminary Conclusions

The kimberlites of the Kuruman province are unusual kimberlites. They show a change in petrographic character from east to west, and toward the south. The perovskites are also atypical, having high REE contents and high Th contents. The U-Pb systematics of the perovskites are complicated by high radiogenic Th contents and large isotopic heterogeneities within individual kimberlites, and within single grains. Preliminary Sr and Nd analyses in perovskite yield Nd values that are equivalent to the bulk Earth at 1.65 Ga and Sr values that are more radiogenic than bulk Earth.

References

- Batumike, J.M., Griffin, W.L., Belousova, E.A., Pearson, N.J., O'Reilly, S.Y., Shee, S.R., 2008. LAM-ICPMS U-Pb dating of kimberlite perovskites: Eocene-Oligocene kimberlites from the Kundelungu Plateau, D.R. Congo. *Earth and Planetary Science Letters* 267, 609-619.
- McDonough, W.F., Sun, S.S., 1995. The composition of the Earth. *Chemical Geology* 120 (304), 223-253.
- Mitchell, R.H., 1995. *Kimberlites, Orangeites and Related Rocks*. Plenum Press.
- Shee, S.R., Bristow, J.W., Bell, D.R., Smith, C.B., Allsopp, H.L., Shee, P.B., 1989. The petrology of kimberlites, related rocks and associated mantle xenoliths from the Kuruman Province, South Africa. In: Ross, J., Jaques, A.L., Ferguson, J., Green, D.H., O'Reilly, S.Y., Danchin, R.V., Janse, A.J.A. (eds), *Proceedings of the Fourth International Kimberlite Conference, Kimberlites and Related Rocks*. Blackwell Carlton, 60-82.

An evidence for the composition of the Ordovician upper mantle beneath West Sangilen (Southeast Tuva, Russia)

Anastasiya Gibsher¹, Vladimir Malkovets¹, Yury Litasov¹,
William Griffin², Suzanne O'Reilly²

¹ Institute of Geology and Mineralogy SB RAS, Novosibirsk, Russia (n.gibsher@gmail.com),

² GEMOC National Key Centre, Macquarie University, Sydney, Australia

Introduction

Ultramafic xenoliths in alkaline basaltic rocks are major source of information on the structure and composition of the lithospheric mantle beneath the continents. Although many studies have been carried out on xenoliths from Tertiary and Quaternary magmatic host, far fewer studies have been undertaken on xenolith suites from older magmatic events of orogenic belts. In this paper, we present a study of ultramafic xenoliths from Ordovician lamprophyre dikes of the West Sangilen Highland (Southeast Tuva, Russia).

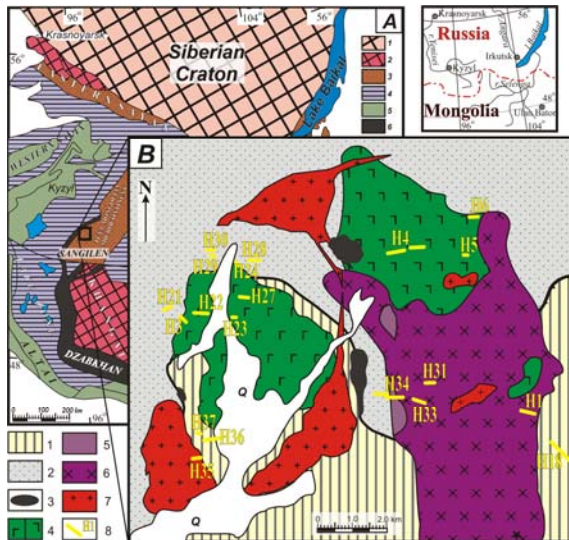


Fig. 1. **A** – Simplified tectonic scheme of the central part of the Central Asian Orogenic Belt (modified after Vladimirov et al., 1999). 1 – Siberian craton; 2 – Precambrian microcontinental megablock; 3 – Riphean microcontinental blocks; 4 – Neoproterozoic mobile belts; 5 – Paleozoic mobile belts; 6 – ophiolites. **B** – (modified after Egorova et al., 2006) Location map of the lamprophyre dikes. 1 – Precambrian metamorphic rocks, 2 – Cambrian volcanogenic – sedimentary rocks; 3 – serpentinites; 4 – gabbroids; 5 – porphyritic monzodiorites; 6 – nonporphyritic monzodiorites; 7 – Ordovician granites; 8 – lamprophyre dikes.

Geological setting

The West Sangilen is a fragment of highly metamorphized structure of Cambrian-Ordovician orogen, which has been formed as a result of Tannuola island arc, Agardag back-arc basin and Sangilen microcontinent piling-up (Gibsher et al., 2000). Recently, a number of mantle-derived xenoliths have been found in the lamprophyre dikes. The dikes correspond to the last stage of magmatic activity within the region, which belongs to the Late Ordovician orogeny. Ar-Ar dating of amphibole and biotite megacrysts from the lamprophyres provides an age of 441.3 ± 1.1 Ma (Izokh et al., 2001).

Sample description

Lamprophyres contain numerous xeno-, mega-, and phenocrysts, as well as abundant xenoliths of lherzolites, harzburgites, clinopyroxenites, and gabbro. The megacryst assemblage includes kaersutite, Al-Ti-augite, anorthoclase, biotite, apatite, and Ti-magnetite.

Peridotite nodules reach up to 50 cm in diameter and are significantly dominant among the mantle-derived xenoliths. They are very fresh, well-preserved rocks. According to the Frey-Prinz classification (1978), the group I xenoliths are presented by spinel lherzolites, of which the some contain the grains of phlogopite and amphibole, and spinel harzburgites; the group II xenoliths are spinel clinopyroxenites with amphibole and plagioclase-spinel-garnet clinopyroxenites. The textures of group I are protogranular (Mercie & Nicolas, 1975). The textures of group II are cumulative.

Whole rock chemical composition

The bulk rock analyses of most peridotites reveal negative correlation between MgO content and TiO_2 , Al_2O_3 , and CaO. It is consistent with traditional concept of partial melting degree of



primitive mantle lherzolite. Correspondingly, the harzburgites contain less amount of TiO_2 , Al_2O_3 , CaO , and higher MgO content.

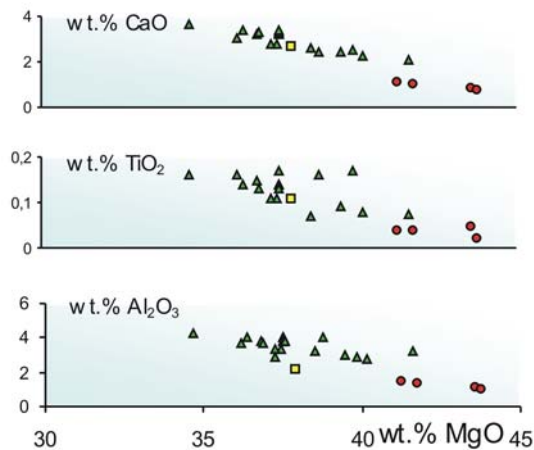


Fig. 2. A plot of MgO versus some major oxides content in bulk rock peridotites. *Symbols*: triangles – lherzolites; square – phlogopite-amphibole-bearing lherzolite; circles – harzburgites.

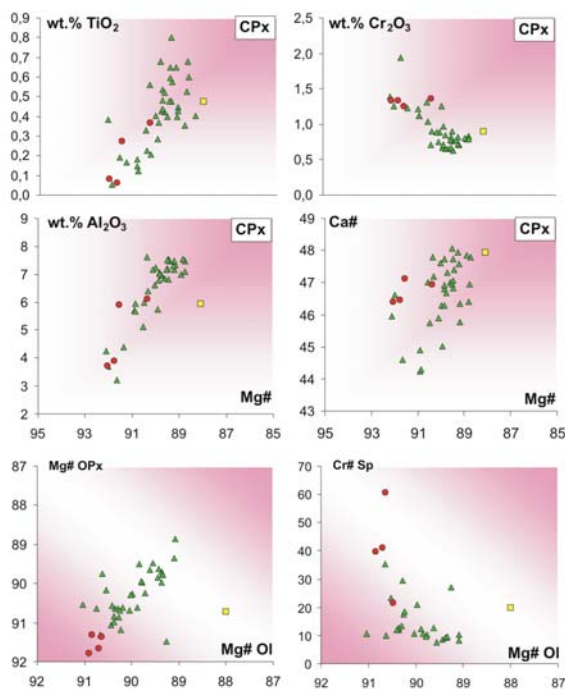


Fig. 3. Compositional variation of major elements in peridotitic minerals. $\text{Mg\#} = 100 \text{ Mg}/(\text{Mg}+\text{Fe})$, $\text{Ca\#} = 100 \text{ Ca}/(\text{Ca}+\text{Mg})$, $\text{Cr\#} = 100 \text{ Cr}/(\text{Cr}+\text{Al})$; CPx – clinopyroxene, OPx – orthopyroxene, Sp – spinel, Ol – olivine. *Symbols*: triangles – lherzolites; square – phlogopite-amphibole-bearing lherzolite; circles – harzburgites.

Mineral chemistry

Composition of minerals gradually changes from fertile lherzolites to harzburgites. Peridotitic olivine composition fits the mantle array. It has Mg\# values

89-91 %. NiO contents plot within 0.3-0.4 wt %. Orthopyroxene from peridotites has $\text{Mg\#} = 87-91 \%$, $\text{Al}_2\text{O}_3 = 2.3-5.5 \text{ wt } \%$, $\text{Cr}_2\text{O}_3 = 0.28-0.86 \text{ wt } \%$. Clinopyroxene from peridotites has $\text{Mg\#} = 86.8-92.3 \%$, $\text{TiO}_2 = 0.01-0.95 \text{ wt } \%$, $\text{Al}_2\text{O}_3 = 3.5-7.5 \text{ wt } \%$, $\text{Cr}_2\text{O}_3 = 0.63-1.94 \text{ wt } \%$. Clinopyroxene from clinopyroxenites has $\text{Mg\#} = 79-89 \%$. Clinopyroxene composition differs for spinel clinopyroxenites and plagioclase-spinel-garnet clinopyroxenites (correspondingly, 8.4-9.4 and 8.0-11.2 wt. % of Al_2O_3 , 0.87-1.75 and 0.02-0.26 wt. % of TiO_2 , and 0-0.03 and 0.05-0.25 wt. % of Cr_2O_3). Spinel from peridotites has $\text{Mg\#} = 60.6-80.3 \%$ and bears $\text{Cr}_2\text{O}_3 = 7.2-47.2 \text{ wt. } \%$, $\text{Al}_2\text{O}_3 = 20.4-59.9 \text{ wt } \%$. Spinel from clinopyroxenites has $\text{Mg\#} = 70.2-80.1 \%$, $\text{Cr}_2\text{O}_3 = 0-2.2 \text{ wt. } \%$, $\text{Al}_2\text{O}_3 = 64.4-69.7 \text{ wt } \%$. Garnet from plagioclase-spinel-garnet clinopyroxenites (Py_{65-73} , Alm_{15-23} , Gross_{12-15}) has $\text{Mg\#} = 73.9-82.7 \%$, $\text{Cr}_2\text{O}_3 = 0.08-0.19 \text{ wt. } \%$, $\text{TiO}_2 = 0.01-0.1 \text{ wt } \%$. Phlogopites of lherzolite have $\text{Mg\#} = 73.8-88.7 \%$, $\text{Na}_2\text{O} = 0.4-0.9 \text{ wt } \%$, $\text{K}_2\text{O} = 8.7-9.5 \text{ wt } \%$, $\text{Al}_2\text{O}_3 = 15.4-17.0 \text{ wt } \%$, $\text{TiO}_2 = 3.7-5.9 \text{ wt } \%$. Amphibole belongs to pargasite with $\text{Mg\#} = 87.3-87.6 \%$, $\text{TiO}_2 = 2.6-4.6 \text{ wt } \%$, $\text{Al}_2\text{O}_3 = 15.3-14.6 \text{ wt } \%$, $\text{Na}_2\text{O} = 2.8-3.1 \text{ wt } \%$. Plagioclase from plagioclase-spinel-garnet clinopyroxenites corresponds to labradorite (An_{52-66}).

Geothermometry

According to mineral geothermometry, calculated temperatures for spinel lherzolites range from 970 to 1100 °C (Ca-OPx, Brey, Kohler, 1990) and from 1040 to 1160 °C (2-Px, Brey, Kohler, 1990), for spinel clinopyroxenites – from 1024 to 1032 °C (Mercier, 1980), for plagioclase-spinel-garnet clinopyroxenites – from 1110 to 1243 °C (Ellis, Green, 1979).

Trace elements characteristics of clinopyroxene

Trace element composition for clinopyroxenes in West Sangilen Highland xenoliths is comparable with those for typical primitive mantle peridotites, which have primitive trace element patterns or minor depletion in LREE, Th, U, and Nb. All clinopyroxenes of fertile spinel peridotites have small negative Zr-Hf-Ti anomalies in chondrite-normalized plots. The La/Yb ratios in the clinopyroxenes vary from 0.06 to 0.98.

Clinopyroxenes from several peridotites are slightly enriched in LREE, Sr and depleted in HREE and HFSE. They have La/Yb ratios in the clinopyroxenes from 0.72 to 40.02.

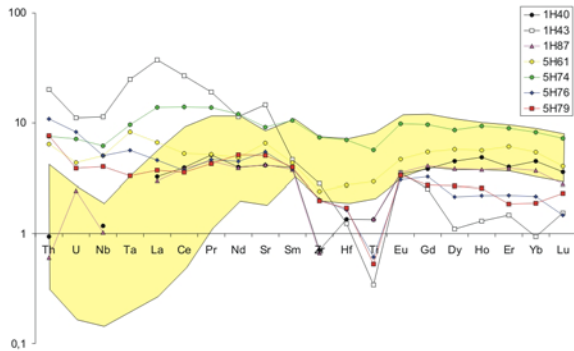


Fig. 4. Chondrite-normalised trace element patterns for clinopyroxene from fertile spinel peridotites. Individual trace elements patterns are shown for spinel peridotites with features of cryptic metasomatism.

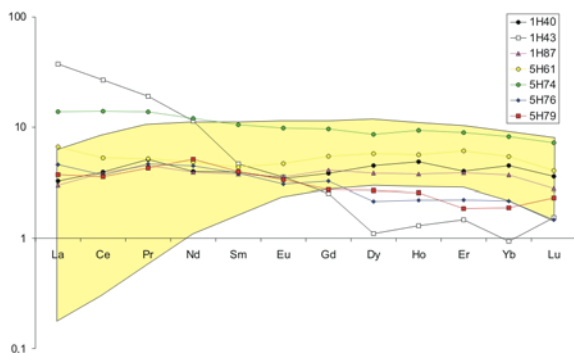


Fig. 5. Chondrite-normalised REE patterns for clinopyroxene from fertile spinel peridotites. Individual trace elements patterns are shown for spinel peridotites with features of cryptic metasomatism.

Results

The Ordovician lamprophyre dikes of the West Sangilen Highland are of special interest, because they sampled and carried up some pieces of most the ancient mantle under orogenic belts.

The chemical and mineralogical data obtained for the lherzolite nodules from Western Sangilen lamprophyre dikes allow us to suggest following:

- (1) The upper mantle domain beneath the Western Sangilen at a depth of the spinel facies consisted of mainly 'dry' lherzolite varieties in the Late Ordovician.
- (2) At that time, the local upper mantle column was heterogeneous ranging from fertile to depleted compositions.
- (3) Locally, mantle metasomatism occurred under volatile influence (preferably CO₂).
- (4) High geothermal gradient beneath the Western Sangilen during the capture of xenoliths is assumed from relatively high calculated temperatures for the depth of spinel facies.

One of important thing is, that a majority of the Ordovician mantle peridotites, in terms of major element compositions, resembles those from numerous xenolith localities of all over the Quaternary basalts of neighboring Baikal Rift System.

References

- Brey G.P., Köhler T., 1990. Geothermobarometry in four-phase lherzolites II. New thermobarometers, and practical assessment of existing thermobarometers, *Journal of Petrology*, 31, 1353-1378.
- Egorova V.V., Volkova N.I., Shelepaev R.A., Izokh A.E., 2006. The lithosphere beneath Sangilen Plateau, Siberia: evidence from peridotite, pyroxenite and gabbro xenoliths from alkaline basalts. *Mineralogy and Petrology*, 88, 419-441.
- Ellis D.J., Green D.H., 1979. An experimental study of the effect of Ca upon garnet-clinopyroxene Fe-Mg exchange equilibria, *Contribution to Mineralogy and Petrology*, 71, 13-22.
- Frey F.A., Prinz M., 1978. Ultramafic inclusions from San Carlos, Arizona: petrologic and geochemical data bearing on their petrogenesis, *Earth and Planetary Science Letters*, 38, 129-176.
- Gibsher A.S.; Vladimirov A.G. & Vladimirov V.G., 2000. The geodynamic nature of Early Paleozoic nappe-folded structure of Sangilen upland (South-Eastern Tuva), *Dokl Akad Nauk*, 370, 489-492.
- Izokh A.E., Polyakov G.V., Mal'kovets V.G., Shelepaev R.A., Travin A.V., Litasov Yu. D., Gibsher A. A., 2001. The Late Ordovician Age of Camptonites from the Agardag Complex of Southeastern Tuva as an Indicator of the Plume-Related Magmatism during Collision Processes, *Doklady Earth Sciences*, 379 (5), 511-514.
- McDonough W.F., Sun S.-S., 1995. The composition of the Earth, *Chemical Geology*, 120, 223-253.
- Mercier J.-C.C., 1980. Single-pyroxene geothermometry, *Tectonophysics*, 70, 1-37.
- Mercier J.-C.C., Nicolas A., 1975. Textures and fabrics of upper-mantle peridotites as illustrated by xenoliths from basalts. *Journal of Petrology*, 16 (2), 454-487.



Petrology and geochemistry of eclogitic sulfides: a new insight on the origin of mantle eclogites?

Yoann Greau^{1,2}, W. L. Griffin², Olivier Alard^{1,2}, Suzanne Y. O'Reilly²

¹GEMOC National Key Centre, Dept of Earth and Planetary Sciences, Macquarie University, NSW 2109, Australia

²Geosciences Montpellier, CNRS UMR-5243, Equipe Manteau-Noyau, Université Montpellier II, France

The alternative hypotheses that mantle eclogites are either rocks produced by mantle processes or fragments of subducted oceanic slabs have been intensively debated for 30 years, and the origin of these rocks is still not well constrained.

In the last decade sulfide assemblages were extensively used to constrain mantle processes. These minerals are the main carrier of the platinum group elements (PGEs) in the mantle. PGEs are useful petrological indicators due to their specific behaviour. The Ir-group PGEs (IPGE- Os, Ir and Ru) are compatible elements while the Pd-group PGEs (PPGEs- Rh, Pt and Pd) are more incompatible (Barnes et al., 1985), in consequence they are useful to trace melting events.

In this study we use the mineralogical and geochemical features of base metal sulfides (BMS) to obtain new information on the history and the origin of mantle eclogites.

Samples

We studied 19 eclogite xenoliths recently sampled at the Roberts Victor mine (South Africa), and 7 samples already within the GEMOC collection. The new suite includes 4 kyanite-bearing eclogites and all the samples except one belong to Type I as defined by McCandless and Gurney (1989) using Na₂O content of garnet and K₂O in clinopyroxene.

The samples are mainly bimineralic eclogites with modal proportions garnet/omphacite varying from 80:20 to 40:60. They are usually coarse grained and show a wide range of microstructures (e.g. layering, patchy accumulation of garnets). Several samples show a microstructural garnet/cpx disequilibrium defined by high-energy surfaces. Most of the rocks also show a destabilisation of the primary omphacite into a spongy inhomogeneous secondary cpx, which is Na-depleted. Garnets are usually fresher than the cpx and are in general chemically homogeneous at the thin section scale. However some specimens (e.g. layered or ky-bearing xenoliths) show variations of the garnet composition within a single thin section. Several accessory minerals such as phlogopite, rutile, amphibole, sulfide, feldspar, spinel, calcite or barite are also commonly present.

Sulfide mineralogy

In the Roberts Victor xenoliths, sulfides occur as veins, as interstitial phases or as inclusions hosted by omphacite and/or garnet. The modal abundance of sulfides varies from 0 to 5%; among 29 thin sections studied only 6 do not contain sulfide phases. Sulfide inclusions are mostly spheres or subhedral polygons 30 to 350 µm long. Intergranular sulfides are generally anhedral with curved or elongate shapes, and grain sizes from < 20 µm to 3 mm. Reflected-light microscopy and backscattered-electron images show that most of the sulfides have been re-equilibrated at low temperature and are polyphase grains composed of pyrite (or Ni-rich pyrite) ± pyrrhotite ± pentlandite ± mono-sulfide solid solution (mss) ± chalcopyrite (Fig.1). The most typical occurrence is a grain of Ni-rich pyrite or pyrrhotite displaying pentlandite flames and euhedral pyrite crystals, with the whole assemblage surrounded by a chalcopyrite corona (Fig 2.).

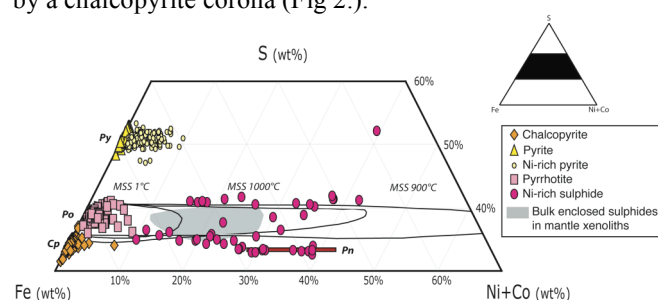


Fig.1 Point analyses of the different sulfide phases plotted in the Fe-Ni-S system. MSS stability field from Kullerud et al., 1969. Grey field, bulk compositions of enclosed sulfides in mantle xenoliths (Lorand & Conquére, 1983; Szabó & Bodnar, 1995). Red bar, compositional range of pentlandite (Lorand, 1989). End-member phases: Cp, chalcopyrite; Po, pyrrhotite; Py, pyrite; Pn, pentlandite.

Sulfide chemistry

Bulk sulfur contents of 21 xenoliths have been analysed by High-Temperature Iodo-Titration (HTIT) and the results range from 0 to 1600 ppm; most are between 200 and 400 ppm with an average of 313 ppm,

similar to accepted values of 200-300 ppm for the subcontinental mantle (O'Neill, 1991). A correlation between sulfide modal abundances and whole-rock S-content confirms that sulfides are controlling the S budget of the eclogites.

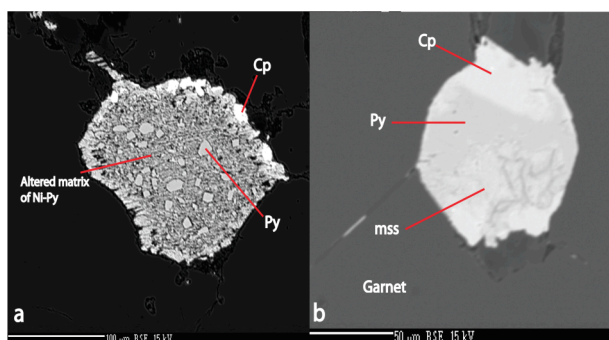


Fig. 2 Back-scattered electron images of polyphased sulfides. a, Typical sulfide with euhedral pyrite crystals within an altered matrix of Ni-rich pyrite and a chalcopyrite corona. b, eclogitic sulfide enclosed within a garnet and showing a pyrite and mss core with a chalcopyrite corona.

LAM-ICP-MS analyses of sulfides from the Roberts Victor samples reveal important variability in the PGE patterns (Fig.3). However it seems that such a feature is mainly due to the low-T subsolidus re-equilibration of the sulfide assemblages. Basically, PGE patterns can be sorted into 4 main groups, 3 of which are related to a specific mineralogy of the ablated phase.

The first kind of occurrence is associated with Ni-rich pyrite with a potential minor component of chalcopyrite. These analyses show enrichment of light PGEs (Ru, Rh and Pd), Os and Ir relative to Pt. The IPGEs show flattened patterns that are essentially chondritic ($0.1-2 \times CI$) and are positively correlated with the nickel concentration (2-6 wt%) of the analysed area. An enrichment in Rh relative to the light PGEs ($Rh/Ir_N = 6.28 \pm 1.34$) is visible on analyses with a chalcopyrite contribution, while the analysis RV07-17S3-1, which has a low Cu content (<1500 ppm), shows $Rh/Ir_N = 1.40$. This positive correlation between the Cu-content and Rh is characteristic of the four groups described here.

The second group is also associated with Ni-rich pyrite but is characterized by a pattern different to those detailed above. In this case, Ru (0.53 ± 0.16 ppm) and Rh (0.048 ± 0.03 ppm) are enriched relative to Os (0.019 ± 0.001 ppm), Ir (0.011 ppm), Pt (0.026 ± 0.011 ppm) and Pd (0.055 ± 0.027 ppm), and $Ru/Rh_N > 1$.

The third type of PGE pattern is related to analyses with a high Cu-content, consisting principally of chalcopyrite and mixtures of chalcopyrite and mss. As previously seen for the second group, there is an enrichment in Ru and Rh relative to the other PGEs, but due the high Cu contents Rh is enriched relative to Ru ($Ru/Rh_N = 0.03 \pm 0.01$). In the chalcopyrite-mss mixture where $Cu/Ni < 1$ the depletion in Pt is less important ($Rh/Pt_N = 21.5 \pm 11.8$) than in the almost pure chalcopyrite ($Rh/Pt_N = 955 \pm 73$). Chalcopyrite patterns are then

similar to those observed for magmatic chalcopyrite described from abyssal peridotite (Luguet et al., 2001,

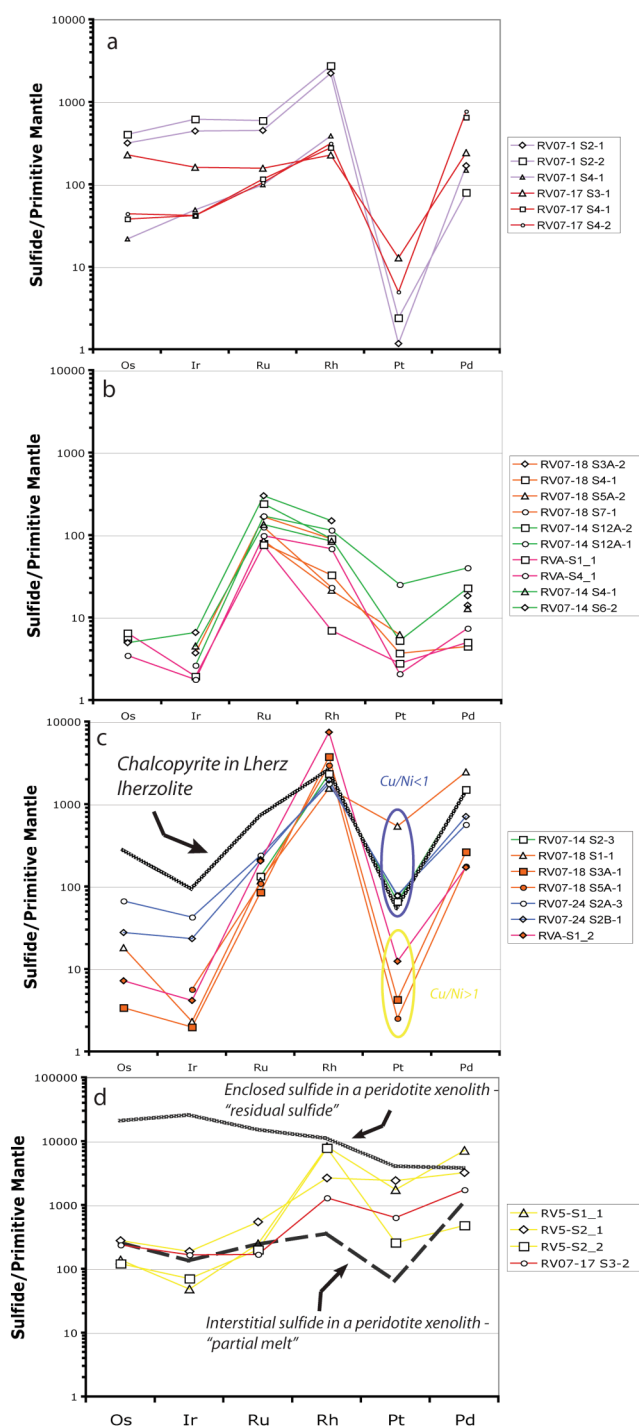


Fig. 3 Primitive mantle normalized PGE abundances of sulfides. a, Ni-rich pyrites (type I) with a minor chalcopyrite component. b, Ni-rich pyrites (type II). c, Chalcopyrites and chalcopyrite/mss mixtures; solid symbols, pure chalcopyrites; black thick line, chalcopyrite in FON B 93 lherzolite (Lherz, France). d, Sulfides with PPGE enrichment relative to IPGEs; black thick line, enclosed sulfides in a peridotite xenolith in alkali basalt (Mt Gambier, Australia); thick dashed line, interstitial sulfides in a peridotite xenolith (Mt Gambier, Australia)

2004) and from peridotite from Lherz (Lorand et al., 2008). There is also a transitional subgroup in which all the steps between the second group (Ni-rich pyrite) and pure chalcopyrite are observable, basically with an increase in Rh and Pd-contents with the addition of chalcopyrite to the mixture.

The fourth type of PGE pattern shows an enrichment in PPGEs relative to IPGEs. IPGEs are generally chondritic while PPGEs show a negative anomaly in Pt. These patterns are similar to those of interstitial sulphide observed in mantle peridotite xenoliths from Australian alkali basalts and interpreted as partial melts of a chondritic sulfide (Alard et al., 2000).

LAM-ICP-MS has been also used to quantify the siderophile and chalcophile element budget of the interstitial sulfides found in crosscutting veinlets. While Se-contents are mostly between 50-90 ppm for the sulfides described above the Se is very low in the veinlet sulfides and do not exceed 4 ppm, and all the PGE are below the minimum detection limit of the instrument. This kind of mineralisation is clearly of secondary origin and can be probably related to the hostkimberlite, whereas the bulk of the observed sulfides must be related to the eclogite formation or later mantle metasomatism.

Preliminary investigations of the sulfur isotopic compositions were carried out using in situ ion-probe techniques (CAMECA IMS-5F, Universite de Montpellier). The results obtained on 3 samples show that the $\delta^{34}\text{S}$ of the sulfides varies from -4.93% to $+2.73\%$ with an average of -0.95% . Considering that the primitive mantle value is defined at $0\pm 2\%$ (Thode et al., 1961) and sulfide inclusions in mantle xenoliths are $1.3\pm 3.8\%$, these first results seem to be consistent with a mantle origin of the sulfides in Roberts Victor eclogites.

Conclusion

Although this study does not provide clear evidence to decide between one hypothesis and the other, the different aspects of the sulfide assemblages in the Roberts Victor eclogites tend to suggest a mantle origin for these minerals. Therefore, it becomes crucial to define whether the BMS origin is related to a late metasomatism or to the origin of the eclogites.

References

- Alard, O., W.L. Griffin, J.P. Lorand, S.E. Jackson, S.Y. O'Reilly., (2000). "Non-chondritic distribution of the highly siderophile elements in mantle sulphides." *Nature* 407: 891-894.
- Kullerud, G., R. A. Yund, et al. (1969). "Phase relations in the Cu-Fe-S, Cu-Ni-S, and Fe-Ni-S systems." *Economic Geology Monographs* 4: 323-343.
- Luguet, A., O. Alard, J.P. Lorand, N.J. Pearson, C. Ryan, S.Y. O'Reilly (2001). "Laser-ablation microprobe (LAM)-ICPMS unravels the highly siderophile element geochemistry of the oceanic mantle." *Earth and Planetary Science Letters* 189: 285-294
- Luguet, A., O. Alard, J.P. Lorand, J.Y. Cottin (2004) "A multi-technique study of platinum-group elements systematic in some ligurian ophiolitic peridotites, Italy" *Chemical Geology* 208: 175-194
- Lorand, J. P. (1989). "Are spinel lherzolite xenoliths representative of the abundance of sulfur in the upper mantle?" *Geochimica et Cosmochimica Acta* 54: 1487-1492.
- Lorand, J. P. and F. Conquere (1983). "Contribution a l'etude des sulfures dans les enclaves de lherzolite a spinelle des basaltes alcalins (Massif Central et Languedoc, France). Contribution to the study of sulfide parageneses in spinel lherzolite xenoliths from alkali basalts, Central Massif and Languedoc, France." *Bulletin de Mineralogie* 106(5): 585-605.
- Lorand, J. P. , A. Luguet, O. Alard, A. Bezos, T. Meisel (2008). "Abundance and distribution of platinum-group elements in orogenic lherzolites; a case study in a Fontete Rouge lherzolite (French Pyrenees)" *Chemical Geology* 248: 174-194
- McCandless, T. E. and Gurney, J. J. (1989). Sodium in garnet and potassium in clinopyroxene: criteria for classifying mantle eclogites. Kimberlites and Related Rocks. J. J. Ross, A L; Ferguson, J; Green, D H; O'Reilly, S Y; Danchin, R V; Janse, A J A. Perth, Special Publication - Geological Society of Australia. 14: 827-832.
- McDonough, W. F. and S.-S. Sun (1995). "The composition of the Earth." *Chemical Geology* 120: 223-253.
- O'Neill, H. S. C. (1991). "The origin of the Moon and the early history of the Earth - a chemical model. Part 2: The earth." *Geochimica et Cosmochimica Acta* 55(4): 1159-1172.
- Szabo, C. and R. J. Bodnar (1995). "Chemistry and origin of mantle sulfides in spinel peridotite xenoliths from alkaline basaltic lavas, Nograd-Gomor Volcanic Field, northern Hungary and southern Slovakia." *Geochimica et Cosmochimica Acta* 59(19): 3917-3927.

Diamonds and carbonatites in the deep lithosphere: Evidence of genetic links

W.L. Griffin¹, D. Araujo¹, S.Y. O'Reilly¹, S. Rege¹, E. van Achterbergh²
¹GEMOC, Dept. Earth & Planetary Sciences, Macquarie Univ., NSW 2109, Australia
²Rio Tinto Technology & Innovation, 1 Research Ave., Bundoora, VIC 3083, Australia

Some diamonds from the A154 kimberlite, in the Lac de Gras area of the Slave Craton, have gem-quality octahedral cores overgrown by porous, fibrous to particulate coats ranging from tens of microns to ≈ 1 mm in thickness (Fig. 1).



Figure 1. Coated octahedral diamond from A154, whole stone and polished plate.

Quantitative trace-element analysis of the cores and coats by LAM-ICPMS (using methods described by Rege et al. (2005)) shows distinct differences in the composition of the metasomatic fluids/me/ts from which each type of diamond grew.

Diamond Analyses

The *cores* have trace-element patterns (Fig. 2) broadly similar to those of monocrystalline diamonds from other localities worldwide. They show LREE depletion ($(La/Nd)_{CN} < 1$), negative Sr and Y anomalies relative to Sm and Ho, respectively, $(Ba/La)_{CN} \approx 1-3$, $(Th/U)_{CN} \approx 0.5$, $(Zr/Hf)_{CN}$ and $(Nb/Ta)_{CN} \ll 1$ and low Mg/Ca. These trace elements are assumed to reside in submicroscopic fluid and solid (daughter mineral) inclusions, rather than in the diamond lattice.

The *coats* are typically homogeneous within each stone, and their trace-element patterns are very similar from stone to stone (> 20 stones analysed). They have CN abundances of the HREE similar to those in the monocrystalline diamonds, but show

strong LREE enrichment ($(La/Nd)_{CN} \geq 30$), $(Ba/La)_{CN} \approx 8-10$, $(Zr/Hf)_{CN}$ and $(Nb/Ta)_{CN} \approx 0.5-2$, $(Th/U)_{CN} \approx 5-10$ and high Mg/Fe. Most analyses show small positive Sr anomalies and negative Y anomalies of widely variable depth. Compared to coated and fibrous diamonds from other localities worldwide, they have high Ba/Th, Ba/K and K/Sr, and anomalies in Sr and Y are rare in other fibrous diamonds.

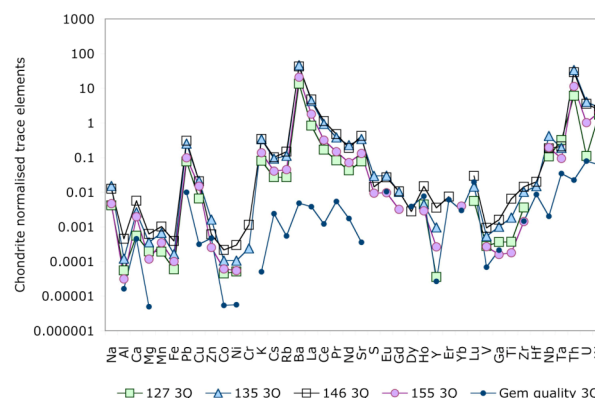


Figure 2. Chondrite-normalised trace-element patterns of coats on four representative diamonds from the A154 kimberlite. Shown for comparison are the third-quartile values for analyses of the gem-quality cores of coated stones.

Trapped Melts and Fluids

The Lac de Gras kimberlites contain xenoliths of megacrystalline garnet lherzolite derived from near the base of the lithosphere (180-200 km) beneath the Slave Craton, and Cr-diopside crystals within these xenoliths contain mm-sized round to oblate inclusions of quenched silico-carbonate melts (van Achterbergh et al. 2002, 2004). Detailed study of a large suite of these melt inclusions (Araujo et al., this conference, abstract A-00139) tracks the evolution of kimberlite-carbonatite melts, through fractionation of olivine and phlogopite and possible immiscible separation into carbonate-rich and silicate-rich melts. Despite wide variation in absolute abundances, the trace-element patterns of the different carbonatitic to silicic melts are broadly similar



to one another, and to those of fibrous and coated diamonds from other localities (Fig. 3; cf Rege et al., 2005; Zedgenizov et al., 2007; Weiss et al., 2008). However, the Diavik diamond coats have higher LREE/HREE, Ba/La, K/La and Na/Ca, and higher contents of chalcophile elements, than the quenched melt inclusions.

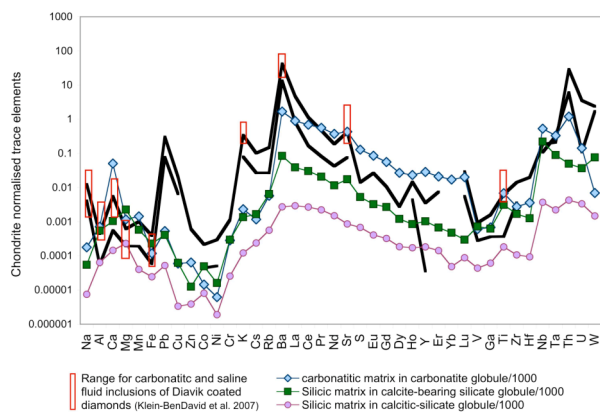


Figure 3. Trace-element patterns of quenched melt inclusions (/1000) in Cr-diopside of megacrystalline lherzolite xenoliths from the A154 kimberlite. High and low patterns of diamond coats from Fig. 2 are shown for comparison. Bars show ranges of concentration (/1000) in fluid inclusions from coats on Diavik diamonds; many Sr and Ti values are <MDL (Klein-BenDavid et al., 2007).

“Major-element” ratios (Na, Al, Ca, Mg, Fe, K, Ba, Ti) in the coats are closely similar to those measured (by EMPA) in individual fluid inclusions in diamond coats from the Diavik mines (Fig. 2; Klein-BenDavid et al., 2007). Relative to the melt inclusions in the Cr-diopsides, the fluid inclusions in the diamond coats have high Na/Ca, K/Ca and Ba/La. Comparison of absolute element abundances in the fluids and the diamond coats indicates that such fluid inclusions make up ca 1% by weight of the coats. These fluid inclusions lie in a spectrum from (dominantly) saline toward carbonatitic, suggesting that they may be genetically related to the silico-carbonatitic melts trapped in the Cr-diopside of the megacrystalline lherzolites.

Detailed analysis of the Cr-diopside adjacent to different types of melt inclusions shows pronounced metasomatic modification of the cpx, with introduction of LREE, Ba, K and Na. Modelled compositions for the metasomatising fluids, calculated using a variety of experimentally-derived values for $D^{cpx/fluid}$ (Fig. 3) closely resemble both the LAM-ICPMS data for the diamond coats, and the measured compositions of the saline-carbonatite fluid inclusions. These observations suggest that similar fluids escaped from the carbonatitic to silicic melts to metasomatise the surrounding Cr-diopside, following their trapping and the necking-down of the fluid-filled veins to produce the present rounded melt inclusions.

Discussion and Conclusions

The Diavik coated diamonds described here clearly reflect two generations of diamond growth, and the trace-element analyses suggest that the two generations formed from radically different metasomatic fluids. The accumulating trace-element data on fibrous and coated diamonds from localities worldwide suggests that most of these have crystallized from low-volume melts in the kimberlite-carbonatite spectrum (Rege et al., 2005; Zedgenizov et al., 2007; Weiss et al., 2008). The coats on the Diavik diamonds have more fractionated patterns than most fibrous diamonds, reflecting their growth from saline- fluids that evolved from such melts, rather than from the melts themselves. The data thus establish a genetic connection between the low-volume

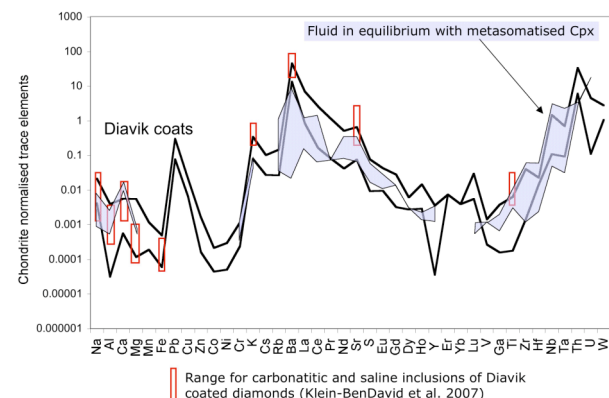


Figure 3. Calculated compositions of fluids (/1000) that metasomatised Cr-diopside adjacent to quenched melt inclusions, compared to patterns (/1000) of diamond coats and their fluid inclusions.

melts, the saline to carbonatitic fluids, and the coats on the Diavik diamonds. The Diavik situation is perhaps unique in preserving samples of both the melts (trapped and quenched within Cr-diopside) and the fluids that may have evolved from them (trapped within the coats on gem diamonds).

However, nearly all monocrystalline diamonds worldwide, including the octahedral cores of the diamonds described here, appear to have crystallized from fluids/melts that are distinctly different from those trapped in fibrous diamonds or coats on diamonds (e.g. Fig. 2). The relationship between the “monocrystalline-diamond” fluid and those that precipitated fibrous diamonds, diamondites (Rege et al., 2008) or the fibrous coats on monocrystalline diamonds remains to be clarified. It may involve the continued evolution of melts and fluids such as those described here. Alternatively, it may be a precursor (CH₄-rich) fluid, the oxidation of which produced CO₂ and H₂O that lowered the peridotite solvus and allowed production of melts in the kimberlite-carbonatite spectrum (Malkovets et al., 2007).

There are many unanswered questions arising from these data, but it is clear that *quantitative, in situ* analysis of trace elements in diamonds by LAM-ICPMS can provide unique information on the

processes in the lithospheric mantle, including those by which diamonds are formed.

References

- Klein-BenDavid, O., Izraeli, E.S., Hauri, E., Navon, O., 2007. Fluid inclusions in diamonds from the Diavik mine, Canada and the evolution of diamond-forming fluids. *Geochimica Cosmochimica Acta* 71, 723-744.
- Malkovets, V.G., Griffin, W.L., O'Reilly, S.Y., Wood, B.J., 2007. Diamond, subcalcic garnet and mantle metasomatism: Kimberlite sampling patterns define the link. *Geology* 35, 339-342.
- Rege, S., Jackson, S.J., Griffin, W.L., Davies, R.M., Pearson, N.J., O'Reilly, S.Y., 2005. Quantitative trace element analysis of diamond by laser ablation inductively coupled plasma mass spectrometry. *Journal of Analytical Atomic Spectroscopy* 20, 601-610.
- Rege, S., Griffin, W.L., Kurat, G., Jackson, S.E., Pearson, N.J., O'Reilly, S.Y., 2008. Trace element chemistry of diamondites: Crystallisation of diamond from kimberlite-carbonatite melts. *Lithos* (in press).
- van Achterbergh, E., Griffin, W.L., Ryan, C.G., O'Reilly, S.Y., Pearson, N.J., Kivi, K., Doyle, B.J. 2002. A subduction signature for quenched carbonatites from the deep lithosphere. *Geology* 30, 743-746.
- van Achterbergh, E., Griffin, W.L., O'Reilly, S.Y., Ryan, C.G., Pearson, N.J., Kivi, K., Doyle, B.J., 2004. Melt inclusions from the deep Slave lithosphere: implications for the origin and evolution of mantle-derived carbonatite and kimberlite. *Lithos* 76, 461-474.
- Weiss, Y., Griffin, W.L., Elhlou, S., Navon, O., 2008. Comparison between LA-ICP-MS and EPMA analysis of trace elements in diamond. *Chemical Geology* (in press)
- Zedgenizov, D.A., Rege, S., Griffin, W.L., Kagi, H., Shatsky, V.S., 2007. Compositional variations of micro-inclusions in fluid-bearing diamonds from Udachnaya kimberlite pipe as revealed by LA-ICP-MS. *Chemical Geology* 240, 151-162.

Contrasting lithospheric mantle across the suture between the Eastern and Western Dharwar Cratons, central India

W.L. Griffin¹, A. F. Kobussen¹, E.V.S.S.K. Babu², S.Y. O'Reilly¹, R. Norris³, P. Sengupta³

¹GEMOC, Dept. Earth & Planetary Sciences, Macquarie Univ., NSW 2109, Australia

²National Geophysical Research Inst., Hyderabad 500 007, India

³Rio Tinto Exploration India, Whitefield, Bangalore 560 066, India

Introduction and Methods

The Dharwar craton consists of two major blocks: in the Western Dharwar (WDC) 3.3-2.6 Ga supracrustal rocks overlie a 3.4-2.9 Ga basement; in the Eastern Dharwar (EDC) 2.6-2.5 Ga calc-alkaline granitoids enclose narrow belts of 2.7 Ga supracrustals. The EDC appears to have been thrust westward over the WDC prior to 2.5 Ga; the suture may be represented by a major mylonite zone (the Chitradurga schist belt) or by the Closepet Granite, a narrow batholith that runs N-S for ca 300 km, 40-50 km E of the schist belt. Garnet concentrates and mantle-derived xenoliths from 1.0-1.1 Ga kimberlite clusters in Andhra Pradesh provide images of the subcontinental lithospheric mantle (SCLM) along a traverse extending SW-NE across the E margin of the Closepet Granite (Fig. 1).

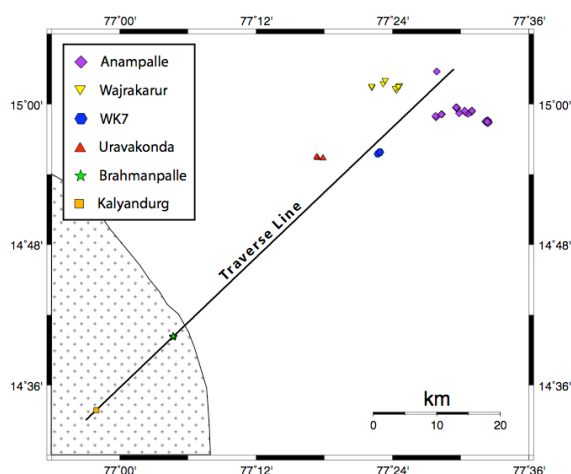


Figure 1. Locations of kimberlite clusters studied with traverse line. Igneous pattern indicates the Closepet Granite.

Geotherms for the SCLM beneath each cluster have been derived from major- and trace-element compositions of peridotitic garnets as described by

Ryan et al. (1996). The calculation of X_{Mg} in olivine coexisting with individual garnet grains is described by Gaul et al. (2000) and the derivation of whole-rock (WR) Al_2O_3 contents from garnets by Griffin et al. (1998). Eclogite data used here are from this work (n=18), Ganguly and Bhattacharya (1987; n=4) and Patel et al. (2006; n=10). Depth estimates for eclogites are defined by the intersection of P-T trajectories (Krogh, 1988) with the garnet geotherm, assuming that eclogites and peridotites have equilibrated to a common geotherm (Griffin and O'Reilly, 2007).

Results

The Kalyandurg and Brahmanpalle clusters at the SW end of the traverse sampled typical Archean SCLM, with a low geotherm (35 mW/m^2) and harzburgitic to lherzolitic rocks with median $X_{Mg}^{\text{olivine}} > 0.93$ and median whole-rock $Al_2O_3 < 1\%$. The base of the depleted lithosphere at 185-195 km depth is marked by a 10-15 km layer of strongly metasomatised peridotites ($X_{Mg}^{\text{olivine}} \approx 88$). The Anampalle and Wajrakarur clusters 60 km to the NW show a distinctly different SCLM; it has a higher geotherm ($37.5\text{-}40 \text{ mW/m}^2$), contains few subcalcic harzburgites, and has median $X_{Mg}^{\text{olivine}} \leq 0.925$ and median whole-rock $Al_2O_3 \approx 2\%$. Kimberlites of the Uravakonda and WK-7 clusters, midway along the traverse, sampled a quite fertile (median $X_{Mg}^{\text{olivine}} \approx 0.915$, median WR $Al_2O_3 \approx 3\%$) SCLM with an elevated geotherm ($>40 \text{ mW/m}^2$).

The data from >1080 peridotitic garnet xenocrysts have been used to map the vertical and lateral variations in key chemical parameters (Figs 2-4). The techniques used for gridding and contouring the data are described by Kobussen et al. (2008).

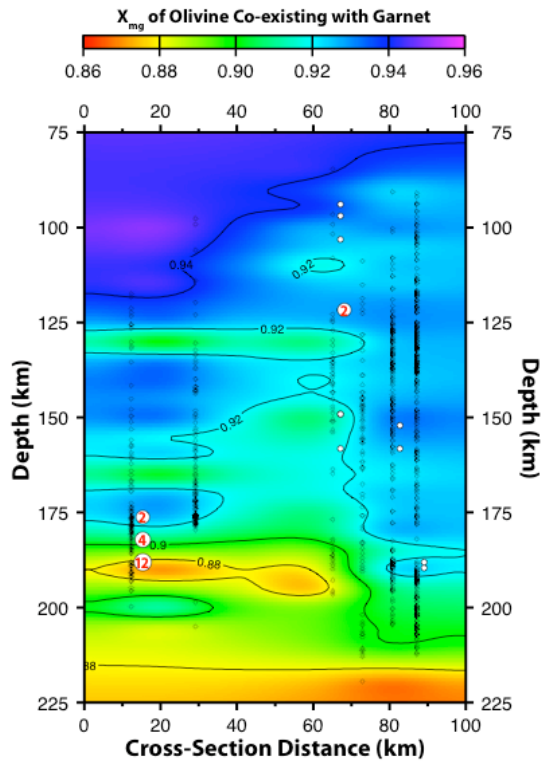


Figure 2. Distribution of median calculated X_{Mg} of olivine coexisting with Cr-pyrope garnets. Diamonds, individual data points. Circles, eclogites (numbers show >1 sample with similar depth estimate). The gridding and filtering algorithm elements used are 20 km wide by 5 km deep.

The X_{Mg} of olivine (Fig. 2) shows marked vertical and lateral variations. In the Kalyandurg (16 km on the traverse) and Brahmanpalle (29 km) sections, relatively depleted material ($X_{Mg} > 0.93$) is interspersed with bands of lower X_{Mg} , and median X_{Mg} drops to ≤ 0.88 between 180-195 km depth. This Fe-enriched layer corresponds to a strong concentration of eclogites. The section beneath the Uravakonda and WK-7 clusters (65-75 km) is strikingly less magnesian, with few values of $X_{Mg} \geq 0.92$. The available data suggest that eclogites are distributed throughout the section from ca 85-160 km. The SCLM beneath the most northerly clusters (80-90 km) is more uniform in composition, but is significantly less magnesian than the SW end of the traverse, especially at depths <125 km. The few eclogite data from these fields spread between 150-190 km depth.

Figure 3 shows sharp rises in the Ti contents of garnets at depths varying from ca 180 km in the middle of the traverse to ca 190 km at the NE end. This pattern is typical of many SCLM sections worldwide, and the chemistry of these higher-Ti garnets can be correlated with the garnets of high-T sheared, meltmetasomatised garnets. We take this signal as defining the base of the depleted SCLM, and a level of

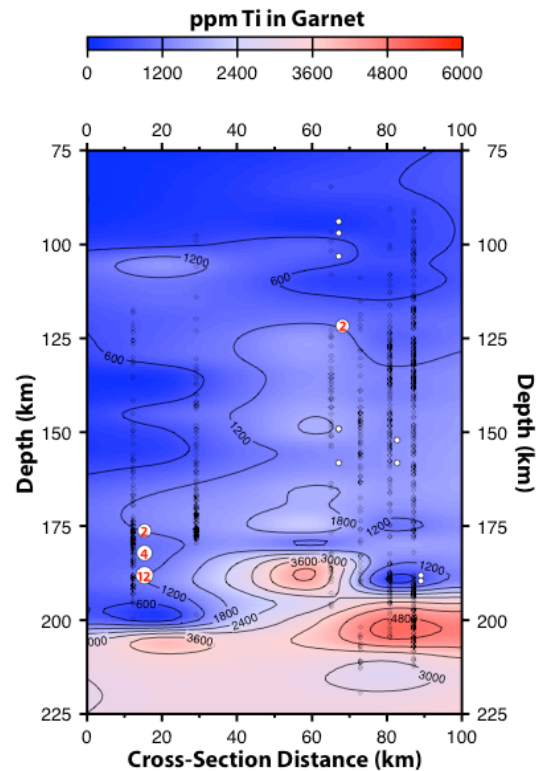


Figure 3. Distribution of median Ti contents (ppm) of Cr-pyrope garnets.

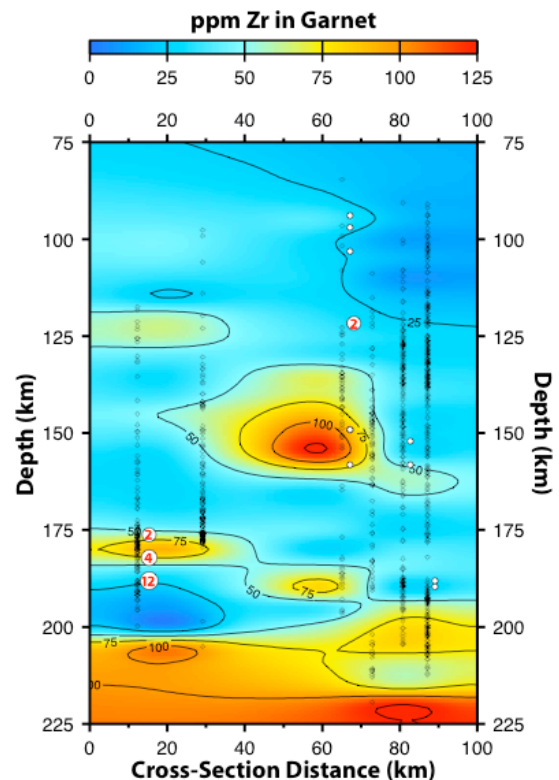


Figure 4. Distribution of median Zr contents (ppm) of Cr-pyrope garnets.

magma ponding and infiltration. This increase in Ti is not well-defined beneath the SW end of the traverse; the intense Fe-metasomatism at 180-195 km depth is accompanied by only a relatively modest rise in the median Ti in garnet. The section beneath the Uravakonda and WK-7 clusters is generally higher in Ti than the SCLM at the NE or SW ends of the traverse. The distribution of median Zr in garnet (Fig. 4) tends to mirror that of Ti, with two marked differences: a large increase at ca 150 km depth in the middle of the traverse, and another at 175-180 km depth beneath the SW end.

Beneath the Kalyandurg cluster (16 km), there is a strong correlation between the distribution of eclogites and enrichment of the peridotites in Fe and Zr. We suggest a genetic connection, with the peridotites being metasomatised by mafic melts and associated fluids. The strong concentration of eclogites in a 10-20 km layer beneath the Kalyandurg cluster is similar to that seen in many SCLM sections (Griffin and O'Reilly, 2007) and contrasts with the broader depth distribution of eclogites beneath the fields to the NE. There is also a marked difference in eclogite types: many of the Kalyandurg eclogites are kyanite-bearing (\pm coesite), and the bimineralic eclogites tend to have the high-Ca garnet that is characteristic of the kyanite eclogites, suggesting they belong to the same suite. The eclogites from the pipes to the NE are more typical bimineralic eclogites with generally higher Mg# and lower-Ca garnets.

Conclusions

- (1) The striking differences in the SCLM (100-200 km depth) along the traverse suggest that the NE and SW ends of the traverse represent distinct lithospheric blocks, corresponding to the EDC and WDC.
- (2) At 100-200 km depth, the EDC - WDC suture lies near the E margin of the Closepet Granite, suggesting that the batholith is the crustal expression of a lithosphere-scale boundary.
- (3) The SCLM near the suture is strongly refertilised, perhaps during craton assembly.
- (4) The differences in the SCLM beneath the WDC and EDC suggest that each cratonic block carried its own "root" at the time of their collision; the root beneath the margin of the EDC may already have been less depleted, or it may have been refertilised by fluids moving along the suture.
- (5) The scarcity of kyanite eclogites beneath the EDC margin suggests that the WDC eclogites were emplaced before craton assembly.

References

- Ganguly, J., Bhattacharya, P.K., 1987. Xenoliths in Proterozoic kimberlites from southern India: petrology and geophysical implications. In Nixon, P.H. (ed.) *Mantle Xenoliths*, Wiley, New York, pp. 249-266.
- Gaul, O.F., Griffin, W.L., O'Reilly, S.Y., Pearson, N.J., 2000. Mapping olivine composition in the lithospheric mantle. *Earth and Planetary Science Letters* 182, 223-235.
- Griffin, W.L., O'Reilly, S.Y., Ryan, C.G., Gaul, O., Ionov, D. 1998. Secular variation in the composition of subcontinental lithospheric mantle. In Braun, J., Dooley, J.C., Goleby, B.R., van der Hilst, R.D., Klootwijk, C.D. (Eds), *Structure and Evolution of the Australian Continent*, Geodynamics Volume 26, American Geophysical Union, Washington D.C. pp. 1-26.
- Griffin, W.L., O'Reilly, S.Y., 2007. Cratonic lithospheric mantle: Is anything subducted? *Episodes* 30, 43-53.
- Kobussen, A.F., Griffin, W.L., O'Reilly, S.Y., Shee, S.R., 2008. The ghosts of lithospheres past: Imaging an evolving lithospheric mantle in southern Africa. *Geology* 36, 515-518.
- Krogh, E. R., 1988. The garnet-clinopyroxene Fe-Mg geothermometer – a reinterpretation of existing experimental data. *Contributions to Mineralogy and Petrology* 99, 44-48.
- Patel, S.C., Ravi, S., Thakur, S.S., Rao, T.K., Subbarao, K.V. 2006. *Mineralogy and Petrology* 88, 363-380.
- Ryan, C.G., Griffin, W.L., Pearson, N.J., 1996. Garnet Geotherms: a technique for derivation of P-T data from Cr-pyroxene garnets. *Journal of Geophysical Research* 101, 5611-5625.

Super-deep diamonds from kimberlites in the Juina area, Mato Grosso State, Brazil

Felix V. Kaminsky^{1,3}, Galina K. Khachatryan¹, Paulo Andrezza²,
Debora Araujo³, William L. Griffin³

¹KM Diamond Exploration Ltd., West Vancouver, Canada

²Diagem do Brasil Mineração Ltda., Brazil

³GEMOC Key Centre, Dept. of Earth and Planetary Sciences, Macquarie University, Sydney, Australia

In the last decade, the study of diamonds from the placer deposits of the Juina area, Mato Grosso State, Brazil has provided important information on the composition and origin of the deepest accessible levels of the Earth's lithosphere and lower mantle (Harte *et al.*, 1999; Kaminsky *et al.*, 2001; Hayman *et al.*, 2005). In 2006-2007, a group of kimberlitic pipes was discovered by Diagem in the Chapadão area. They form a new kimberlite cluster containing high-grade (0.2-1.8 ct/m³) volcanoclastic layers. Diamondiferous layers, considered a primary kimberlitic ash-fall, were bulk-sampled, and representative quantities of diamonds were gained.

Diamond morphology and coloration

Diamonds from the Juina kimberlitic pipes, like ones from previously studied Juina placer deposits, are very homogeneous in their morphology and optical properties. There are only two major crystallographic forms in these crystals, dodecahedral (from 27.8 % to 41.8 % of the stones) and octahedral (from 9.3 % to 12.7 % in Pandrea pipes, and from 5.0 % to 6.6 % in pipes Aripuana-1 and Collier-4 respectively). A very limited variety of face accessories is present on the stones. No cubic crystals or even cubic faces were found among the diamonds studied. The diamonds from the Juina kimberlitic pipes are colourless, grey/greyish, brown/ brownish, and yellow/ yellowish. In some cases, the smoky-brown colour of the diamonds is due to plastic deformation, while the yellow colour is caused by a nitrogen impurity in the diamond. Grey colouration is caused by the presence of numerous small black graphite-like inclusions.

Infrared spectroscopy of diamonds

The diamonds from the Juina pipes, like those from the placer deposits, are substantially different in their nitrogen impurity characteristics from most other kimberlite-related diamonds. In the Pandrea pipes, 25-56 % of diamonds are 'nitrogen-free'. Type IaB-diamonds comprise 40-65 % of all studied pipe

diamonds. The diamonds form two populations: a major population with a highly aggregated nitrogen impurity (% N_B = 75-100 %), and a secondary population with a moderately aggregated nitrogen impurity (% N_B = 20-65 %). The total nitrogen contents in both diamond populations are the same (Fig. 1).

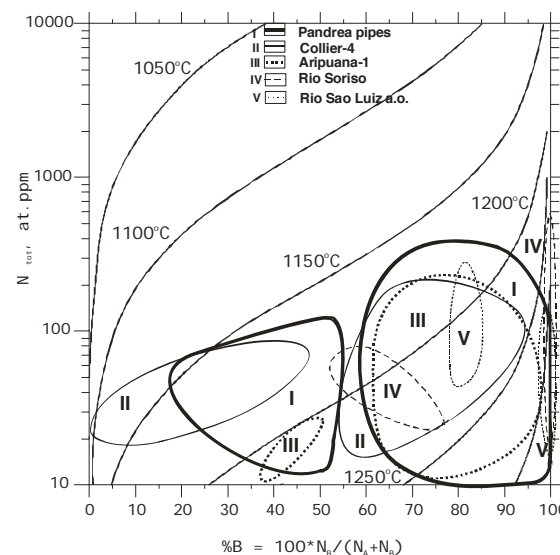


Fig. 1. Distribution of total nitrogen content against proportion of aggregated nitrogen in diamonds from the pipes and placer deposits (Rio Soroso, Rio Sao Luiz, a.o.) in the Juina area. Isotherm curves for 3 Ga after Taylor and Milledge (1995).

In contrast to most diamond deposits worldwide, almost all diamonds from the Juina pipes (80-89 %) have noticeable (up to 4.2 cm⁻¹) levels of hydrogen H-centres.

Mineral inclusions in diamonds

Ferropericlase, chrome spinel, microilmenite, Mn-ilmenite, a MgCaSi-perovskite phase, rutile, sulphides, and native iron were identified among inclusions in Juina pipe diamonds. Some of them form associations: ferropericlase + spinel + native Fe, chrome spinel + MgCaSi-perovskite, and microilmenite + Mn-ilmenite.



Ferropericlasite is the most abundant mineral inclusion in the diamonds studied, as in other Juina diamonds. It has a range of *mg* from 0.518 to 0.810, within the wider range defined by other ferropericlasite compositions from the Juina placer deposits (0.38-0.85). The major impurities are Ni (0.59-1.48 wt.% NiO), Cr (0.09-0.65 wt.% Cr₂O₃), Mn (0.14-0.73 wt.% MnO), Na (0.01-0.72 wt.% Na₂O), and Zn (0.02-0.10 wt.% ZnO).

Chrome spinel is the second most common inclusion phase. Compositionally it differs drastically from spinel identified in placer diamonds. In contrast to titaniferous chrome spinel with 10-11 wt.% TiO₂ from placer diamonds, the studied grains have only 0.12-0.58 wt.% TiO₂ and cannot be called 'titaniferous'. The Fe_{tot} content in the studied spinel grains is also lower (FeO = 14.11-22.29 wt.% against 35-37 wt.% in the earlier-studied inclusions from placer deposits). Al and Cr concentrations in the studied grains are significantly higher: Al₂O₃ = 12.85-19.75 wt.%, and Cr₂O₃ = 45.93-58.16 wt.% against 5-6 % and 35-37 %, respectively, in 'placer' inclusions. The *mg* of the studied spinel inclusions is generally higher: 0.347-0.558 against 0.35-0.36. The compositions of the studied chrome spinel inclusions within a single diamond vary in both Cr content (by several per cent) and *mg* ($\Delta = 0.07-0.14$). In newly studied chrome-spinel grains, concentrations of Ti, V, Cu, Zr, and Nb are two orders of magnitude lower, while Co and Zn are significantly higher than in the titaniferous spinels from the placer diamonds (Fig. 2).

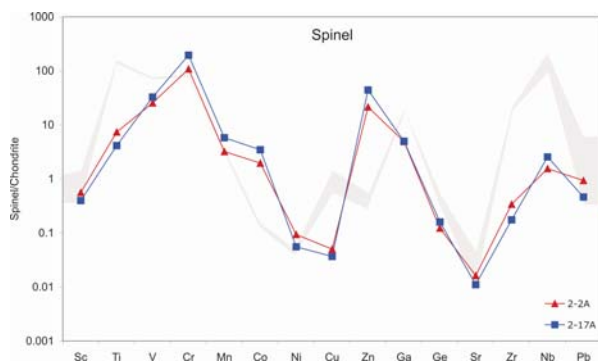


Fig. 2. Chondrite-normalized trace element distribution in chrome spinel inclusions in Juina kimberlitic diamonds. Shaded area – trace element distribution in spinel from Juina placer diamonds [after Kaminsky *et al.*, 2001].

Two grains of MgCaSi-perovskite were identified in a single diamond from pipe Pandrea-2. The chemical composition of this mineral has not been reported before. The *mg* numbers of these grains are extremely high (0.966 and 0.969); the highest reported value even for MgSi-perovskite from all areas with lower-mantle diamonds. The average formula for two grains is as following: Mg_{1.2}Fe_{0.03}Ca_{0.6}Al_{0.04}Si_{2.05}O₆. Since the grain is opaque, and the two analyses show a spread,

especially in Al and Ca, it is possible that the grains were originally a mixture of Mg- and Ca-perovskites, and are now a fine-grained mixture due to decompression breakdown.

Rutile is recorded as a mineral inclusion in Juina diamonds (as well as in the ultra-deep association worldwide) for the first time. It has a low concentration of FeO, compared to other rutile grains included in diamond, 0.21-0.44 wt.% FeO, while rutile included in diamond typically has 1.3-1.8 wt.% (Sobolev, 1974). The studied rutile grains have also low Cr contents (0.09-0.13 wt.%); they belong to the eclogitic association. There are also minor admixtures of Al and V in the studied grains. Low totals (91.6-98.5 %) suggest the presence of other elements.

Native iron has significant contents of Cr₂O₃ (2.37 wt.%), NiO (0.40 wt.%), MgO (0.94 wt.%), and MnO (0.17 wt.%).

The sulphide grains are composed mainly of iron and sulphur, with a small admixture of Cu (0.39-0.80 wt. %) and minor amounts of Ni (0.02-0.06 wt.%), and may be attributed to the eclogitic paragenesis. One of the grains has small (3-10 μm long) lamellae which are very rich not only in Ni (22.2 wt.%) but in Co (14.19 wt.%).

Carbon isotopic composition of diamonds

The isotopic composition of carbon in most diamonds from the Pandrea pipes ranges from -2.67 ‰ to -7.46 ‰, *i.e.*, it is almost exactly the same as for the previously studied placer diamonds (Kaminsky *et al.*, 2001). 6.5 % diamonds have a 'light' (< -9 ‰) isotopic composition (Fig. 3). Three of the 'light' diamonds have mineral inclusions of the eclogitic paragenesis (rutile and sulphide); this suggests that the other isotopically 'light' diamonds are also of the eclogitic paragenesis.

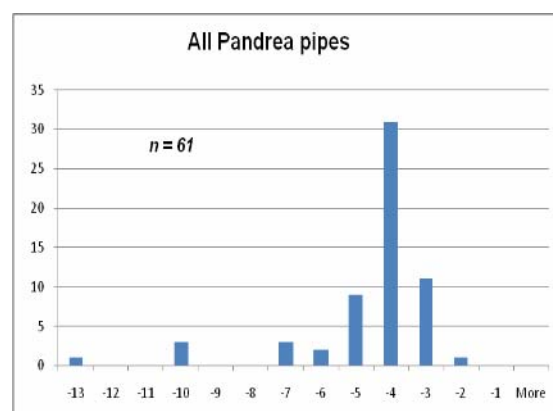


Fig. 3. Carbon isotopic composition of diamonds (in ‰ $\delta^{13}\text{C}$) from Pandrea pipes.

Discussion and conclusions

All Juina diamonds (both kimberlitic and placer) revealed the features that are different to diamonds from other regions. Firstly, there are high proportions of nitrogen-free and low-nitrogen crystals amongst the Juina diamonds. Secondly, the high proportion of IaB diamonds among the nitrogen-containing crystals suggests that they had a prolonged thermal history, which resulted in the almost complete transformation of single-atomic and paired nitrogen centres into polyatomic complexes. Probably, the crystallization and later annealing of Juina diamonds occurred at high temperatures.

A study of mineral inclusions in diamonds from the Juina pipes reveals that they have the same mineral assemblage as previously studied samples from Juina placer deposits (Harte *et al.*, 1999; Kaminsky *et al.*, 2001; Hayman *et al.*, 2005). Most of the inclusions belong to the lower-mantle paragenesis; however some (rutile and sulphide) are of eclogitic paragenesis. Besides, 6.5 % of the studied diamonds have a 'light' (< -9 ‰), 'eclogitic' isotopic composition. This agrees with the identification of carbonates and nanometre-sized crystals of a hydrous aluminium silicate phase (so-called 'phase Egg', $\text{AlSiO}_3(\text{OH})$), in other Juina diamonds (Brenker *et al.*, 2007; Wirth *et al.*, 2007). These data may be considered as proofs that formation of diamondiferous kimberlites in Juina has been initiated by the subduction of crustal material to the depth of the transition zone and lower mantle.

By a complex of characteristics (morphology, mineral inclusions, IR spectra, and carbon isotopic composition) diamonds from the Juina pipes and placer deposits are similar to each other. Diamonds from both groups, kimberlites and placer deposits, belong to the same genetic population with most of the stones originating within the superdeep (lower-mantle and transition zone) conditions.

However, there are some quantitative differences between the placer diamonds and the pipe diamonds. (1) The number of octahedral diamonds is 2-3 times higher in the Pandrea pipes than in the previously studied placer deposits. The average D/Oct ratio for the Pandrea pipes is 2.9 against 13.1 in placer deposits. (2) Two diamond populations exist in the Pandrea pipes: the major population with a highly aggregated nitrogen impurity, and a secondary population with a moderately aggregated nitrogen impurity, while only one major population is present in the diamonds from placers; and in diamonds from placer deposits type IaB-diamonds are strongly, by several times, predominate over type II-diamonds, while in the Pandrea diamonds the ratio of these groups is almost even. (3) Mineral inclusions in diamonds from kimberlitic pipes appeared to be different in composition than the same minerals in placer diamonds. Some of these differences are minor,

however, other differences are substantial, such as the differences in spinel compositions: instead of 'titaniferous' spinel inclusions in placer diamonds, there are chrome spinel inclusions in pipe diamonds. (4) Both kimberlitic and placer diamonds belong to the same population, but have differences in the $\delta^{13}\text{C}$ distribution; and were probably formed from different local carbon sources. These data indicate that besides the discovered Pandrea pipes which may have at least partly supplied diamonds to the studied earlier placer deposits, there may be other, still unknown primary sources of diamonds in the Juina area.

References

- Brenker, F.E., Vollmer, C., Vincze, L., Vekemans, B., Szymanski, A., Janssens, K., Szaloki, I., Nasdala, L., Kaminsky, F., 2007. Carbonates from the lower part of transition zone or even the lower mantle. *Earth and Planetary Science Letters* 260 (1-2), 1-9.
- Harte, B., Harris, J.W., Hutchison, M.T., Watt, G.R., Wilding, M.C., 1999. Lower mantle mineral associations in diamonds from Sao Luiz, Brazil. In: Fei, Y., Bertka, C.M., Mysen, B.O. (Eds), *Mantle Petrology: Field Observations and High Pressure Experimentation*. Geochemical Society Special Publication 6, 125-153.
- Hayman, P.C., Kopylova, M.G., Kaminsky, F.V., 2005. Lower mantle diamonds from Rio Soriso (Juina, Brazil). *Contributions to Mineralogy and Petrology* 149 (4), 430-445.
- Kaminsky, F.V., Zakharchenko, O.D., Davies, R., Griffin, W.L., Khachatryan-Blinova, G.K., Shiryaev, A.A., 2001. Superdeep diamonds from the Juina area, Mato Grosso State, Brazil. *Contributions to Mineralogy and Petrology* 140 (6), 734-753.
- Sobolev, N.V., 1974. Deep-seated inclusions in kimberlites and the problem of the composition of the upper mantle. Nauka Press, Novosibirsk, 264 p. (in Russian). English Translation (1977), ed. by F.R. Boyd, American Geophysical Union, Washington, D.C., 279 p.
- Taylor, W.R., Milledge H.J., 1995. Nitrogen aggregation character, thermal history and stable isotope composition of some xenolith-derived diamonds from Roberts Victor and Finch. In: Sixth Internat. Kimberlite Conf. Extended Abstr., Novosibirsk, August 1995, 620-622.
- Wirth, R., Vollmer, C., Brenker, F., Matsyuk, S., Kaminsky, F., 2007. Nanocrystalline hydrous aluminium silicate in superdeep diamonds from Juina (Mato Grosso State, Brazil). *Earth and Planetary Science Letters* 259 (3-4), 384-399.



The scale and scope of Cretaceous refertilisation of the Kaapvaal lithospheric mantle, Kaapvaal Craton, South Africa

Alan F. Kobussen, William L. Griffin, and Suzanne Y. O'Reilly

GEMOC ARC National Key Centre, Dept. Earth & Planetary Sciences, Macquarie University NSW 2109, Australia

Introduction

There are more than 1000 known kimberlite occurrences scattered throughout southern Africa. These kimberlites can be divided into Group I and Group II, on the basis of their Pb, Sr, and Nd isotopic ratios (Smith, 1983). The vast majority of these kimberlites were emplaced during the Jurassic and Cretaceous Periods. Within this subset, there is a firm relationship between group and age of intrusion: Group II kimberlites were emplaced between ~150 and 115 Ma and Group I kimberlites were emplaced between ~105 and 70 Ma (Smith et al., 1985, 1994). Many of these kimberlites carry peridotitic garnet xenocrysts. Major- and trace-element analysis of these xenocrysts yields a wealth of geochemical information about the underlying sub-continental lithospheric mantle (SCLM), including paleogeotherms and several geochemical indicators of depletion or metasomatism. The wide distribution of kimberlites hosting garnet xenocrysts allows the mapping of geochemical parameters over a broader area than usually possible. In addition, the difference in age between Group II and Group I kimberlites allows the comparison of the same volume of SCLM during different intervals of the Jurassic-Cretaceous intrusive episode in areas where these kimberlites overlap spatially.

Methods

We have obtained major- and trace-element analyses of 14,480 peridotitic garnets hosted in 34 Group II kimberlites and 29 Group I kimberlites (Fig.1). The kimberlites occur in environments both on and off craton. For each suite of garnet xenocrysts from a particular kimberlite, we constructed a paleogeotherm based on the Ni-in-garnet thermometer and Cr solubility barometer (Ryan et al., 1996). At the depth where garnets very low in Y become scarce, we introduce a point of inflection and run the deeper part of the geotherm parallel to the diamond-graphite stability line (O'Reilly and Griffin, 2006), similar to geotherms derived from xenolith suites in southern Africa (Finnerty and Boyd, 1987). Once the geotherm is established, all garnets are forced onto the geotherm based on their Ni temperature.

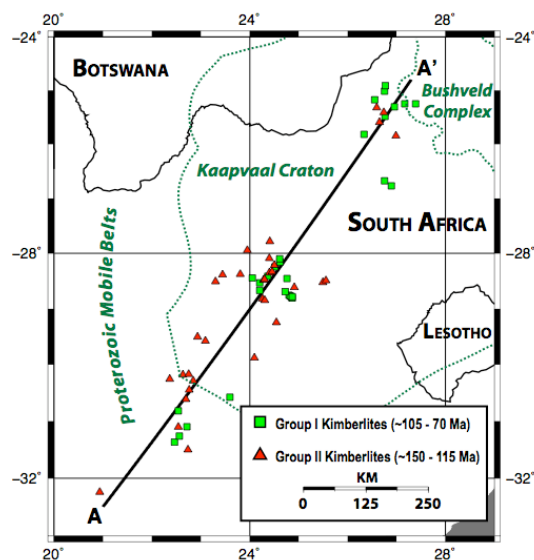


Figure 1. Location map for kimberlites and traverse line. Major tectonic units are outlined in dark green.

Assuming the kimberlites sample the mantle vertically, we have created a cross-section spanning the craton and its southwest margin (A-A'; Fig. 1). Each garnet data point is projected onto the cross-section at its interpreted depth. All kimberlites used are within 100 km surface distance of the cross-section. Then, using the spline method of Smith and Wessel (1990), we contour the Ti contents, the Zr contents, the Zr-Y ratio, and X_{Mg} of olivine co-existing with the garnets along the cross-section using a framework similar to that of Kobussen et al. (2008). We chose to use these four geochemical parameters because they are sensitive indicators of depletion and different styles of metasomatism in cratonic peridotites.

Results

For each geochemical parameter imaged, we have created two plots. The upper panels for each figure are constructed using garnets hosted in Group II kimberlites and thus sample the mantle between 150-115 Ma. The lower panels in each figure are constructed using garnets hosted in Group I kimberlites, which sample the same mantle region later (<105 Ma) during the same intrusive episode. Individual garnets are shown on each plot as open black symbols where they project onto the cross-section, enabling the visual recognition of where plot

resolution is poor. All sections have 2x vertical exaggeration.

The Ti content in garnet ranges from nearly zero to >6000 ppm (1% wt. TiO₂). Typical values for Ti in garnet in cratonic peridotites range from 1250 to 2500 ppm. Values less than 1250 ppm are considered extremely depleted and values higher than 2500 ppm indicate metasomatism. Figure 2 compares the Ti value in garnets from Group II and Group I kimberlites.

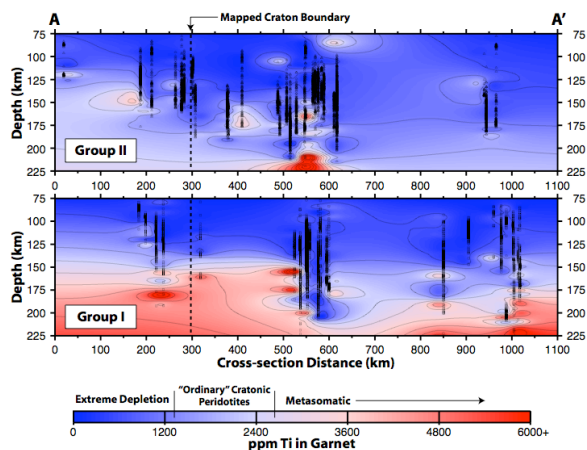


Figure 2. Contoured Ti contents in garnet hosted in Group II (top panel) and Group I kimberlites (bottom panel) along cross-section A-A' from Figure 1.

In the shallower parts of both sections the garnets have Ti contents typical of cratonic peridotites, or much more commonly with extremely depleted signatures. Garnets from the lowermost parts of the lithosphere, in contrast, show signatures typical of strongly melt metasomatised peridotites and such garnets are more common in Group I kimberlites.

The southwest part of the section (0 to 500 km) displays a huge enrichment in Ti between the emplacements of the Group II and Group I kimberlites. The Ti content of the lithospheric mantle in the Kimberley area (~500 to 600 km) is nearly unchanged during this time. It is unclear how much change there is in the northeast because of sampling patterns, but there appears to be some enrichment in Ti in the later (Group I) time slice.

The Zr contents of garnets show a different pattern of depletion/metasomatism (Fig. 3). Again, the shallower parts of both sections show a depleted signature, but the depth extent of depletion is much less and more irregular than for Ti. Particularly noticeable is the large Zr enrichment in the Kimberley area (~500-600 km along section), which can be related to the "phlogopite style" metasomatism commonly observed in xenoliths from the Kimberley area (e.g. Grégoire et al., 2002).

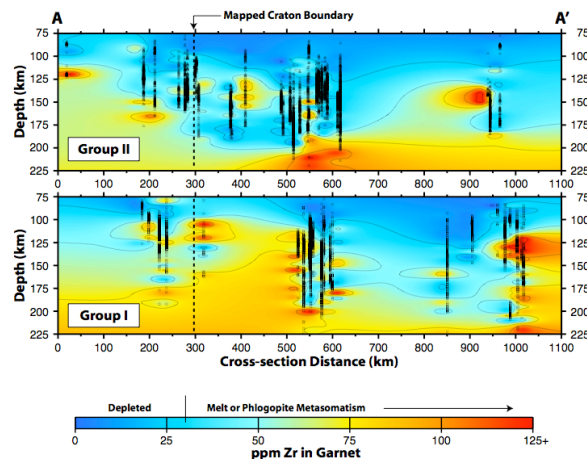


Figure 3. Zr contents of garnet plotted as in Fig. 2.

Another indicator of phlogopite-style metasomatism is the Zr-Y ratio measured in garnets (Griffin et al., 2002; Fig. 4). High ratios suggest either phlogopite metasomatism or enrichment related to extreme melt metasomatism. The overlap of high Zr values (Fig. 3) with high Zr-Y ratios (Fig. 4) in the Kimberley area during Group I time indicates phlogopite metasomatism. The phlogopite signature is not observed in the southwest part of the section where there is strong enrichment in Ti between the intrusion of Group II and Group I kimberlites (Fig. 2).

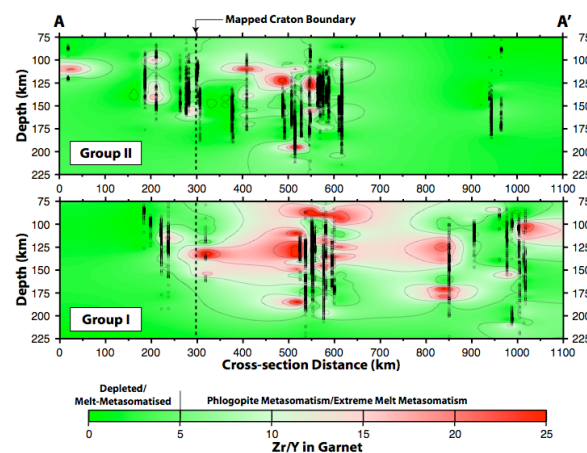


Figure 4. Measured Zr-Y ratio in garnets plotted as in Figure 2.

Finally, the X_{Mg} of olivine coexisting with the garnets was calculated using the method of Gaul et al. (2000; Fig. 5). The pattern of X_{Mg} of olivine more closely resembles the pattern observed for Ti than for Zr, but there are important differences. In the NE part of both Group II and Group I sections there is considerable Fe enrichment compared with the other shallow parts of the sections. This is not accompanied by a rise in Ti.

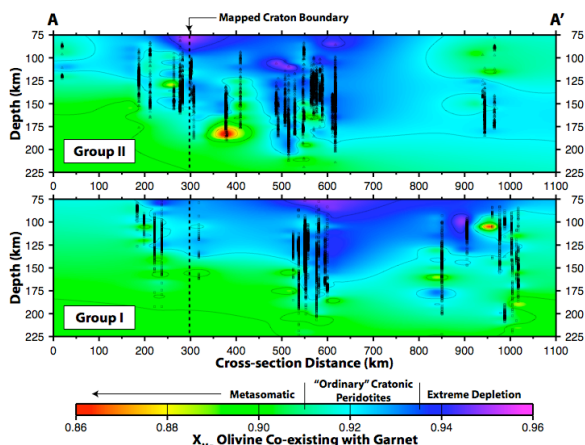


Figure 5. Calculated X_{Mg} for olivine coexisting with garnet, plotted as in Figure 2.

Discussion

Previous work on the Kaapvaal Craton using compilations of data from xenoliths/xenocrysts hosted in Group II and Group I kimberlites have indicated that there was a change in both geotherm and lithosphere chemistry between the eruption of the two groups (Griffin et al., 2003). This conclusion was supported and defined in a spatial context using garnet xenocrysts hosted in kimberlites from the Prieska cluster by Kobussen et al. (2008). In that study, we found a significant change in lithosphere chemistry as defined by Ti in garnet and the calculated X_{Mg} of coexisting olivine in a short and well-defined time window of 9 m.y. between the eruption of the Group II and Group I kimberlites.

Here we confirm this conclusion, but find that the change in lithosphere chemistry appears to be more complex than previously proposed. In the Kimberley area, the changes observed between the eruption of the Group II and Group I kimberlites are dominated by phlogopite-style metasomatism in which garnets are enriched in Zr, but not in Ti and Y.

Melt-related metasomatism is the most likely cause of large-scale modification of the lithosphere in the Prieska area along the SW part of the section (Gurney and Harte, 1980; Kobussen et al., 2008). Bell et al. (2003) suggest that silicate melts might more easily be able to penetrate and metasomatise formerly depleted Proterozoic-age lithosphere due to zones of weakness or melt pathways along tectonic boundaries. This type of infiltration could be assisted by changes in the stress field associated with the opening of the South Atlantic (Bailey, 1992).

Acknowledgements

We thank De Beers and its staff (especially Dave Apter, Rob Preston, Jock Robie, Simon Shee and Bruce Wyatt) for data, discussions and much assistance.

References

- Bailey, D. K., 1992. Episodic alkaline igneous activity across Africa: Implications for the causes of continental break-up. In Storey, B. C. et al., eds. *Magmatism and the causes of continental break-up: Geological Society [London] Special Publication 68*, 91-98.
- Bell, D. R., Schmitz, M. D., and Janney, P. E., 2003. Mesozoic thermal evolution of the southern African mantle lithosphere. *Lithos*, 71, 273-287.
- Finnerty, A. A., and Boyd, F. R., 1987. Thermobarometry for garnet peridotite xenoliths: A basis for mantle stratigraphy. In Nixon, P. H. ed., *Mantle Xenoliths: Chichester, UK, Wiley*, p. 381-402.
- Gaul, O. F., Griffin, W. L., O'Reilly, S. Y., Pearson, N. J., 2000. Mapping olivine composition in the lithospheric mantle. *Earth and Planetary Science Letters*, 182, 223-235.
- Grégoire, M., Bell, D. R., and le Roux, A. P., 2002. Trace element geochemistry of phlogopite-rich mafic mantle xenoliths: their classification and their relationship to phlogopite-bearing peridotites and kimberlites revisited. *Contributions to Mineralogy and Petrology*, 142, 603-625.
- Griffin, W. L., Fisher, N. I., Friedman, J. H., O'Reilly, S. Y., Ryan, C. G., 2002. Cr-pyrope garnets in the lithospheric mantle 2. Compositional populations and their distribution in time and space. *Geochemistry, Geophysics, Geosystems*, 3, doi:10.1029/2002GC000298.
- Griffin, W. L., O'Reilly, S. Y., Natapov, L. M., and Ryan, C. G., 2003. The evolution of lithospheric mantle beneath the Kalahari Craton and its margins. *Lithos*, 71, 215-241.
- Gurney, J. J., and Harte, B., 1980. Chemical variation in upper mantle nodules from southern African kimberlites. *Philosophical Transactions of the Royal Society of London, Series A*, 297, 273-293.
- Kobussen, A. F., Griffin, W. L., O'Reilly, S. Y., and Shee, S. R., 2008. Ghosts of lithospheres past: Imaging an evolving lithospheric mantle in southern Africa. *Geology* 36, 515-518.
- O'Reilly, S. Y., and Griffin, W. L., 2006. Imaging global chemical and thermal heterogeneity in the subcontinental lithospheric mantle with garnets and xenoliths: Geophysical implications. *Tectonophysics*, 416, 289-309.
- Ryan, C. G., Griffin, W. L., and Pearson, N. J., 1996. Garnet geotherms: Pressure-temperature data from Cr-pyrope garnet xenocrysts in volcanic rocks. *Journal of Geophysical Research*, 101, 5611-5625.
- Smith, C. B., 1983. Pb, Sr and Nd isotopic evidence for sources of southern African Cretaceous kimberlites. *Nature*, 304, 51-54.
- Smith, C. B., Allsopp, H. L., Kramers, J. D., Hutchinson, G., and Roddick, J. C., 1985. Emplacement ages of Jurassic-Cretaceous South African kimberlites by the Rb-Sr method on phlogopite and whole-rock samples. *South African Journal of Geology*, 88, 249-266.
- Smith, C. B., Clark, T. C., Barton, E. S., Bristow, J. W., 1994. Emplacement ages of kimberlite occurrences in the Prieska region, southwest border of the Kaapvaal Craton, South Africa. *Chemical Geology*, 113, 149-169.
- Smith, W. H. F., and Wessel, P., 1990. Gridding with continuous curvature splines in tension. *Geophysics*, 55, 293-305.

Diamondiferous microxenoliths and xenocrysts from the Nyurbinskaya kimberlite pipe, Yakutia

Vladimir Malkovets^{1,2}, Dmitry Zedgenizov¹, William Griffin², Alexey Dak³,
Suzanne O'Reilly², Nikolai Pokhilenko¹, Sergei Mityukhin⁴

¹ Institute of Geology and Mineralogy SB RAS, Novosibirsk, Russia (vladimir.malkovets@gmail.com)

² GEMOC, Australian Research Council National Key Centre, Department of Earth and Planetary Sciences, Macquarie University, Sydney, Australia;

³ Savannah Diamonds Limited, Tanzania;

⁴ ALROSA Co. Ltd, Mirny, Russia

Introduction

Mineral inclusions in diamonds and their intergrowths provide important information about the composition of the subcontinental lithospheric mantle involved in the processes of diamond formation. Newly discovered kimberlitic pipes of the Nakyn kimberlite field (Yakutia) are characterised by the very high proportion (more than 50%) of diamonds of eclogitic paragenesis (Botuobinskaya pipe; Mityukhin, Spetsius, 2005). Here we present the new results of study of five samples of diamondiferous microxenoliths and garnet xenocrysts from the Nyurbinskaya kimberlite pipe, located in this field. The studied samples are microxenolith of diamondiferous peridotite, microxenolith of diamondiferous eclogite, and 3 intergrowths of single pyrope grains with diamonds. Samples are up to 4 mm in diameter and all of them fall in a sieve class -4+2 mm.

Geological Background

The Nakyn kimberlite field is located in the east of the Siberian platform, in the Vilui-Markha deep fault zone, a northeast-trending structure associated with the middle Paleozoic Vilui rift system. The well-known Mir pipe (Malobotuobia kimberlite field) also is located in that zone ~350 km southwest of the Nakyn field, a magmatic complex that includes tholeiitic and alkaline basalts, kimberlites, and explosion breccias (Tomshin et al., 1998). Only two kimberlite pipes (Botuobinskaya and Nyurbinskaya) have been discovered; both are diamondiferous. The kimberlites originally intruded an early Paleozoic terrigenous-carbonate sequence and were covered by Jurassic terrigenous sediments 30-80 m thick. The Rb-Sr isochron method gives an age of 364 +/-9 Ma for the Botuobinskaya pipe and 364 +/-5 Ma for the Nyurbinskaya pipe (Agashev et al., 2001).

Sample Description

Samples Nyurb-1, Nyurb-2 and Nyurb-3 are intergrowths of single pyrope grains with diamonds. Nyurb-1 sample consists of purple pyrope grain and irregular intergrowth of several diamonds of octahedral habit (Fig. 1 and 2a). Nyurb-2 is intergrowth of purple pyrope grain and single diamond crystal of octahedral habit (Fig. 2b). Nyurb-3 is red pyrope grain with a

system of parallel cracks. Two diamond crystals of octahedral habit found along one of such cracks. Both diamonds are colorless and have step-like structure of octahedral surfaces (Fig. 2c).



Figure 1: Nyurb-1 - pyrope xenocryst and irregular intergrowth of several diamonds of octahedral habit. Width of sample ~4 mm.

Clinopyroxene of the diamondiferous biminerall eclogite microxenolith (Nyurb-4) is completely altered. Diamond in this xenolith is colorless step-like octahedron with slightly rounded edges (Fig. 2d).

Microxenolith of diamondiferous peridotite (Nyurb-5) mainly consists of two large diamond crystals. Cpx, Grt and Chr are fresh, while Ol and Opx are completely altered. Diamonds are colorless crystals of cubooctahedral shape (Fig. 2e). One diamond crystal contains mineral inclusion of chromite and olivines (Ol - visual identification). The chromite diamond inclusion was exposed to the surface by polishing and studied *in situ*.

Mineral Chemistry

The compositions of the primary phases and chromite diamond inclusion (Nyurb-5) are presented in Figure 3 and Tables 1 and 2. Garnets in all samples are homogeneous. Pyropes from heavy concentrate and from studied samples are plotted on the Fig. 3 for comparison.



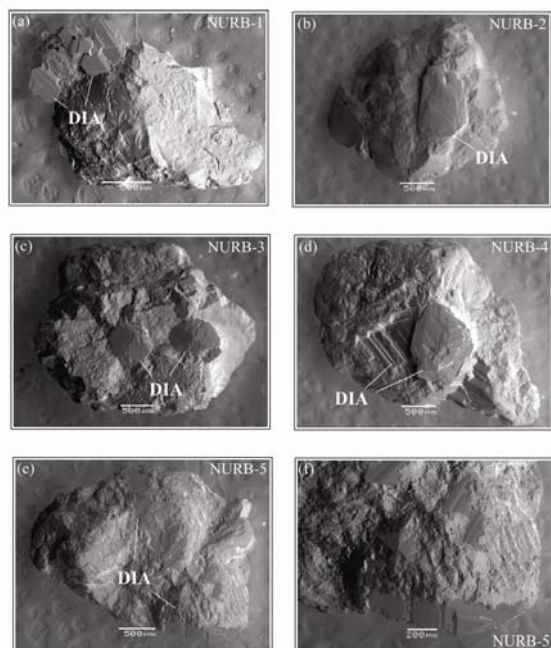


Figure 2: SEM images of individual samples.

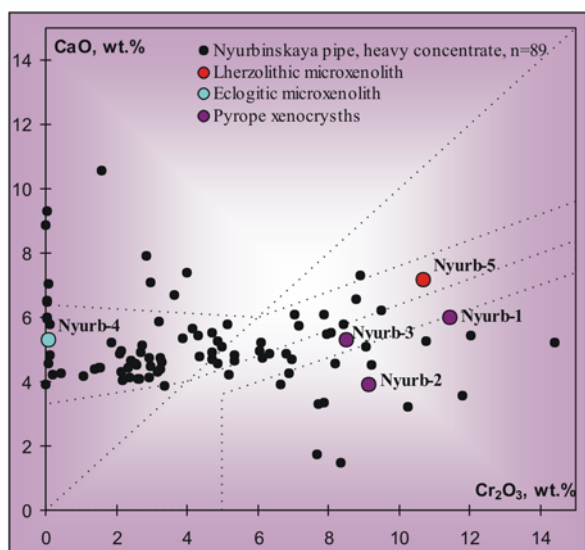


Figure 3: Cr₂O₃ vs CaO in garnets. Fields after Sobolev et al. (1973).

Nyurb-1 and Nyurb-2 are high-chromium subcalcic pyropes with Cr₂O₃ - 11.4% and 9.1%, and CaO contents - 6% and 3.9%, accordingly. Nyurb-3 is lherzolitic pyrope (Cr₂O₃ - 8.5%, CaO - 5.3%). Garnet composition from the eclogitic microxenolith (Nyurb-4) corresponds to pyrope-almandine series (65.8Pyr21.3Alm7.9Gross). The contents of CaO, Cr₂O₃, and TiO₂ are 5.3, 0.09 and 0.53 wt.%, accordingly.

Garnet from peridotitic microxenolith has a high CaO (7.1%) content and fall into lherzolitic field (Cr₂O₃ - 10.8%). Chromite from xenolith fall into diamond inclusion field (Cr₂O₃ - 63.6%, TiO₂ - 0.61%). Chromite diamond inclusion has lower TiO₂ - 0.09%

and FeO - 16.0%. Chromite diamond inclusion also has lower Fe³⁺ content than chromite from xenolith and Fe³⁺/(Cr+Al+Fe³⁺) ratio fall into typical worldwide chromite diamond inclusion range from 0 to 0.06 (Fig.4; Malkovets et al., 2007).

Table 1: Composition of garnets.

Sample Mineral	Nyurb-1 Gar	Nyurb-2 Gar	Nyurb-3 Gar	Nyurb-4 Gar	Nyurb-5 Gar
SiO ₂	40.7	41.7	41.8	40.9	41.2
TiO ₂	0.28	0.08	0.20	0.53	0.20
Al ₂ O ₃	14.3	16.4	16.7	21.8	15.1
Cr ₂ O ₃	11.4	9.12	8.52	0.09	10.7
FeO	7.03	7.30	7.35	15.0	7.23
MnO	0.43	0.42	0.42	0.44	0.47
MgO	19.2	20.8	19.7	15.6	17.9
CaO	5.99	3.93	5.30	5.32	7.16
Na ₂ O	0.07	0.02	0.03	0.14	0.01
K ₂ O	0.002	0.004	0.008	0	0.017
Total	99.49	99.79	99.97	99.89	99.91

Table 2: Composition of clinopyroxene and chromites.

Sample Mineral	Nyurb-5 CPx	Nyurb-5 Chr DI	Nyurb-5 Chr
SiO ₂	55.6	n/d	n/d
TiO ₂	0.05	0.09	0.61
Al ₂ O ₃	1.48	6.19	5.43
Cr ₂ O ₃	3.24	64.9	63.6
FeO	1.75	16.0	18.8
MnO	0.09	0.21	0.26
MgO	15.5	11.7	10.7
CaO	19.12	n/d	n/d
Na ₂ O	2.21	n/d	n/d
K ₂ O	0.04	n/d	n/d
NiO	n/d	0.09	0.08
Total	99.07	99.17	99.48
Fe ³⁺ /(Cr+Al+Fe ³⁺)		0.018	0.032

Diamond Study

Diamond aggregate from Nyurb-1 show corrosion surface features. The individual crystals are colorless with nitrogen content from 325 to 377 ppm and aggregation state from 30 to 35 %B1. The diamond from Nyurb-2 has nitrogen content of around 100 ppm at aggregation state of 18 %B1. CL reveals their zonal structure with rounded core and octahedral overgrowth (Fig.4 a). No significant variation of carbon isotope composition is observed in this sample. Two diamonds recovered from Nyurb-3 have nitrogen content varying from 250 to 540 ppm and nitrogen aggregation state from 36 to 51 %B1. CL of one of them show cuboctahedral core overgrown with octahedron (Fig.4 b). The variations of δ¹³C is non-systematic and insignificant (-5.1 to -6.2 ‰). Diamonds from Nyurb-5 with nearly cubic habit have nitrogen content and aggregation state in both crystals is closely similar (660-690 ppm and 10-13 %B1 accordingly). They show complex growth history with changing growth from octahedral to cuboid and back to octahedral (Fig.4 d). Carbon isotope ratio systematically changes from core to rim toward lighter compositions. One diamond from eclogite microxenolith (Nyurb-4) has 450 ppm nitrogen and 15 %B1 aggregation state. At least two

growth stages are deduced from CL imagery and carbon isotope variations (Fig. 4 c).

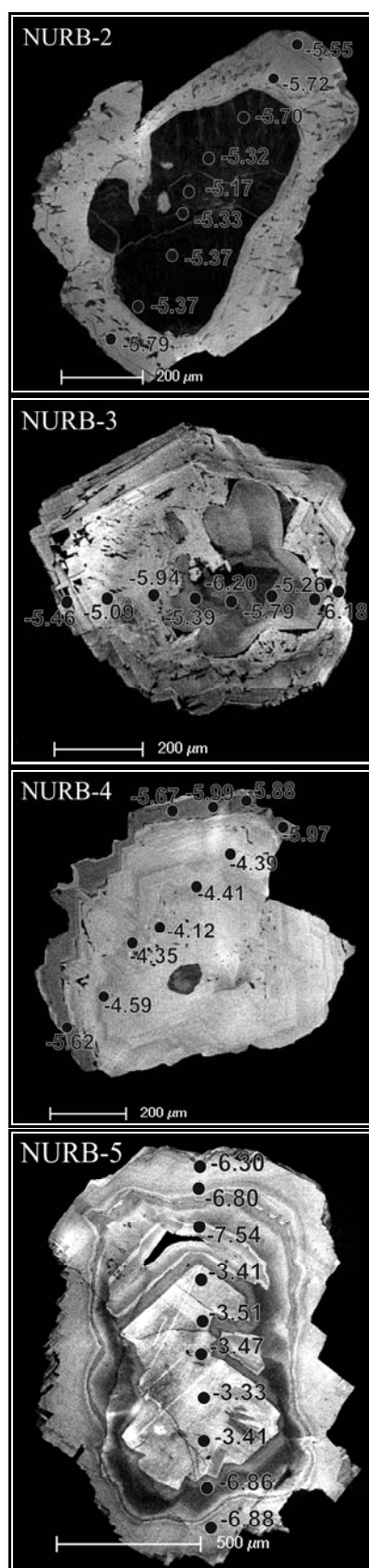


Figure 4: CL images and ion probe C-isotope data points.

Conclusions

Preliminary conclusions of this study are:

- (i) P-type garnet of studied samples are of harzburgitic to lherzolitic compositions. Garnet from diamondiferous eclogite microxenolith has high Na₂O content (0.14%), suggesting its formation under high pressure conditions.
- (ii) Typical mantle C-isotope data for our diamonds don't support the previously stated conclusion that the most diamondiferous microxenoliths from the Nyurbinskaya pipe are related to the crustal subduction (Spetsius et al., 2008).
- (iii) Diamonds from studied samples have complex growth histories with several episodes of growth and resorption. The last growth stages for some diamonds are characterized by carbon isotope evolution toward lighter compositions.

This work was supported by Russian Foundation for Basic Research grants No.08-05-00751 (V.Malkovets) and No.07-05-00345 (N.Pokhilenko), a Macquarie University Research Fellowship (V.Malkovets), Macquarie University Research Grants, and an Australian Research Council (ARC) Discovery Grant (O'Reilly, Griffin).

References:

- Agashev, A.M., Watanabe, T., Bydaev, D.A., Pokhilenko, N.P., Fomin, A.S., Maehara, K., Maeda, J., 2001. Geochemistry of kimberlites from the Nakyn field, Siberia: evidence of unique source composition. *Geology* 29 (3), 267-270.
- Malkovets, V.G., Griffin, W.L., O'Reilly, S.Y., Wood, B.J., 2007. Diamond, subcalcic garnet, and mantle metasomatism: kimberlite sampling patterns define the link. *Geology* 35 (4), 339-342.
- Mityukhin, S.I., Spetsius, Z.V., 2005. Paragenesis of inclusions in diamonds from the Botuobinskaya pipe (Nakyn field, Yakutia). *Russian Geology and Geophysics* 46 (12), 1225-1236.
- Pokhilenko, N.P., Pearson, D.G., Boyd, F.R., Sobolev, N.V., 1991. Megacrystalline dunites: sources of Siberian diamonds. *Carnegie Institution of Washington Yearbook* 90, 11-18.
- Sobolev, N.V., Lavrent'ev, Y.G., Pokhilenko, N.P., Usova, L.V., 1973. Chrome-rich garnets from the kimberlites of Yakutia and their paragenesis. *Contribution to Mineralogy and Petrology* 40, 39-52.
- Spetsius, Z.V., Taylor, L.A., Valley, J.W., DeAngelis, M.T., Spicuzza, M., Ivanov, A.S., Banzeruk, V.I., 2008. Diamondiferous xenoliths from crustal subduction: garnet oxygen isotopes from the Nyurbinskaya pipe, Yakutia. *European Journal of Mineralogy* 20, 375-385.
- Tomshin, M.D., Fomin, A.S., Kornilova, V.P., Chernyi, S.D., Yanygin, Y.T., 1998. Peculiarities of magmatic formations from the Nakyn kimberlite field of the Yakutian province. *Russian Geology and Geophysics* 39, 1693-1703.

Evolved carbonatitic kimberlite from the Batain Nappes, eastern Oman continental margin

S. Nasir⁽¹⁾, S. Al-Khribash⁽¹⁾, H. Rollinson⁽¹⁾, A. Al-Harthy⁽¹⁾, A. Al-Sayigh⁽¹⁾, A. Al-Lazki⁽¹⁾, E. Belousova⁽²⁾, F. Kaminsky⁽³⁾, T. Theye⁽⁴⁾, H.-J. Massonne⁽⁴⁾, S. Al-Busaidi⁽⁵⁾

¹Department of Earth Sciences, Sultan Qaboos University, Oman

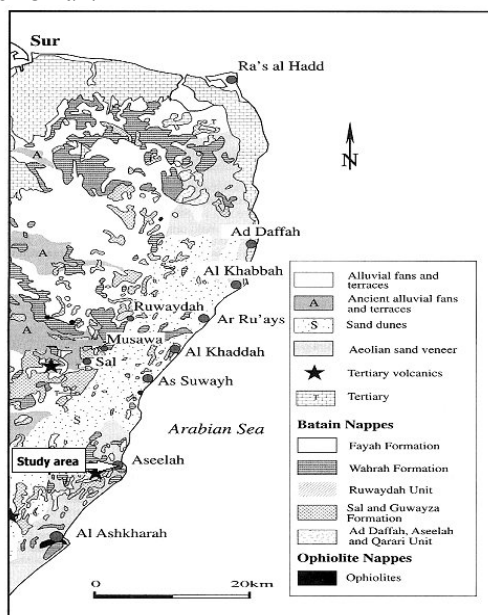
²GEMOC ARC National Key Centre, Macquarie University, Australia

³KM Diamond Exploration Ltd, Vancouver, Canada

⁴Institut für Mineralogie und Kristallchemie, Universität Stuttgart, Germany

⁵Directorate General of Minerals, Oman

The geology of northeastern Oman is dominated by the Batain nappes, which comprise an allochthonous sequence of Permian to uppermost Cretaceous marine sedimentary and volcanic rocks (Map below). At the Cretaceous-Paleogene transition (~65 Ma), oblique convergence between India and Afro-Arabia caused fragments of the early Indian Ocean to be thrust onto the Batain Basin, eastern Oman. The Lower Permian to Maastrichtian sediments and volcanic rocks of the Batain basin and fragments of the Indian Ocean floor (eastern ophiolite of Oman "Masirah ophiolite") were obducted northwestward onto the northeastern margin of Oman.



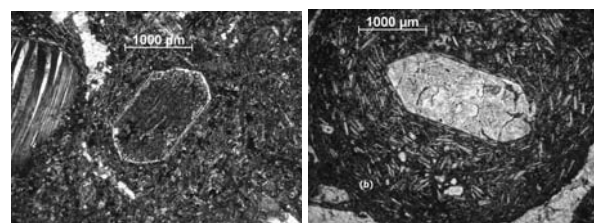
Field description and Petrography

The ultramafic lamprophyric rocks outcrop on the beach of the Asceelah village as a few, almost house-sized blocks. The diameter of the corresponding pipe is suggested to be 200-300 m. In general, the rocks are macrocrystic, spinel, and phlogopite bearing diatreme facies calcite ultramafic lamprophyres with globular

segregationary textures. The lamprophyres intrude the cherts of the Late Jurassic-Cretaceous Wahra formation of the Batain Nappe with a sharp contact. The main body of the Asceelah pipe is comprised of two rock varieties with a sharp contact between them:

(1) Heterolithic breccia (HB)

The rocks are fine-grained, carbonate-rich, and porphyritic (Left figure below). They contain olivine microcrysts and phenocrysts, which are completely pseudomorphed by chlorite, calcite, and saponite. Xenocrysts of phlogopite up to 2 cm in size, and rounded grains of chromite are common in a carbonate-phlogopite-rich matrix. The breccias have distinct autolithic structures, cemented into a carbonate matrix, and range in size from microscopic to as large as 15 cm. Large ovoidal carbonatitic xenoliths are common.



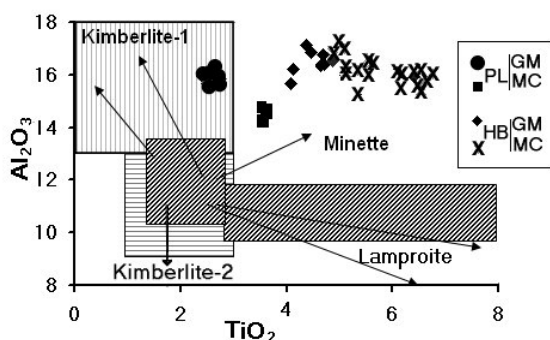
(2) Pelletal volcanoclastic lapilli tuff (PL)

The PL tuff consists of lapilli, 1-20 mm in sizes, which are composed of fine-grained aggregates of mica, magnetite, spinel, chlorite, and calcite, often with cores of mineral macrocrysts or phenocrysts (right figure above). The cored lapilli contain kernels of olivine pseudomorphs, and/or calcite which are surrounded by phlogopite-rich microlites. Xenoliths are common in the pipe of Asceelah. They comprise a suite ranging from carbonatite (up to 30 cm in diameter), discrete green chlorite xenoliths (1-8 cm) to high-alumina ultrabasic rocks (e.g., glimmerite). Abundant xenoliths of upper crustal wall rocks also occur in the pipe ranging from cherts and shales of the Wahra Formation to serpentinite.

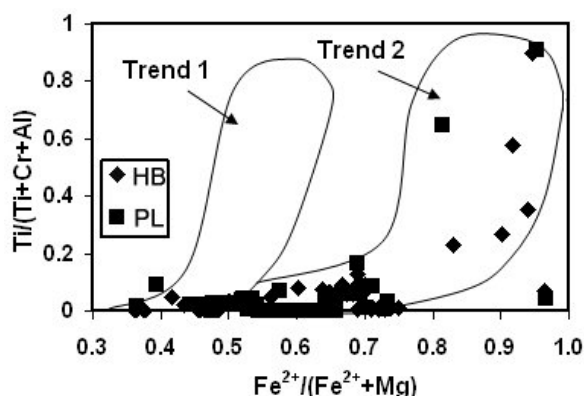
Mineralogy

Calcite is fairly pure with low SrO (up to 0.21 wt.%), MnO (up to 0.9 wt.%), MgO (up to 1.36 wt.%) and FeO (0.97 wt.%) contents.

Phlogopite grains exhibit a wide compositional range ($Mg\# = 0.69-0.86$, $Al_2O_3 = 14.2-17.4$, $TiO_2 = 2.4-6.7$ wt.%, $Cr_2O_3 = 0.03-0.57$, $BaO = 0.29-1.44$ wt. %). The figure below demonstrates that the majority of PL groundmass phlogopite plot along a trend described for kimberlitic rocks (Mitchell, 1986) whereas phlogopite from the HB plots along a trend described for minette and ultramafic lamprophyres. Matrix phlogopite in HB exhibits zoning with cores having higher Ti but lower Al and Fe contents than the rim, whereas phlogopite macrocrysts show the opposite trend.



Spinels are mostly chrome spinels with up to 5 wt. % TiO_2 , 0.6 wt. % ZnO and 0.8 wt. % MnO . Larger groundmass grains (0.04 to 0.1 mm) are zoned with titanomagnetite rims. Groundmass chromites in the PL plot on two different trends (Figure below). A small number of grains plot on the main kimberlite trend (magmatic trend 1 of Mitchell, 1986); these have higher TiO_2 contents and show Ti-enrichment as Fe^{3+} increases and the $Cr\#$ decreases.



Ilmenite falls into the "Cr-poor" population, characterized by Cr_2O_3 contents of <1 wt. % with MgO contents ranging from 4.1 to 9.9 wt.

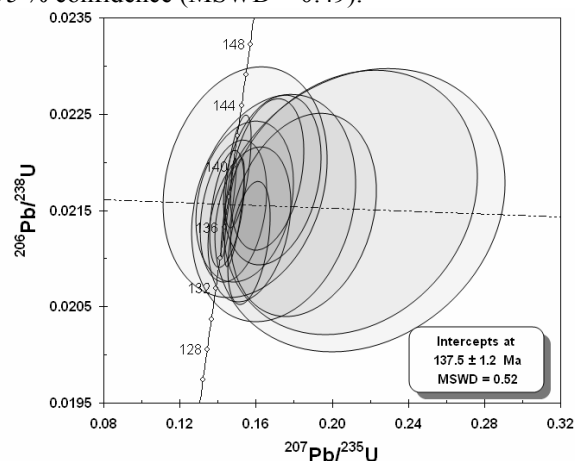
Zircon: Hafnium, Y, Yb, Lu, Th and U contents in the

Asseelah zircons show that their trace-element composition is typical of zircons found in carbonatites and kimberlites (26 % of the zircon grains classified as carbonatitic, 26% kimberlitic, and 48% as carbonatitic/kimberlitic; Belousova et al., 2002).

Other minor minerals are GO garnet, apatite, rutile, chlorite, vermiculite and serpentine.

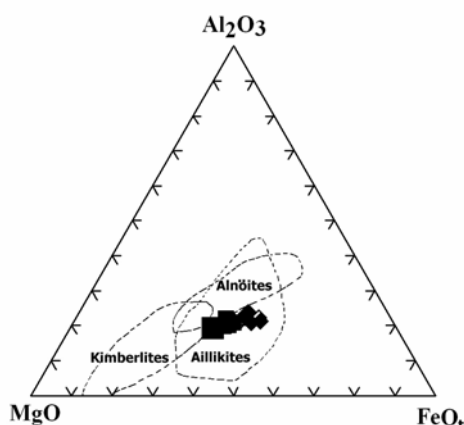
U-Pb LAM-ICPMS Geochronology

The U-Pb zircon data are plotted on a conventional concordia diagram below. All grains produced a weighted average $^{206}Pb/^{238}Pb$ age of 137.5 ± 1 Ma with 95 % confidence (MSWD = 0.49).



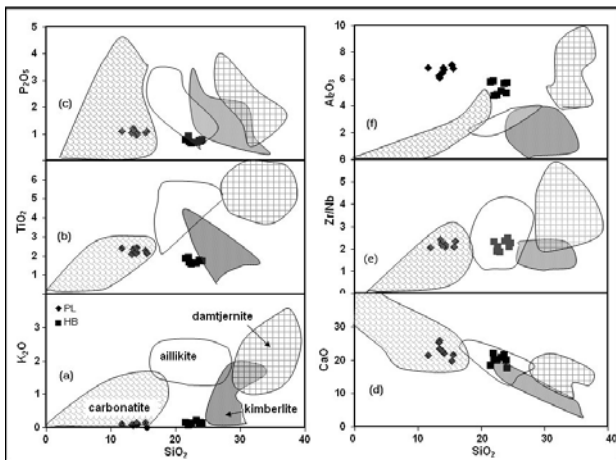
Whole Rock Geochemistry

The Asseelah rocks are characterized by low SiO_2 (11.6–24.1 wt%) and MgO contents (9.5–12.4 wt%). In the figure below, all the Asseelah rocks plot in the aillikite field.

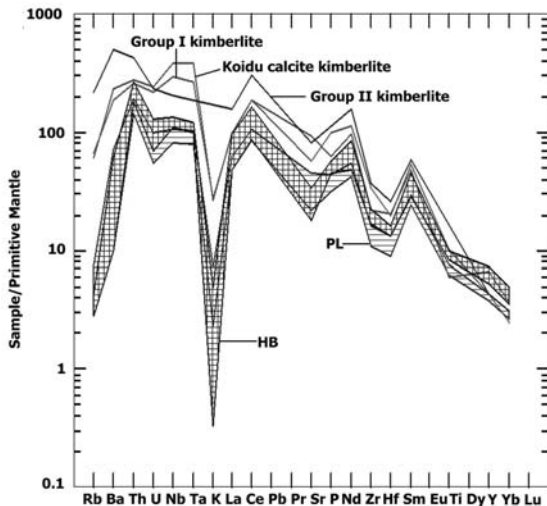


In a plot of K_2O vs. SiO_2 and TiO_2 vs. SiO_2 , the HB samples plot near the kimberlite field, whereas the PL samples plot within the carbonatite field. However, the HB samples plot within the aillikite field and the PL samples within the carbonatite field on P_2O_5 , CaO and

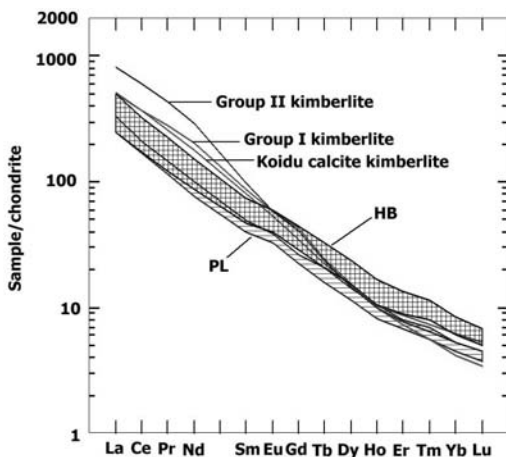
Zr/Nb vs. SiO₂ diagrams (Figure below). Both groups show K₂O depletion and Al₂O₃ enrichment (>4.75 wt.%) compared to other ultramafic rocks and carbonatite.



Trace element abundances (Figure below) show a strong enrichment in most LILE and Nb, Th, U and Pb, typical of Group-I kimberlites with small-degree partial melts.



All HB and PL samples exhibit smooth, sub-parallel patterns and steep slopes, with (La/Sm)_N of 6-10. (Figure below).



Sr-Nd and Pb Isotopes

Initial ⁸⁷Sr/⁸⁶Sr ratios (at 137 Ma) vary from 0.70472 and 0.70625, whereas initial ¹⁴³Nd/¹⁴⁴Nd ratios vary between 0.512603 and 0.512696. The ²⁰⁸Pb/²⁰⁴Pb_i ratios are high relative to MORB and group I kimberlite, but are similar to the Reunion mantle plume rocks.

Hf-isotope

The ¹⁷⁶Hf/¹⁷⁷Hf ratio in all analysed zircon grains is identical within error (0.282862 ± 12). The mean εHf for the zircons is 6.18 ± 0.42. A minimum Depleted-Mantle model age, calculated using the measured Lu/Hf ratio is 0.54 Ga. A “crustal” model age of 0.8 Ga, that gives a maximum model age, is produced when assuming a Lu/Hf ratio corresponding to the average continental crust (0.015).

Discussion

Using the whole-rock chemistry as the primary classification criterion, the Asseelah rocks should be termed either aillikite and/or magnesio-carbonatite. From the similarity in mineralogy and texture to kimberlite, aillikite, and carbonatite, coupled with evidences from specific major, and trace elements, it is possible to infer that the Asseelah rocks before evolution represent a relatively cohesive group with a restricted compositional range intermediate between kimberlite, aillikite and/or carbonatite. The highly hybrid nature of the Asseelah rocks are not likely to represent a direct crystallization product from a mantle-derived magma. The composition of the Asseelah rocks may represent the late stage magmatic evolution of kimberlitic or more likely aillikitic melt in an oceanic environment.

The characteristic incompatible element enrichment and fractionated REE patterns of the Asseelah rocks are consistent with derivation by very low degrees of partial melting of metasomatically enriched sources. The enrichment of the Asseelah aillikite source region could be a consequence of upward percolation of alkaline melt from upwelling Mesozoic mantle plumes (e.g. Reunion) that impinged on the base of the sub-continental lithosphere just prior to Gondwana break-up. In a geodynamic context, the Reunion plume is inferred to have provided both material, in the form of metasomatizing alkaline fluids or melts, and heat to initiate melting to give rise to Batain magmatism.

References

- Belousova, E.A., Walters, S., Griffin, W. L., O'Reilly, S. Y., and Fisher, N. I., 2002. Igneous zircon: trace element composition as an indicator of source rock type. *Contributions to Mineralogy and Petrology*, 143, 602-622.
- Mitchell, R. H., 1986. *Kimberlites: Mineralogy, Geochemistry and Petrology*, Plenum, New York

Late Jurassic-Early Cretaceous kimberlite, carbonatite and ultramafic lamprophyric sill and dyke swarms from the Bomethra area, northeastern Oman

S. Nasir⁽¹⁾, S. Al-Khribash⁽¹⁾, H. Rollinson⁽¹⁾, A. Al-Harthy⁽¹⁾, A. Al-Sayigh⁽¹⁾, A. Al-Lazki⁽¹⁾, E. Belousova⁽²⁾, F. Kaminsky⁽³⁾, T. Theye⁽⁴⁾, H.-J. Massonne⁽⁴⁾, S. Al-Busaidi⁽⁵⁾

¹Department of Earth Sciences, Sultan Qaboos University, Oman

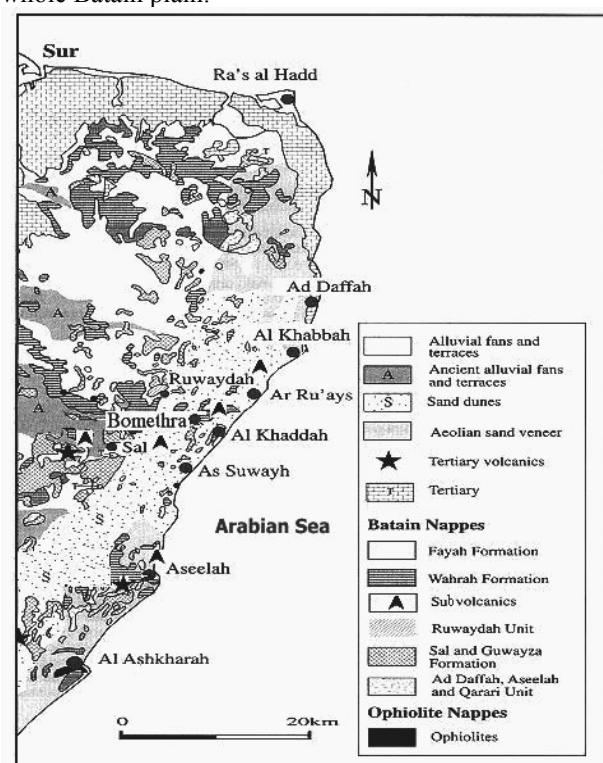
²GEMOC ARC National Key Centre, Macquarie University, Australia

³KM Diamond Exploration Ltd, Vancouver, Canada

⁴Institut für Mineralogie und Kristallchemie, Universität Stuttgart, Germany

⁵Directorate General of Minerals, Oman

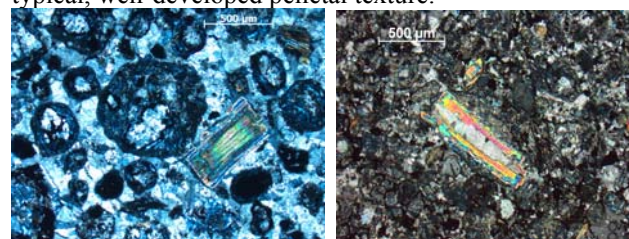
The Batain Nappes in Oman is represented by an allochthonous unit mainly consists of sedimentary rocks with subordinate volcanic rocks and minor intrusions, deposited in the Batain Basin along the eastern Oman continental margin during the Permian to the Late Cretaceous times. The allochthonous units in the Batain Plain were emplaced in a NW direction on to the Arabian plate at the Cretaceous/Tertiary boundary. The Nappes contain ophiolite, ultramafic lamprophyres, carbonatite and kimberlites occurring as pipes in the Asseelah area and as plugs, sills and dykes of several meters thick and about 6 km long in the Bomethra area. The majorities of these rocks are hosted by the Late Jurassic to Early Cretaceous Wahra Formation, which comprises a series of radiolarian cherts, shales and clay stones, and are found over the whole Batain plain.



Petrography and Mineralogy

The dyke and sill swarms are located approximately 20 km northeast of the Aseelah pipe (Nasir et al., 2008) in the Bomethra area (Map above). The main sill has a thickness of 1-2 m and extends to 6 km in N40°E direction. Two blows, 200x500 m exposure of effusive rocks occur within the main sill. They are composed of lapilli and bombs, mixed with pieces of radiolarian cherts.

Two varieties of ultramafic rocks have been observed: one is medium- to coarse-grained mica-carbonate-rich damtjernite with abundant calcite-ocelli and/or pelletal lapilli, and the other is massive fine-grained tuffitic aillikite (Figures below). Microscopically, the damtjernite exhibits a range of textures from well-developed segregations of calcite and phlogopite with abundant microlitic apatite and phlogopite, to the more typical, well-developed pelletal texture.

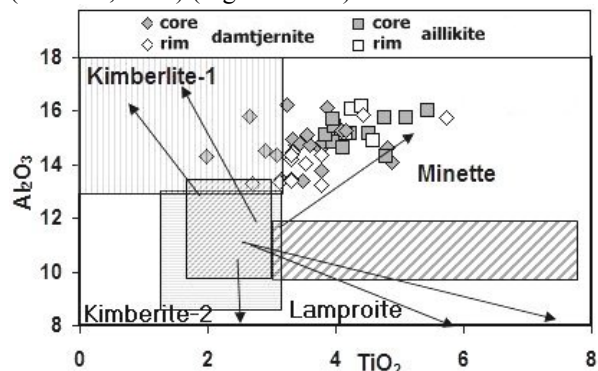


The groundmass in both varieties is composed of mainly of calcite, phlogopite, and apatite. Cr-Spinel, magnetite and rutile are common. Orthoclase, diopside and richterite occur mainly in the damtjernite.

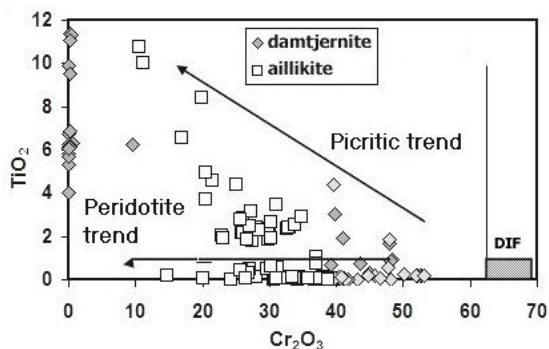
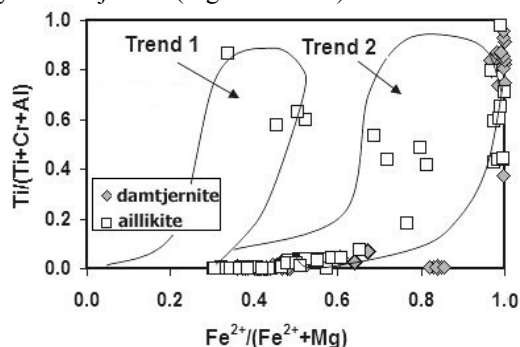
Carbonate typically occurs together with phlogopite and apatite as fine-grained (<0.1 mm) aggregates of xenomorphic grains in the ground mass. Primary Sr-bearing calcite (0.1 to 0.15 wt%) is the dominant carbonate phase and is commonly present in the groundmass of all samples.

Apatite is a late-crystallizing groundmass phase. The grains are euhedral, prismatic with hexagonal base sections. Abundant apatite occurs as acicular grains and as larger more prismatic grains grown primarily within calcite segregations. They are relatively Si-rich (0.9-1.8 wt% SiO₂) and Sr-poor (<1.5 wt% SrO).

Phlogopite is a major constituent in the Bomethra ultramafic rocks, generally forming > 30 vol. % of the mineral assemblage. It occurs as euhedral six-sided macrocryst, phenocrysts, and unehedral microphenocrysts and as small groundmass crystals characterized by subhedral to euhedral laths (0.05 to 0.1 mm). The phlogopite is titania aluminous and plots along a trend described for minette and alnöite rocks (Mitchell, 1986) (Figure below).



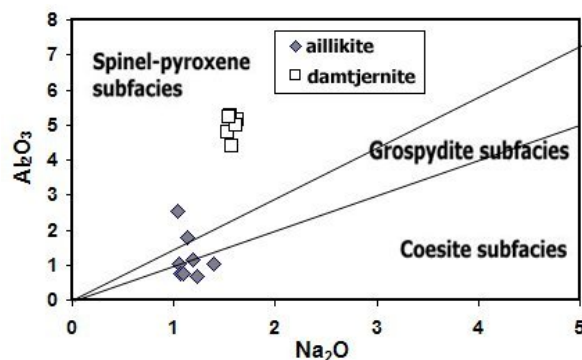
Spinel is a ubiquitous mineral phase in all samples. It occurs as macrocrysts, primary groundmass minerals, and occasionally in association with ilmenite and rutile. Small (<0.2 mm) euhedral-to-subhedral spinels comprise a significant portion of the groundmass mineral assemblage of both aillikite and damtjernite. TiO₂ contents are typically <1 wt.%, increasing with evolution to as high as ≈11.5 wt.%. Two separate evolutionary trends of primary magmatic groundmass spinels are found: magnesian ulvöspinel magmatic trend (trend 1) and titanomagnetite magmatic trend (trend 2). The former occurs in the aillikite groundmass spinels, while the latter is characteristic only of damtjernite (Figures below).



One forsteritic olivine grain and one G4 garnet grain, beside abundant chromite grains were recovered from the heavy mineral concentrates. Garnet grain has a size

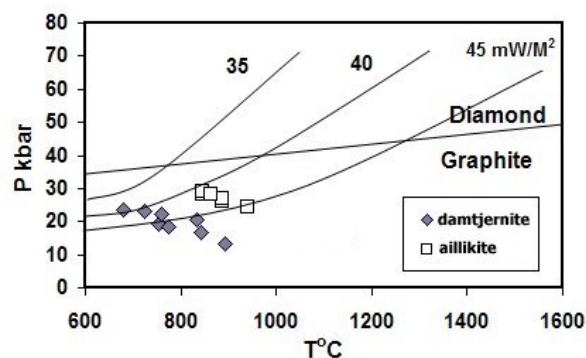
of 0.43 x 0.35 mm. It is a spalled, oval-flattened, pale yellow-orange grain. Pure orthoclase occurs only in the damtjernite.

Cr-diopside and richterite occur sporadically in the carbonate groundmass. Diopside from the damtjernite has lower Al₂O₃ and Na₂O than those from the aillikite (Figure below). Rutile, chlorite and serpentine are common accessory minerals.



P-T estimation

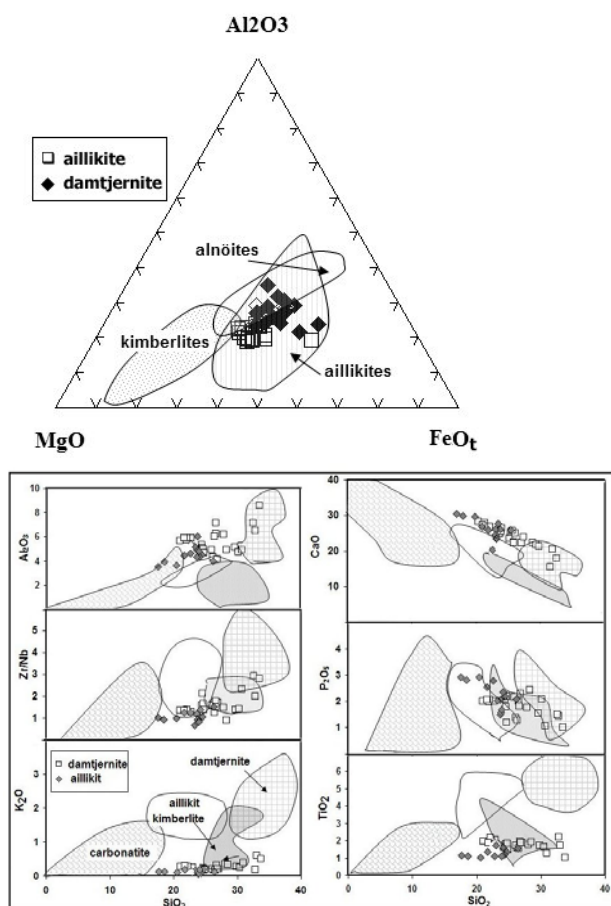
The crystallization pressure of clinopyroxene as estimated by the clinopyroxene barometer of Nimis (1995) can be bracketed between 1.3 and 2.4 GPa for the damtjernite and between 24-29 GPa for the aillikite. Temperatures vary between 680 and 890°C for the damtjernite and between 840-940°C for the aillikite, (Figure below).



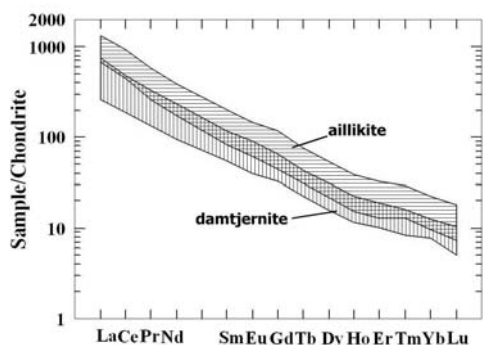
Whole Rock Geochemistry

The Bomethra rocks are strongly silica undersaturated (17-34 wt. % SiO₂), with high Al₂O₃ (3.5-9.5 wt.%) and variable TiO₂ (1-3 wt.%). They have low MgO (5-11 wt. %), which never approach MgO-values similar to kimberlites. The Bomethra rocks have petrographic and geochemical affinities with aillikite. On the FeO_T-MgO-Al₂O₃ ternary discriminant plot, and SiO₂ vs. selected major elements (Figures left below), these rocks generally fall in the aillikite field.

The incompatible trace element abundances show a significant enrichment in most elements, particularly Nb, Ta and LREEs and pronounced troughs at Rb, K, Pb, P, Hf, and Ti (Figure left below).



The REE patterns are all remarkably similar and show strong LREE enrichment with La_n/Yb_n between 30-70 (Figure below).



K-Ar whole rock age dating yielded an age between 130-140 Ma, similar to that of the Asseelah aillikites and carbonatites (Nasir et al., 2008). The initial Sr, Nd and Pb isotope compositions of the aillikite and damtjernite have strong affinity with ultramafic lamprophyres and are similar to the Reunion mantle plume

Discussion

The Bomethra rocks show very low SiO₂ and MgO contents, much lower than most common alkaline magmas. They have petrographic and geochemical affinities with aillikite, damtjernite, and kimberlite, and resemble experimentally produced melts of synthetic carbonated garnet peridotite in the simple CMAS-CO₂ system close to 3 GPa. The high abundance of REE and most incompatible elements may be interpreted as a result of derivation from a lower degree of partial melts or due to enrichment in the mantle source. The K and Ti depletions may be related to a residual phlogopite phase in the source mantle during partial melting. The abundance of magmatic carbonate suggests that the primary magmas were derived from a carbonated mantle. The initial Sm-Nd and Pb isotope are close to the value of the Reunion mantle plume.

There is no obvious age progression for the various types of magmatic activity in the Batain Nappes. It is quite possible, therefore, that all of the magmatic rocks seen in the Batain plain originated in a single event, triggered by the arrival of upwelling mantle plume beneath the metasomatised Indo-Arabian lithosphere. The influx of heat caused melting of the carbonated garnet peridotite asthenospheric mantle forming carbonatite, aillikite, damtjernite and other more fractionated alkaline magmas. The Late Jurassic-Early Cretaceous magmatism in eastern Oman is related spatially and compositionally to mantle upwelling associated with the Reunion mantle plume.

References

- Mitchell, R. H., 1986. Kimberlites: Mineralogy, Geochemistry and Petrology, Plenum, New York
- Nasir S., Al-Khribash, S, Rollinson, H., Al-Harthy, A., Al-Sayigh, A., Al-Lazki, A., E. Belousova, E. Kaminsky, F., Theye, T., Massonne H-J., Al-Busaidi, S. 2008. Evolved carbonatitic kimberlite from the Batain Nappes, eastern Oman continental margin. 9IKC-A- 00002.
- Nimis, P 1995. A clinopyroxene geobarometer for basaltic systems based on crystal-structure modeling. Contribution to Mineralogy and Petrology, 121, 115-125

Archean Lithospheric mantle: its formation, its composition and today's refertilised remains

Suzanne Y. O'Reilly¹, W.L. Griffin¹, Ming Zhang¹ and Graham Begg^{1,2}

¹ GEMOC ARC National Key Centre, Dept of Earth and Planetary Sciences, Macquarie University, NSW 2109, Australia, ² Minerals Targeting International PL, 17 Prowse Street, West Perth, WA 6005, Australia. (sue.oreilly@mq.edu.au) / FAX: +61298508953

Continental Archean lithospheric mantle

Archean subcontinental lithospheric mantle (SCLM) is distinctive in its highly depleted composition, commonly strong stratification, and the presence of rock types absent in younger SCLM. Is Archean SCLM part of a compositional continuum that shows a secular evolution varying broadly with the age of the last major tectonothermal event in the overlying crust, or was the Archean mantle formed in a different way in a distinctive tectonic regime? Did subduction play a major role in Archean SCLM formation? What is the composition of original Archean mantle and how much persists today?

The "typical" Archean mantle composition used in geochemical/geophysical modelling is a depleted garnet lherzolite. This composition is derived from peridotite xenoliths in kimberlites, mainly from the SW Kaapvaal Craton, and a few from Siberia. However, most such "typical" Archean xenoliths have experienced repeated metasomatism, leading to a progression from dunite/harzburgite through "depleted" lherzolite to "fertile" lherzolite, mirroring the secular evolution of the SCLM as a whole (Fig. 1; Griffin et al., 2007). Similar refertilisation processes can be studied *in situ* in peridotite massifs (e.g. Western Norway, Lherz), showing the lherzolites to be the products of melt infiltration into magnesian dunite/harzburgite protoliths (e.g. Beyer et al., 2004). The most depleted rocks are poorly represented in the published record; the bias partly reflects the collecting of rocks useful for P-T studies, but also has a geological basis. High-resolution seismic tomography of Archean cratons shows high-Vs volumes surrounded and dissected by zones of lower Vs. The low-Vs parts can be modelled using the "typical" garnet lherzolite compositions, while the higher-Vs volumes require much more depleted rocks. In detail, kimberlites avoid the high-Vs volumes to preferentially follow older zones of fluid passage and metasomatism, hence biasing our "mantle sample" toward the metasomatised zones. A revised estimate of the composition of "original" Archean SCLM yields a dunite/harzburgite

with 49% MgO, 6.6% FeO, 0.4% Al₂O₃, 0.34% Cr₂O₃ and 0.2% CaO (Griffin et al., 2008). Seismic tomography suggests that this material still underlies the bulk of Archean cratons to depths of 1 km but is poorly sampled by kimberlites. Relict Archean mantle is also imaged as buoyant high-Vs blobs in oceanic regions (see below), a likely source for "recycled" geochemical signatures in some ocean island basalts and old Os-isotope ages in abyssal peridotites. These observations provide new evidence on actual mechanisms of continental breakup and the behaviour of ancient lithospheric mantle domains.

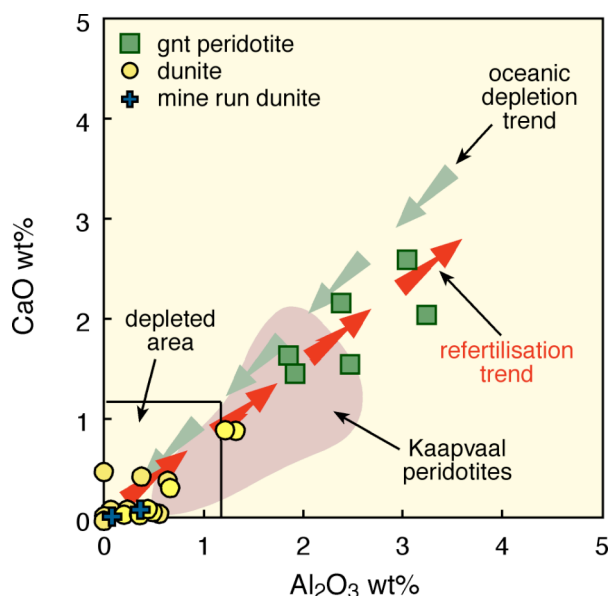


Fig. 1 The refertilisation trend shown in a depleted peridotite massif (Western Norway) mimics the compositional range of the classic Archean xenolith population from the SW Kaapvaal Craton, which usually is interpreted as a depletion trend ("oceanic trend" of Boyd, 1999). After Beyer et al. (2006).

Hf-isotope data on zircons show that much Proterozoic crust, especially in shield areas, has Archean protoliths, suggesting that the underlying SCLM also was originally Archean. Seismic tomography commonly

shows high-Vs roots, requiring depleted compositions and low geotherms, under many of these areas; clearly juvenile Proterozoic belts (e.g. SW Scandinavia) lack such roots. Re-Os isotopic data for sulfides in xenoliths from the mantle beneath some Proterozoic shields preserve Archean signatures. These observations suggest that much of the observed secular evolution in SCLM composition reflects progressive reworking of buoyant Archean SCLM, rather than secular changes in the mechanisms of SCLM production. Seismic tomography suggests that $\geq 50\%$ of existing continental crust is underlain by relict Archean SCLM, modified to varying degrees. This implies a much larger volume of originally Archean crust than currently accepted, and hence very high early crustal growth rates.

Melt-modelling exercises that treat "typical" Archean peridotites as simple residues are invalid, and cannot be used to support "lithosphere stacking" models for SCLM formation. The "primitive" Archean dunites and harzburgites are best modelled as restites and cumulates from high-degree melting at 3-6 GPa, in ascending plumes or mantle upwellings and overturns. This uniquely Archean regime may have coexisted with a more modern plate-tectonic regime, which produced weakly depleted residues similar to Phanerozoic SCLM. This "modern-type" SCLM would be inherently unstable, easily recycled and lost to the modern record.

Oceanic Archean mantle

High-resolution global seismic tomography (Fig. 2; Deen et al., 2006) images high-velocity regions, persisting in some cases to over 300 km, beneath cratons and also beneath the oceans. In the Pacific Ocean, these regions are irregularly and densely distributed and probably reflect to a large extent the widespread subduction into the upper convecting mantle in that region. However, in the Atlantic Ocean (Fig. 2) these high-velocity regions show a more regular distribution. They extend significantly towards the mid-ocean ridge from the continental margins in the 1-100km depth slice. At deeper levels, many become discrete blobs that persist to depths of up to 300km, and some of these lie directly below oceanic basalt centres including Trinidad, Ascension and Crozet, and are adjacent to parts of others such as the Cape Verde Archipelago.

Old Re-Os ages for mantle sulfides in some depleted mantle rock types beneath rift zones (e.g. Brandon et al., 2000; Wang et al., 2003) and oceanic areas (e.g. Coltorti et al., 2008) suggest that these high-velocity (inferred high-Mg and therefore low-density) blobs represent relict original Archean to Proterozoic SCLM (now refertilised to varying degrees, during episodes of mantle fluid infiltration reflecting larger-scale tectonic events), that has been mechanically disrupted and thinned during the formation of the oceanic

lithosphere. This implies that ocean basins do not form by clean breaks at now-observed continental boundaries, but that significant volumes of old mantle form buoyant volumes within the newly generated oceanic lithosphere.

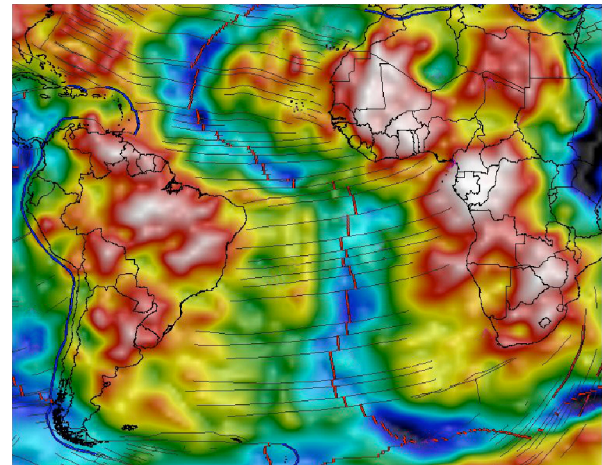


Fig. 2 Seismic tomography (Vs) slice for 0-100km for the Atlantic Ocean (from S. Grand, see Deen et al., 2006). Note the colour reversal with red spectrum for fast and blue for slow velocities.

If the higher-velocity coherent blobs observed to depths of up to 300 km below the Atlantic Ocean do represent remnant Archean mantle roots, this has important implications for the nature of global convection. Models involving large-scale horizontal components would be difficult to reconcile with these observations. Instead, convection may be dominantly in the form of upwelling vertical conduits with shallow horizontal flow (Fig. 3). The locus of these conduits may be controlled by the geometry of the margins and the coherence of the buoyant lithospheric blobs. The convective plate motions are "eddies" between these buoyant blobs and are preserved in some continental assembly configurations as the observed plate stress directions and anisotropy (e.g. Simons and van der Hilst). Mobile belts represent lithosphere accretion between the blobs.

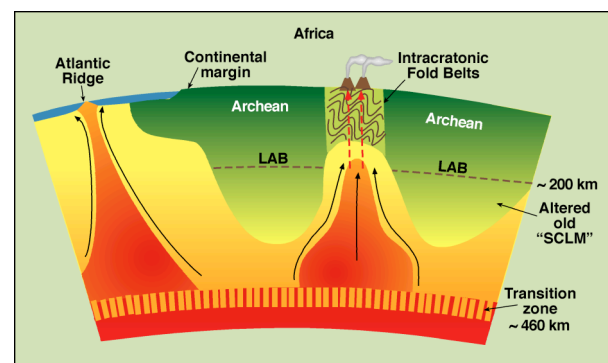


Fig. 3 Cartoon indicating how high-Vs (low-density), vertically coherent regions extending to up to > 250 km could control convection pathways.



The persistence of ancient SCLM beneath younger mobile belts and oceans also provides a logical explanation for the alphabet soup of mantle sources created by geochemists (EM1, EM2, HIMU, DMM (e.g. Hofman, 1997)). All of these geochemical fingerprints are found in lithospheric material and have been well characterised in mantle xenolith studies (e.g. Zhang et al., 2001, 2008). If lithospheric volumes persist to deep mantle levels (e.g. 250 - 300 km) then interaction with upwelling mantle can “contaminate” these plumes and fluids. The requirement for mysterious hidden source regions to provide the geochemical alphabet is removed. Magma interaction with deep ancient SCLM roots also provides a simple explanation for observations such as Archean Re-depletion model ages and old continental geochemical signatures in oceanic basalts.

Conclusions

- * The primitive Archean SCLM appears to have been much more depleted than estimates from xenoliths.
- * Seismic tomography images indicate that volumes of high-Vs ancient lithosphere (metasomatised and altered but identifiable as discrete higher velocity domains) have persisted through time and may extend to depths of at least 300 and 250 km beneath continental and oceanic regions respectively. The presence of disrupted ancient lithospheric roots in ocean basins provides new information on the mechanisms of continental breakup and mechanical disruption.
- * Magma interaction with such deep lithospheric mantle roots can explain many geochemical signatures in asthenosphere-derived primitive magmas.
- * Original Archean lithospheric mantle is apparently more extensive, both laterally and vertically, than previously considered and proposed processes for the formation of Archean lithosphere have to consider this.

References

- Beyer, E.E., Brueckner, H.K., Griffin W.L., O'Reilly, S.Y., Graham, S., 2004. Archean mantle fragments in Proterozoic crust, Western Gneiss Region, Norway. *Geology* 32, 609-612.
- Boyd F.R., 1989. Composition and distinction between oceanic and cratonic lithosphere. *Earth and Planetary Science Letters* 96, 15-26
- Coltorti M., Bonadiman C., O'Reilly S., Griffin W., Pearson N., 2008. Heterogeneity in the oceanic lithosphere as evidenced by mantle xenoliths from Sal Island (Cape Verde Archipelago). Abstracts 33rd International Geological Congress, Oslo.
- Wang, K.-L., O'Reilly, S.Y., Griffin, W.L., Chung, S.-L., Pearson, N.J., 2003. Proterozoic mantle lithosphere beneath the extended margin of the South China Block: in situ Re-Os evidence. *Geology* 31, 709-712.
- Brandon A. D., Snow J. E., Walker R. J., Morgan J. W., Mock T. D., 2000. ¹⁹⁰Pt-¹⁸⁶Os and ¹⁸⁷Re-¹⁸⁷Os systematics of abyssal peridotites. *Earth and Planetary Science Letters* 177, 319-355.
- Deen, T., Griffin, W.L., Begg, G., O'Reilly, S. Y., L.M. Natapov, L., Hronsky, J., 2006. Thermal and compositional structure of the subcontinental lithospheric mantle: Derivation from shear-wave seismic tomography. *Geochemistry, Geophysics, Geosystems* 7 (7), (doi:10.1029/2005GC001120).
- Griffin, W.L., O'Reilly, S.Y., 2007. The earliest subcontinental mantle. In: Van Kranendonk, M.J., Smithies, R.H. and Bennett, V.C. (eds.), *The Earth's Oldest Rocks*. Elsevier, Amsterdam pp 1013-1035.
- Griffin, W.L., O'Reilly, S.Y., Afonso, J.C., Begg, G.C., 2008. The Composition and Evolution of Lithospheric Mantle: A Re-evaluation and its Tectonic Implications. *Journal of Petrology* (accepted June 2008).
- Hofmann, A.W., 1997. Mantle geochemistry: the message from oceanic volcanism: *Nature* 385, 219-229.
- Simons, F.J., van der Hilst, R.D., 2003, Seismic and mechanical anisotropy and the past and present deformation of the Australian lithosphere. *Earth and Planetary Science Letters* 211, 271-286.
- Zhang, M., Stephenson, J., O'Reilly, S.Y., McCulloch, M.T., Norman, M., 2001. Petrogenesis of late Cenozoic basalts in North Queensland and its geodynamic implications: trace element and Sr-Nd-Pb isotope evidence. *Journal of Petrology* 42, 685-719.
- Zhang, M., Wang, K.-L., O'Reilly, S.Y., Hronsky, J., Griffin, W.L., 2008. Flood Basalts and Metallogeny: The Lithospheric Mantle Connection. *Earth Science Reviews* 86, 145-174.

In-situ isotope ratio measurement: a decade of development of applications for mantle peridotites and kimberlites

N.J. Pearson, W.L. Griffin, S.Y. O'Reilly

GEMOC Key Centre, Department of Earth and Planetary Sciences, Macquarie University, NSW 2109, Australia;
npearson@els.mq.edu.au

In the last decade the geochemistry and geochronology of kimberlites and mantle xenoliths has advanced dramatically through the precise in-situ measurement of trace element compositions and isotope ratios. This increased analytical capability is the product of coupling a laser-ablation microprobe (LAM) to an induced coupled plasma mass spectrometer (ICP-MS) and the rapid development of the multi-collector (MC-) ICP-MS. The higher precision of the MC-ICP-MS has enabled the development of in-situ high precision isotope ratio measurements for a range of geologically important isotopic systems (e.g. Rb-Sr, Nd-Sm, Lu-Hf, Re-Os). The impact of these advances is that the isotopic data can be used to place constraints on the timing of processes in the lithosphere and to better characterize the nature of these processes. In-situ analysis also allows the isotopic data to be interpreted within a microstructural context and the acquisition of multiple datasets (e.g. trace REE-Pb, PGE-Os, Pb-Hf, Pb-Os) on single grains or parts of grains.

The MC-ICPMS has been developed to a level where the typical within-run (internal) precision and between-run (external) precision for solution analyses are comparable to those for thermal ionization mass spectrometers (TIMS). The introduction of the second-generation sector-field MC-ICPMS brought a number of advantages over the quadrupole ICPMS, including simultaneous detection, flat-topped peaks and greater sensitivity. All of these factors contributed to the more precise measurement of isotope ratios that made the results from the MC-ICPMS directly comparable with those obtained by TIMS. The MC-ICPMS has two great advantages over TIMS: (1) due to the high efficiency of the ICP source to ionise refractory elements, the MC-ICPMS has become the instrument of choice to investigate mass-dependent isotopic fractionation of stable isotopes of light and heavy metals (e.g. Li, Mg, Fe, Cu, Mo, Tl); (2) a LAM system can be coupled to the MC-ICPMS for in situ high-precision microanalysis of isotopic ratios. This has led most notably to the combined U-Pb and Lu-Hf isotopic analysis of zircon (e.g. Griffin et al. 2000) as well as studies of a range of other radiogenic isotopic systems (e.g. Sr - Schmidberger et al., 2003, Neumann et al., 2004; Woodhead et al., 2005; Nd - Foster & Vance, 2006, McFarlane & McCulloch, 2007; Os -

Pearson et al., 2002, Alard et al. 2002, Aulbach et al., 2004).

There are many advantages to be gained by LAM-MC-ICPMS analysis, the most important being the potential information that can be obtained at the high spatial resolution. Like other microanalytical techniques laser ablation MC-ICPMS produces data that can be interpreted in a spatial context and integrated with microstructural and other geochemical datasets. Other advantages include the removal of the sample digestion and chemical purification procedures, high sample throughput, little or no memory and no solvent interferences. Despite the advances in recent years there remains a perception that the accuracy and precision of the in-situ measurements suffer in comparison to solution measurements because of matrix effects and isobaric interferences.

Many factors contribute to the accuracy and precision of in-situ measurements. These can be considered as the interplay between parameters related to the sample, the laser operating conditions and processes in the mass spectrometer. In the in-situ studies that have concentrated on radiogenic isotope systems the elements of interest are trace or minor elements in common rock-forming minerals (e.g. Sr in clinopyroxene, carbonate, feldspar, perovskite) or accessory phases (e.g. Hf in zircon, rutile; Nd in apatite, titanite; Os in mantle sulfide). The precision of an individual measurement is primarily a function of the number of ions counted and therefore depends on the concentration of the element in the mineral, the size of the laser pit, the sensitivity of the mass spectrometer and the counting time. In comparison with conventional solution analysis, the added complexity associated with the in-situ method primarily concerns the 'dirty' nature of the sample. This may cause matrix effects that can change instrumental mass fractionation and produce isotopic interferences (isobaric and other molecular overlaps) that also require procedures to correct mass bias. Isobaric interferences present a major problem in nearly all of the radiogenic isotopic systems of most interest: ^{87}Rb on ^{87}Sr , ^{144}Sm on ^{144}Nd , ^{176}Lu and ^{176}Yb on ^{176}Hf , ^{187}Re on ^{187}Os . As a consequence, precision is also dependent on the parent-daughter ratio in the mineral, as well as the absolute element abundances.



The combination of the size of the mineral grain and the sensitivity of the mass spectrometer dictates the size of the laser pit (static hole or traverse) or whether multiple analyses can be undertaken to investigate zoning. In some cases the laser is used simply as a solid-sampling device in order to maximise the volume of material introduced in the mass spectrometer, thereby homogenising the sample but improving precision. The alternative approach is to use the laser as a microprobe to add isotopic data to internal variations identified using optical images or other geochemical data. This technique invariably involves using a smaller spot size with the consequent effect on precision. In deciding which approach to use it is worth considering that the first may give a very precise but geologically meaningless result if the sample is heterogeneous. This is also true for the comparison of data obtained by solution analysis of mineral separates and by LAM-MC-ICPMS.

The two most significant developments in LAM-MC-ICPMS in the past decade have been the analysis of Lu-Hf isotopes in zircon and Re-Os isotopes in sulfides and PGE alloys. Zircon and the sulfide minerals represent micro time capsules for the crust/mantle and mantle respectively, and the isotopic studies provide information about the evolution of each layer. By determining the timing of events in the crust and the underlying lithospheric mantle, linkages between crustal and mantle processes can be assessed and used to address key problems in geodynamics.

Zircon megacrysts represent a late stage in the crystallisation of the magmas that produced the low-Cr megacryst suite (Ol+Opx+Cpx+Gnt+Ilm+Phl+Zir) found in many kimberlites. U-Pb dating of zircon in kimberlite has been widely performed on single- and multiple-collector instruments with accuracy and precision comparable to ion microprobe techniques (e.g. Belousova et al., 2001). More recently the method has been extended to the U-Pb systematics of rutile and perovskite (Batumike et al., 2008), with the latter providing a rapid, cost-effective method for dating eruption ages of kimberlites.

Griffin et al. (2000) were the first to demonstrate the significance of the isotopic composition of Hf in mantle-derived zircon megacrysts as an indicator of the sources of the parent magmas and the interaction of these magmas with the cratonic lithosphere. The study included zircons from African, Siberian and Australian kimberlites, with a range in age from 90 Ma to 2500 Ma. Most of the zircons have ϵHf values between 0 and 10, but values down to -16 were obtained. In plots of Nd-Hf isotopes the Group I and Group II kimberlites define long trends pointing to low values below the terrestrial array. Combined with published Nd data on the silicate members of the low-Cr megacryst suite, the Hf isotopic data indicate crystallisation of zircon from magmas also lying well below the terrestrial array. The depleted and metasomatised lherzolites and harzburgites that make up much of the Archean lithospheric mantle have Lu/Hf ratios (≤ 0.15), low enough to account for the lowest ϵHf observed in the zircons over time spans of

1–3.5 Ga. This led Griffin et al. (2000) to suggest that the magmas from which the kimberlitic zircons crystallised were derived from Depleted Mantle or OIB-type sources, and developed negative ϵHf through reaction with the subcontinental lithospheric mantle.

The development of in-situ techniques has also enabled the investigation of the scale of isotopic variation at the microscopic level. The significance of this capability is shown in a study of the origin of MARID xenoliths using in-situ analysis of Lu-Hf isotopes of rutile and zircon (Choukroun et al., 2005). The rutiles are isotopically very heterogeneous, both within and between grains, with an overall range in $^{176}\text{Hf}/^{177}\text{Hf}$ from 0.2812–0.2858. The low Hf isotopic signatures indicate that the MARID rocks initially formed by interaction of asthenospheric melt with ancient (3Ga) harzburgitic mantle, which dominated their Hf budget. The range to high Hf isotopic signatures, well above the mean value for the present-day Depleted Mantle, was produced by later metasomatism by a fluid/melt with highly radiogenic Hf derived from the breakdown of eclogitic or peridotitic garnet. The low $^{176}\text{Hf}/^{177}\text{Hf}$ preserved in MARID rutiles also helps to resolve one of the minor controversies about the origin of kimberlites. The in-situ rutile data, combined with published data on MARID rocks show that the Nd-Hf isotopic systematics of kimberlites and lamproites also can be explained by contamination of asthenospheric melts with the ancient subcontinental lithospheric mantle, without any hidden reservoirs.

A major advance in the application of Re-Os to mantle-derived rocks came with the recognition that the Os budget of such rocks is controlled by trace sulfide phases, and that these rocks typically contain multiple generations of sulfide with widely differing Os contents and Re/Os (Alard et al., 2000). In-situ Re-Os isotope analysis of mantle sulfides has enabled the dating of depletion and metasomatism events in the lithospheric mantle and forced a reappraisal of the relevance of whole-rock measurements. GEMOC pioneered the development of LAM-MC-ICPMS techniques for the in-situ analysis of Os isotopes in individual sulfide grains and showed that different sulfide generations also have widely varying Re/Os and $^{187}\text{Os}/^{188}\text{Os}$ (Pearson et al., 2002; Alard et al., 2002). The isotopic data indicate that there are multiple generations of sulfides in most mantle peridotites and whole-rock Re-Os ages thus reflect a mix of these different sulfide populations. In many samples the isotopic record preserved in enclosed residual primary sulfides gives older ages for original lithospheric mantle stabilization than obtained from the whole-rock data. Superimposed on this record is the post-stabilisation history preserved in mainly interstitial sulfides. The implication is that whole-rock Os-isotope analyses of sulfide-bearing peridotites must represent mixtures of components with different ages and isotopic compositions. In such cases, the model ages of these rocks can only be regarded as minimum estimates of melt-depletion ages, and are unlikely to date any particular event (Griffin et al., 2004). ‘Age’

spectra for these mantle events commonly mirror temporal signatures for thermal and tectonic events in the overlying crust. The application of in-situ Re-Os analysis to mantle-derived xenoliths is demonstrating that much of the cratonic SCLM is older than previously thought, and that old SCLM is very persistent despite later tectonic reworking.

The in-situ isotopic techniques now available allow the integration of age information with other isotopic datasets to constrain the origin of a sample, but also to unravel the processes that have subsequently modified it. An example of this is the combined Pb-Sr-Nd-Hf study of individual grains of LIMA (Lindsleyite-Mathiasite) minerals from the Jagersfontein kimberlite to constrain the timing of mantle metasomatism and the sources of the metasomatic material. The in-situ isotopic analyses show significant within-grain and inter-grain variability in Sr and Pb isotopic composition, less variation in Nd isotopic composition, and little variation in the isotopic composition of Hf. The LIMA phases are related to the Phlogopite-K-richterite-Peridotite (PKP) style of metasomatism and modeling of the U-Pb isotopes gives a maximum age for this metasomatism at ca 180 Ma. The results suggest an interaction between a plume-related fluid or melt with the isotopic characteristics of the “HIMU” reservoir, and a refertilised SCLM with relatively high $^{87}\text{Sr}/^{86}\text{Sr}$ but low $^{206}\text{Pb}/^{204}\text{Pb}$ and $^{143}\text{Nd}/^{144}\text{Nd}$, similar in many respects to the “EM1” component. This multi-isotope approach has recently been applied to the U/Pb-Sr-Nd study of groundmass perovskite in kimberlites to assess the roles of contamination and alteration (see Donnelly et al., 9IKC-A-00125).

The impact of in situ isotope ratio analysis has advanced modern geochronology beyond the acquisition of dates. Not only does the method provide rapid and precise data, but it places these data in a micro-structural framework and allows integration with datasets produced by other micro-analytical techniques. The integration of these multiple sources of data is crucial in constraining the origin of the sample and the processes leading to its formation, so that we can understand the meaning of a date in terms of geological events. The development of these analytical techniques over recent years have made it possible to compare the large scale evolution of the crust and the history of its underlying mantle (O'Reilly et al., 2008). However this still remains possible only where xenolith-bearing volcanic rocks are available.

References

- Alard, O., Griffin, W.L., Lorand, J.P., Jackson, S.E., O'Reilly, S.Y. 2000. Non-chondritic distribution of the highly siderophile elements in mantle sulfides. *Nature* 407, 891-894.
- Alard, O., Griffin, W.L., Pearson, N.J., Lorand, J.-P., O'Reilly, S.Y. 2002. New insights into the Re-Os systematics of sub-continental lithospheric mantle from

in situ analysis of sulphides. *Earth & Planetary Science Letters* 203, 651-663.

- Aulbach, S., Griffin, W.L., Pearson, N.J., O'Reilly, S.Y., Kivi, K., Doyle, B.J. 2004. Mantle formation and evolution, Slave Craton: constraints from HSE abundances and Re-Os isotope systematics of sulfide inclusions in mantle xenocrysts. *Chemical Geology* 208, 61-88.
- Batumike, J.M. Griffin, W.L., Belousova, E.A., Pearson, N.J., O'Reilly, S.Y., Shee, S. 2008. LAM-ICPMSU-Pb dating of kimberlitic perovskite: Eocene-Oligocene Kimberlites from the Kundelungu Plateau, D.R. Congo. *Earth & Planetary Science Letters* 267, 609-619.
- Belousova, E.A., Griffin, W.L., Shee, S.R., Jackson, S.E., O'Reilly, S.Y. 2001. Two age populations of zircons from the Timber Creek kimberlites, Northern Territory, Australia, as determined by laser-ablation ICPMS analysis. *Australian Journal of Earth Sciences* 48, 757-766.
- Choukroun, M., O'Reilly, S.Y., Griffin, W.L., Pearson, N.J., Dawson, J.B. 2005. Hf isotopes of MARID (mica-amphibole-rutile-ilmenite-diopside) rutile trace metasomatic processes in the lithospheric mantle. *Geology* 33, 45-48.
- Foster, G.L., Vance, D. 2006. In situ Nd isotopic analysis of geological materials by MC-ICP-MS. *Journal of Analytical Atomic Spectrometry* 21, 288-296.
- Griffin, W.L., Pearson, N.J., Belousova, E., Jackson, S.E., van Achterbergh, E., O'Reilly, S.Y., Shee, S.R. 2000. The Hf isotope composition of cratonic mantle: LAM-MC-ICPMS analysis of zircon megacrysts in kimberlites. *Geochimica et Cosmochimica Acta* 64, 133-147.
- Griffin, W.L., Graham, S., O'Reilly, S.Y., Pearson, N.J. 2004. Lithospheric evolution beneath the Kaapvaal Craton: Re-Os systematics of sulfides in mantle-derived peridotites. *Chemical Geology* 208, 89-118.
- McFarlane, C.R.M., McCulloch, M.T., 2007. Coupling of in-situ Nd-Sm systematics and U-Pb dating of monazite and allanite with application to crustal evolution studies. *Chemical Geology* 245, 45-60.
- Neumann, E., Griffin, W.L., Pearson, N.J., O'Reilly, S.Y. 2004. The evolution of the upper mantle beneath the Canary Islands: Information from trace elements and Sr isotope ratios in minerals in mantle xenoliths. *Journal of Petrology* 45, 2573-2612.
- O'Reilly, S.Y., Griffin, W.L., Pearson, N.J., Jackson, S.E., Belousova, E.A., Alard, O., Saeed, A., 2008. Taking the pulse of the Earth: linking crustal and mantle events. *Australian Journal of Earth Sciences*. In press.
- Pearson, N.J., Alard, O., Griffin, W.L., Jackson, S.E., O'Reilly, S.Y. 2002. In situ measurement of Re-Os isotopes in mantle sulfides by laser ablation multicollector-inductively coupled plasma mass spectrometry: Analytical methods and preliminary results. *Geochimica et Cosmochimica Acta* 66, 1037-1050.
- Schmidberger, S.S., Simonetti, A., Francis, D., 2003. Small-scale Sr isotope investigation of clinopyroxenes from peridotite xenoliths by laser ablation-MC-ICP-MS - implications for mantle metasomatism *Chemical Geology* 199, 317-329.
- Woodhead, J.D., Swearer, S., Hergt, J., Maas, R., 2005. In situ Sr-isotope analysis of carbonates by LA-MC-ICP-MS: interference corrections, high spatial resolution and an example from otolith studies. *Journal of Analytical Atomic Spectrometry* 20, 22-27.



Trace-element Geochemistry of Diamond

Sonal Rege¹, W.L. Griffin¹, N.J. Pearson¹, Suzanne Y. O'Reilly¹, S.E. Jackson¹, D. Zedgenizov², G. Kurat³

¹ GEMOC, Dept. Earth and Planetary Sciences, Macquarie University, Sydney, NSW 2109, Australia;

² Institute of Mineralogy and Petrography, Novosibirsk, Russia

³ Naturhistorisches Museum, Vienna, Austria

Quantitative trace-element analyses of > 40 elements in >500 diamond (diamondite, fibrous and monocrystalline); have been carried out by LAM-ICPMS, using a multi-element-doped cellulose standard; detection limits range to low-ppb levels for many elements (Rege et al., 2005). These trace elements are present in microscopic and submicroscopic inclusions that are believed to represent the fluid from which the diamonds have crystallised.

Diamondites

In general the trace-element patterns of the peridotitic and eclogitic diamondites show enrichment of the LREE compared to the MREE with abundances continuously decreasing from Ba to Ho. Pb and Cu are enriched relative to Fe. Ti, Zr and Hf are depleted, and Nb, Ta, Th and U are enriched, relative to chondrites.

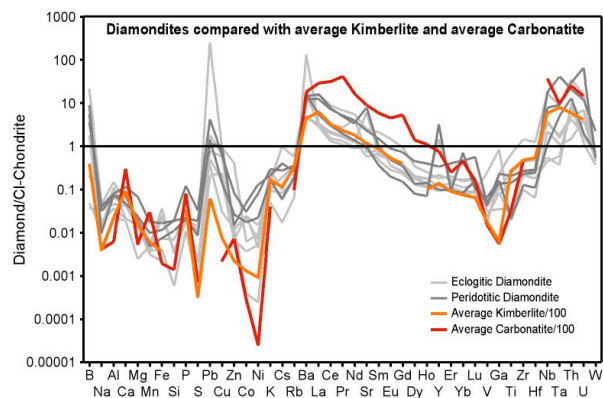


Fig. 1 Comparison of Chondrite-normalised trace-element patterns for Average Peridotitic and Average Eclogitic diamondites with Average Kimberlite and Average Carbonatite. (Data for B, Si, S and P are semi-quantitative only)

Results show that peridotitic and eclogitic diamondites (polycrystalline diamonds or framesite) have probably formed from the same type of fluid, with trace-element and major-element distribution comparable with a kimberlitic-carbonatitic fluid (Rege et al., 2008). Spikes in the time-resolved signals suggest the presence of several, probably submicroscopic, solid phases (garnet, clinopyroxene, Y-Yb rich fluoride

phase, Cu-Pb-Zn-Co-Ni sulphide phase, LIMA-type phase, a carbonate phase, ilmenite, chromite, mica), inferred to have crystallised from the fluid that deposited the diamond matrix. Small differences in Sr, Y and Yb, anomalies, Nb/Ta ratios and abundances of Cr, Mn, Co and Ni between the P and E type diamondites suggest that the fluid may have evolved from "peridotitic" to "eclogitic" by the removal of chromite ± sulphide ± ilmenite.

Fibrous diamonds

Some fibrous diamonds have distinctive TE patterns, with the cores displaying LREE-enriched patterns (broadly similar to the TE pattern observed for the diamondites) whereas the rims have patterns that resemble those of monocrystalline diamonds (see below), suggesting that individual stones grew from an evolving fluid. Significant differences are also seen from locality to locality, suggesting that the fluids from which the fibrous diamonds grew vary in composition from place to place.

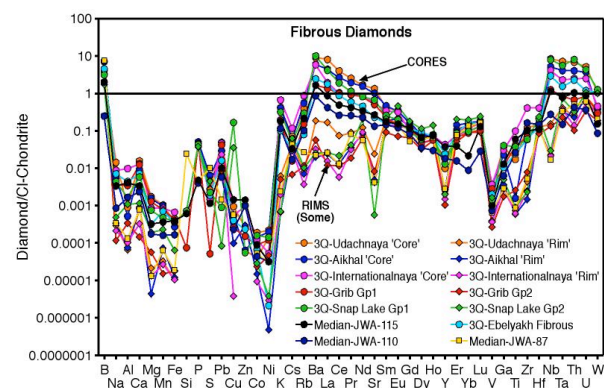


Fig. 2 Chondrite-normalised trace-element patterns of fibrous diamonds. (Data for B, Si, S and P are semi-quantitative only)

Monocrystalline diamonds

Monocrystalline diamonds in general show relatively flat to LREE-depleted REE patterns, with negative Ce, Y and Sr anomalies, Co/Ni >1, and fractionated HFSE. Strong similarities between the TE patterns of peridotitic and eclogitic diamonds from single localities suggest that the fluids from which diamonds

of these two parageneses grew are essentially identical. This would imply that interaction between the fluid and the diamond host rocks is minimal, and suggests high fluid/rock ratios.

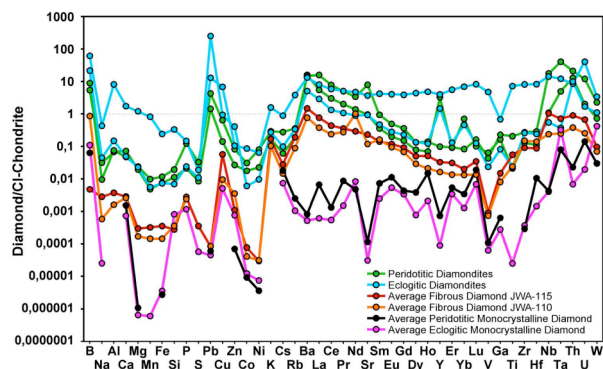


Fig. 3 Average Peridotitic and Eclogitic Diamondites, Average Fibrous Diamonds JWA-110 and JWA-115 and Average Peridotitic and Eclogitic Monocrystalline diamonds from Botswana.

Based on their trace-element patterns, the monocrystalline diamond samples could be roughly separated into two groups: **GRUIPLSJ** (Grib, Udachnaya, Internationalnaya, Komsomolskaya, Aikhal, Lac de Gras, Snap lake, Premier and Jagersfontein and possibly Finsch, Koffiefontein, Bingara, Argyle and Wellington) and **DOJKZC** (Dalnaya, Zarnitsa, Jwaneng, Orapa, Kelsey Lake, Liaoning, Hongqi and Shengli). The principal differences are that most of the samples in the first group show depletion in the LREE relative to the HREE and MREE and have higher overall REE abundances than the second group, which have flatter trace-element patterns and show slight negative anomalies in Yb.

Discussion

The formation of polycrystalline, fibrous and monocrystalline diamonds can be explained by the evolution of a single parent fluid that had a trace-element pattern similar to kimberlite or carbonatite, but which shows significant compositional variation from locality to locality. This fluid/melt is inferred to have formed by the interaction of a $\text{CH}_4\text{-H}_2$ fluid with peridotite in the lithospheric mantle.

Diamondites and the cores of many fibrous diamonds may have crystallised directly from this kimberlitic-carbonatitic fluid. The ubiquitous development of pronounced negative Y anomalies (relative to Ho-Dy) may reflect the separation of fluoride phases or immiscible fluoride melts; microinclusions with positive Y anomalies are observed during ablation of diamondites.

However, many fibrous/particulate diamonds show an abrupt change in trace-element patterns as crystallisation proceeds. Strong fractionations in the

REE and HFSE are difficult to explain by fractional crystallisation, but can be modelled as the result of liquid immiscibility: a separation into broadly hydrous-silicate and carbonatite fluids. This is consistent with observations of carbonate-silicate immiscibility in melt inclusions trapped in Cr-diopside derived from ca 180 km beneath the Slave craton (van Achterbergh et al., 2002).

The rims of some fibrous diamonds, and most monocrystalline diamonds, have crystallised from the silicate-rich end member.

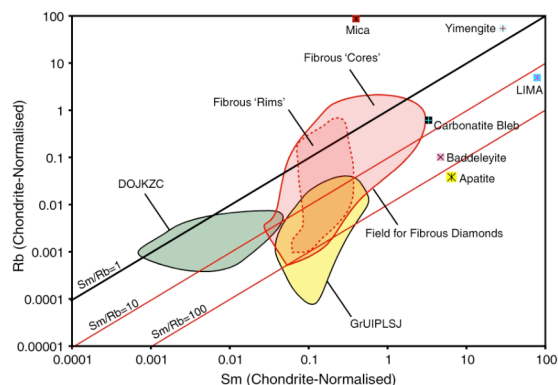


Fig. 4 Plot of Sm vs. Rb (chondrite-normalised) for Fibrous and Monocrystalline Diamonds.

Despite significant variation from one deposit to another, nearly all monocrystalline diamonds show low LREE/HREE, Ba/MREE and Sr/MREE, as well as low (ie subchondritic) Nb/Ta and Zr/Hf, suggesting that they have crystallised from the hydrous-silicate member of the proposed immiscible-liquid couple. Crystallisation of mica minerals in some sample suites (fractionation of Rb from Sm) and the fractionation between Cs and Rb, and between LREE and Ba, suggests a further separation into a hydrosilicate fluid and a brine.

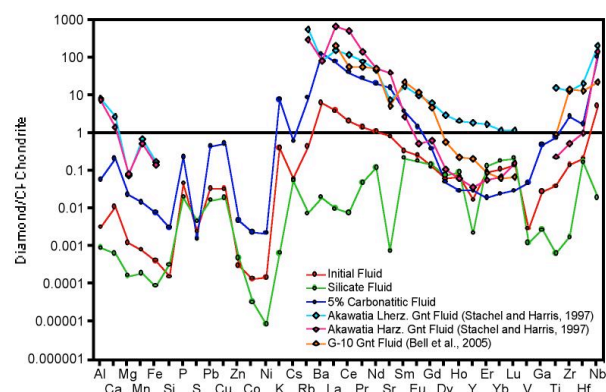


Figure-5 Compositions of melts in equilibrium with harzburgitic and lherzolic garnet inclusions in diamond compared with the 'initial', 'silicate' and 'carbonatitic' fluids.

Modelling of the conjugate Mg-rich "carbonatite" fluid shows it would have extremely high LREE/HREE and



Sr. The reaction of this fractionated carbonatitic fluid with chromite + olivine + opx can produce subcalcic Cr-pyrope garnets (G-10 garnets) with "sinuous" REE patterns and high Sr contents, which are a characteristic inclusion in diamonds of the peridotitic paragenesis, providing a genetic link between diamonds and their most common indicator minerals (Malkovets et al., 2007).

We therefore suggest that the development of immiscibility during the evolution of low-volume melts of the kimberlite-carbonatite spectrum produces conjugate fluids, one of which crystallises most monocrystalline diamonds, and the other of which interacts with mantle harzburgites to produce the most ubiquitous inclusions in peridotitic diamonds. Preliminary comparative studies show little difference in the trace-element patterns of peridotitic and eclogitic diamonds from single localities. This implies limited interaction between fluid and wall rock, which in turn suggests high fluid/rock ratios during diamond crystallisation.

References

- Malkovets, V.G., Griffin, W.L., O'Reilly, S.Y. and Wood, B.J. 2007. Diamond, subcalcic garnet and mantle metasomatism: Kimberlite sampling patterns define the link. *Geology* 35, 339-342.
- Rege, S., Jackson, S.J., Griffin, W.L., Davies, R.M., Pearson, N.J. and O'Reilly, S.Y., 2005. Quantitative trace element analysis of diamond by laser ablation inductively coupled plasma mass spectrometry. *Journal Analytical Atomic Spectroscopy* 20, 601-610.
- Rege, S., Griffin, W.L., Kurat, G., Jackson, S.E., Pearson, N.J. and O'Reilly, S.Y. 2008. Trace element chemistry of diamondites: Crystallisation of diamond from kimberlite-carbonatite melts. *Lithos*, in press
- Van Achterbergh, E., Griffin, W.L., Ryan, C.G., O'Reilly, S.Y., Pearson, N.J., Kivi, K. and Doyle, B.J., 2002. A subduction signature for quenched carbonatites from the deep lithosphere. *Geology* 30, 743-746

Natural silicon carbide from different geological settings: polytypes, trace elements, inclusions

Andrei A. Shiryaev¹, William L. Griffin², Emil Stoyanov^{3,4}, Hiroyuki Kagi⁵

¹*Institute of Crystallography, Moscow, Russia*

²*GEMOC, Sydney, Australia*

³*Bayerisches Geoinstitut, Bayreuth, Germany*

⁴*Arizona State University, Tempe, USA*

⁵*Tokyo University, Japan*

Silicon carbide is a material of significant interest for various fundamental and applied fields: from high-power electronics to crystallography and the oxidation state of Earth's mantle. Since the stability of SiC requires extremely low fO_2 values, some geologists consider moissanite as a "geological aberration". However, a growing body of data confirms the rather widespread existence of small SiC grains in various geological settings. Moissanite has been found not only in mantle derived rocks (e.g., kimberlites, diamonds), but also in high- and low-grade metamorphic rocks, limestones and pegmatites (for a review see Derkachenko et al., 1972, Lyakhovich, 1980, Marshintsev, 1990). SiC is also reported in meteorites and interstellar dust. Interestingly, isotopic analyses show that SiC is always enriched in ^{12}C (Marshintsev, 1990, Mathez et al., 1995). The genesis of natural SiC remains a matter of debate.

In this work we report results of a detailed investigation by complementary techniques of natural SiC grains recovered from two contrasting geological settings: 1) from the heavy fraction of the Mir kimberlite pipe (Yakutia), and 2) from Triassic limestones in Bulgaria. Structural perfection, major and trace element chemistry of natural SiC grains and description of inclusions of other phases are presented.

Samples and methods

Issues of contamination were carefully addressed during extraction of kimberlitic SiC and the contamination is completely excluded in the case of Bulgarian samples. The rocks containing the latter set of SiC grains were collected at the geographical location and from strata described as moissanite-bearing by Gnoevaja and Grozdanov (1965). They were recovered from the heavy fraction of the acid-resistant residue of these rocks, containing well-preserved Triassic fossils. Note, that the SiC grains are genetically unrelated to the host limestones.

The kimberlitic moissanite grains ($n=106$) are up to 1 mm across and the Bulgarian grains ($n=22$) are less than 100 microns. The grains are usually transparent and show various colors, but usually are bluish-green. Similar to earlier observations (Derkachenko et al., 1972, Marshintsev, 1990) most grains are fractured, but

some sides preserve well-formed crystallographic faces.

Raman microspectroscopy was employed to determine the polytypes, to assess degree of crystalline perfection, and to identify of some inclusions. Major and trace elements in SiC bulk and in inclusions exposed by polishing were measured using Electron Microprobe (EMP) and by LAM-ICP-MS. For comparative purposes we studied synthetic SiC samples produced by very different methods: the Acheson and the modified Lely (sublimation) methods. The SiC grains were cast in epoxy and polished prior to analyses. Transmission Electron Microscopy (TEM) was used for direct investigation of submicroscopic inclusions. Loose grains were mechanically crushed and suspension brought to the Cu grid.

Results

Raman spectroscopy

Due to differences in band gap the color of SiC is polytype-dependent. Therefore, already from optical examination the majority of natural SiC grains are identified as the 6H variety. However, doping strongly influences SiC coloration and a more reliable method should be employed to identify the polytypes. Raman spectroscopy is a powerful tool to identify SiC polytypes and to assess degree of lattice disorder (Nakashima and Harita, 1997). Typical spectra are shown in Fig. 1. Grains of pure 6H SiC make 55% of both samples sets. The second most abundant pure polytype is 15R: 8% of the kimberlitic population (pure 15R is not present in the more limited Bulgarian set). Some other grains show the presence of 6H+15R mixtures in different proportions. In total the grains made of pure or intermixed 6H and 15R polytypes make up 83% (73%) of kimberlitic (Bulgarian) sets. It is well-known that the 6H and 15R polytypes generally form at temperatures exceeding 1300 °C. Several grains (~5%) contain mixtures of 6H and 4H polytypes. The rest of the studied populations consist of various mixtures of 6H, 8H, 15R and 21R polytypes; such crystals may be thought of as containing long-period polytypes. As is known, disorder in SiC is not completely random and disordered regions consist of mixtures of randomly disordered simple polytype



domains and those containing stacking faults distributed periodically or near-periodically. Some of the grains (~10%) show extremely complex spectra clearly indicating heavily disordered structures.

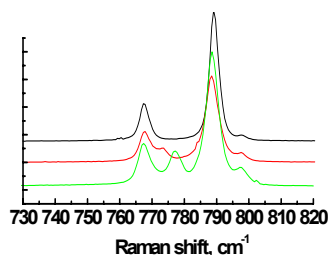


Fig. 1. Parts of the Raman spectra (TO modes) of SiC grains with various degree of perfection (disorder increases from top to bottom).

The shape and position of the LO phonon mode of SiC provides information about stresses and concentration of charge carriers. Only few spectra of the studied grains show stress-related features. At the same time, many grains show the presence of various levels of uncompensated charge carriers (presumably Al, B, perhaps N, see below), whose concentrations reach several hundred ppm in some grains. On average, the 15R grains contain higher concentrations of uncompensated impurities than the 6H ones. The Bulgarian set is, on average, also richer in dopants in comparison with the kimberlitic set.

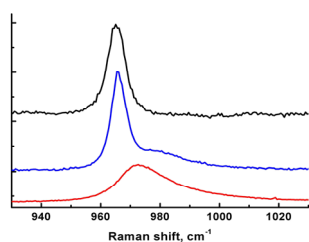


Fig. 2. LO phonon of SiC. Concentration of uncompensated dopants increases from top to bottom. The middle curve shows superposition of two domains.

The LO peak of some grains clearly reflects the superposition of at least two components (fig. 2). This suggests the existence of domains with markedly different type and/or concentration of uncompensated dopants. Judging from the size of the laser spot this heterogeneity is present at a scale of <10 microns. Cathodoluminescence images (Fig. 3) confirm the existence of such zoning. Recently Shiryaev et al., (2008) reported C and Si isotopic zoning in some of the grains.

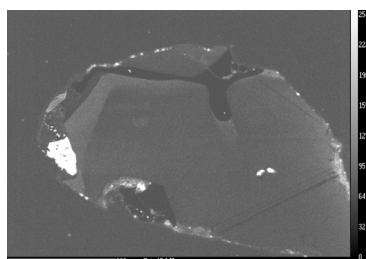


Figure 3. Cathodoluminescence of one of SiC grains showing growth(?) zoning and inclusions of Si.

Several grains (though the statistics are limited) show features in the OH vibrations region (fig. 4). However, it is not yet clear whether these bands are due to structural defects such as C-H complexes in SiC matrix or are due to microscopic H-rich inclusions.

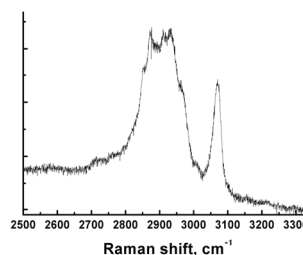


Fig. 4. H-related bands in Raman spectrum on a Yakutian SiC grain.

Major and trace elements

Moissanite grains are typically quite pure SiC with small admixture of oxygen (0.1-0.3 wt%). In the synthetic samples only Al, B, Ti, V, Sc were observed. These impurities (also N) are typical of synthetic SiC. Concentrations of these elements are roughly similar in synthetic and natural samples studied. However, the trace element chemistry of natural SiC is much richer than that of synthetic SiC samples. The most plausible explanation of chemical differences between natural and synthetic materials lies in amount of submicroscopic accessory phases. The SiC lattice is similar to diamond in its extremely low capacity for impurities except some substitutional elements (Al, N, B). Therefore, it is believed that most trace elements are present in unresolved syngenetic inclusions and not in the SiC crystalline lattice. The contents of most trace elements in studied natural SiC grains are low (1-200 ppm), but several important conclusions can be drawn from the chondrite-normalised patterns.

- Al contents show a wide range, as do Cr and Ni;
- The contents of several chalcophile elements (Cu, Zn, Mo) are high compared to Ni, suggesting that no sulfide phase coexisted with the SiC;
- REE contents rise weakly from HREE to MREE, but decline on average from Nd to La;
- Sr shows a pronounced negative anomaly relative to Nd and Sm, and Y shows a negative anomaly relative to Dy and Ho; these features are also characteristic of trace elements in diamonds;
- Eu shows no anomaly relative to Sm and Gd;
- Contents of Sn are high and relatively constant;
- Zr/Hf is strongly subchondritic; limited data suggest the same is true of Nb/Ta; again, these features are characteristic of diamond trace-element patterns.

Several SiC grains from both localities contain inclusions of other phases. The most common is silicon metal, followed by an iron silicide (FeSi_2) and an oxygen-bearing $\text{Si}(\text{C},\text{O})$ phase. Intergrowths of these phases in several grains indicate that they form a single primary assemblage. Raman spectroscopy provides unambiguous confirmation of presence of metallic Si. A slight shift of the Si Raman peak indicates residual pressure of several kbars. The presence of Si metal and various silicides in natural SiC was reported previously (Gnoevaja and Grozdanov 1965, DiPierro et al., 2003, Lyakhovich, 1980, Marshintsev 1990, Mathez et al., 1995). However, the chemical composition and crystal chemistry of previously reported compounds differ from our observations.

A BSE image of an inclusion-bearing kimberlitic SiC grain is shown in fig. 5 (see also Fig. 3). A semi-euhedral crystal of SiC (150x350 μm) contains three inclusions with negative-crystal forms; each consists of Si⁰ with blebs of FeSi₂ nucleated along the contacts. At the top of the grain, a large irregular grain of FeSi₂ is surrounded by a halo of cauliflower-shaped SiC grains set in a matrix of SiO₂. The SiO₂ also forms botryoidal outgrowths along the edge of the SiC crystal.

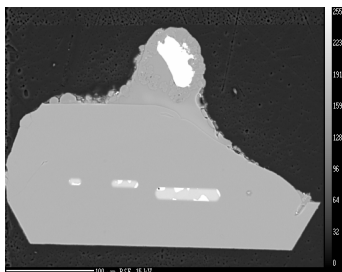


Figure 5. BSE image of inclusion-rich kimberlitic SiC grain.

The large FeSi₂ grain has a complex internal structure, with anastomosing “worms” of metallic Ti set in the FeSi₂ matrix (not shown); the microstructure strongly suggests exsolution of the Ti⁰ from the FeSi₂, and the presence of subgrains within the FeSi₂. The Ti⁰ strongly concentrates Ni and Mn.

The complex intergrowth of SiC and SiO₂ around the FeSi₂ grain suggests a secondary replacement process, which may have oxidised Si⁰ and, to some extent, SiC. The relationships between the phases in these complex grains suggest that SiC coexisted with a melt phase dominated by Si⁰ and Fe⁰; this melt was trapped as inclusions in the SiC and formed a grain-boundary phase. On cooling, FeSi₂ appears to have crystallised (exsolved?) from the Si⁰, typically along contacts with SiC. This relationship between Si and FeSi₂ makes trace element analysis of Si problematic due to contamination by microscopic silicide inclusions.

The TEM study shows presence of submicroscopic FeSi₂ inclusions dispersed in the SiC matrix (fig. 6) Electron diffraction confirms identification of the phase as a FeSi₂-based solid solution. Presumably, deviations of the composition from an ideal formula lead to absence of characteristic Raman signal.

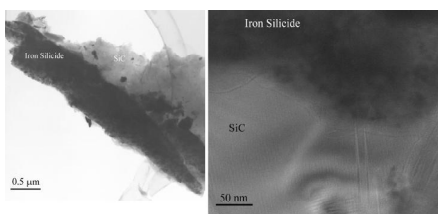


Figure 6. TEM image of FeSi₂ inclusion in a Bulgarian SiC.

Iron Silicide is compositionally variable: Fe ranges from 43.6-46.3 wt% (mean 45.4); Si from 49.2-55.4 wt% (mean 50.8). Ti varies widely; the mean value is 2.0 wt%, but many grains contain 2.5-3.8 wt% Ti, while others contain <0.3 wt%. Ni varies from 0.04 – 0.33 %, and Mn from 0.03 – 1.3 wt%. The calculated structural formula is (Fe,Ti,Mn,Cr,Ni)Si₂. This is clearly different from the Fe₃Si₇ composition reported as inclusions in moissanite by DiPietro et al. (2003).

The FeSi₂ phase has high contents of many trace elements; it appears to concentrate most of these elements in the system, and thus may give an

indication of the nature of the environment in which the SiC and its associated phases formed. The key observations from the chondrite-normalised trace-element patterns are:

- High levels of elements such as Al, Cr, Mn, Fe;
- High levels of chalcophile elements, again indicating that no sulfide phase was present;
- A steep increase in REE contents from Lu to Ce, but chondritic (on average) La/Pr; Ba levels are low relative to La;
- A striking negative Eu anomaly; Eu is below detection limits in all analyses, even those with several hundred ppm of Nd and Gd;
- Smaller, but still marked, negative anomalies in Sm and Yb (as well as Y);
- High levels of Sn, as noted in the SiC;
- Zr/Hf ranges from subchondritic in some grains to suprachondritic in others; Nb/Ta is generally subchondritic.

The FeSi₂ phase clearly accepts highly charged, small ions (e.g., REE and HFSE). The REE pattern of the FeSi₂ suggests that nearly all Eu, and much of the Sm, has been reduced to the 2+ state and entered another phase. The lack of Eu and Sm anomalies in the moissanite suggests that the SiC does not discriminate against Eu²⁺ or Sm²⁺. Without samples of other coexisting phases, it is not clear where the Eu and Sm are concentrated in this environment.

The Si-C-O phase contains 55-56 % Si, 9.6-12.0 wt% O; we assume that the balance is made up of C. The stoichiometry of this phase appears to be close to Si₄(C,O)₇, which would require a mixed valence (between 3 and 4) for Si.

The present study suggests that formation of natural SiC was related to the cooling of Fe-Al-Si-C melt. However, the geochemical environment of its genesis remains unclear.

References

- Derkachenko L.I., Zaretskaya G.M., Obuhov A.P., Sokolova T.V., Filonenko N.E., (1972) Mineralogy of silicon carbide, "Nauka," Leningrad (in Russian).
- DiPietro S., Gnos E., Grobety B.H., Armbruster T., Bernasconi S.M., and Ulmer P., (2003) *American Mineralogist*, 88 1817-1821.
- Gnoevaja N., Grozdanov L., Moissanite from Triassic rocks, NW Bulgaria (1965), *Proceedings of Bulgarian Geological Society*, 26, 89-95.
- Lyakhovich, V.V. (1980) Origin of accessory moissanite. *International Geology Review*, 22, 961–970.
- Marshintsev V.K., (1990) Natural silicon carbide in Yakutian kimberlites. *Mineralogicheskii Zhurnal* 12 17-26 (in Russian).
- Mathez E.A., Fogel R.A., Hutcheon I.D., Marshintsev V.K., (1995) *Geochimica et Cosmochimica Acta* 59 781-791.
- Nakashima S., Harita H., (1997) Raman investigation of SiC polytypes. *Physica Status Solidi A* 162 39-64.
- Shiryaev A.A., Wiedenbeck M., Reutsky V., Polyakov V.B., Mel'nik N.N., Lebedev A.A., Yakimova R., (2008) Isotopic heterogeneity in synthetic and natural silicon carbide. *Journal of Physics and Chemistry of Solids*, in press, doi:10.1016/j.jpcs.2008.05.005



Trace Elements and Oxygen Isotopes in Garnets from Diamondiferous Xenoliths, Nurbinskaya pipe, Yakutia: Implications for Diamond Genesis

Z. V. Spetsius¹, W.L. Griffin², L. A. Taylor³, S.Y. O'Reilly², S.I. Mityukhin⁴, J.W. Valley⁵ and M. Spicuzza⁵

¹YaNIGP CNIGRI, ALROSA Co. Ltd., Mirny, Yakutia, Russia, spetsius@cnigri.alrosa-mir.ru

²GEMOC ARC National Key Centre, Macquarie University, NSW 2109, Australia;

³Planetary Geosciences Institute, Dept. of Geological Sciences, Univ. of Tennessee, USA;

⁴ALROSA Co. Ltd., Mirny, Yakutia, Russia;

⁵Dept. of Geosciences and Geophysics, Univ. of Wisconsin, Madison, WI 53706 USA.

A large collection (160) of xenoliths and garnet-megacrysts with diamonds from the Nyurbinskaya pipe shows several extreme features: exceptionally high diamond grade in individual samples, a predominance of diamonds with eclogitic paragenesis, evidence for metasomatic diamond growth and anomalous $\delta^{18}\text{O}$ values of garnets in diamondiferous xenoliths (Fig. 1). The mineral chemistry, isotopic compositions and diamond characteristics of this suite provide new insights into the origin and modification of eclogites, the composition of the lithospheric mantle under this kimberlite field and the metasomatic origin of diamonds.



Fig. 1. Diamondiferous xenoliths from Nyurbinskaya pipe. Size of diamonds is 4 and 5 mm.

Methodology

Major element compositions of garnets in the xenoliths were determined with a Superprobe JXA-8800R electron microprobe at the ALROSA Co Ltd. (Mirny,

Yakutia). Natural minerals and synthetic were used as standards. Analytical conditions included an accelerating voltage of 15 keV, a beam current of 20 nA, beam size of 5 μm , and 20 seconds counting time for all elements. All analyses underwent a full ZAF correction.

The trace elements (TRE) have been measured in garnets of eclogites and other xenoliths by laser Ablation ICP-MS (LAM) at the Macquarie University in Sydney, with NIST 610 glass as external standard and Ca as internal standard; pit diameters were 40 – 50 μm . Rare earth elements (REE) and other trace elements were analyzed by LAM-ICPMS in garnets of 80 mafic and ultramafic xenoliths.

Fresh garnet grains for oxygen determinations were selected from 121 garnets. Pure separates were obtained using heavy liquids, magnetic separation, but mostly by careful hand picking. The oxygen-isotope analyses were performed on garnet mineral separates, approximately 1-2 mg per run, using a 32 W CO_2 laser, BrF_5 , and a dual-inlet Finnigan MAT 251 mass spectrometer. Replicate analyses were performed on many samples, particularly those that had oxygen values outside that of mantle. The procedure for the laser technique is discussed in Valley et al. (1998). The long-term precision for analyses of UWG-2 is $\pm 0.07\text{‰}$ (1SD), and daily precision is typically $\pm 0.05\text{‰}$.

Results

Factor analysis of garnet major-element chemistry identifies 8 paragenetic groups of xenoliths and megacrysts with diamonds, corresponding to different types of mantle xenolith (Spetsius et al., 2006). Of the entire suite of samples in this study, >60% are eclogitic and websteritic, whereas dunite-harzburgite xenoliths constitute <10% of the entire population of diamondiferous xenoliths. The large range in garnet compositions of the investigated xenoliths is apparent in the ternary plot in Fig. 2. It is obvious that most diamondiferous samples from the Nyurbinskaya pipe occupy fields of groups B and C eclogites. Most garnets are homogeneous in terms of major- and trace-element contents but about 20% of the samples have slightly zoned garnets.

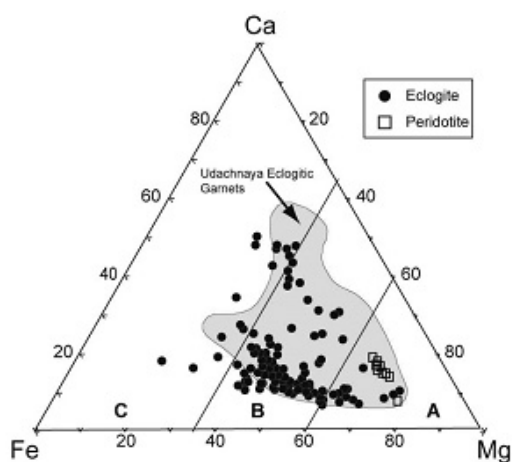


Fig. 2. Garnet compositions in xenoliths from the Nyurbinskaya pipe. The envelope outlines the compositional field of diamondiferous xenoliths from the Udachnaya pipe, after Spetsius (2004).

Trace elements distribution in garnets of xenoliths

Garnets from ultramafic xenoliths define two groups, one with sinusoidal REE_N (chondrite normalised) patterns (10 harzburgites, two lherzolites) and one with flat MREE_N (lherzolites, some websterites). Most eclogitic garnets have LREE-depleted patterns (Ce_N as low as 0.1), and no Eu anomalies. HREE are variably enriched; most Lu_N varies from 20-50 (Fig. 3). Most websteritic garnets show REE patterns similar to this but they are typically enriched in LREE with Ce_N (0.2-0.5). Another group of garnets (n=9) from eclogites and websterites has small negative Eu anomalies. Garnets

with nearly flat HREE and small positive Eu anomalies are common in coesite eclogites and those containing kyanite and/or corundum. Garnets of corundum-bearing eclogites commonly have positive slopes within the LREE_N, peaking at Sm and then slowly decreasing to about chondritic abundance for Lu. LAM-ICPMS analyses show how different populations within an eclogite xenolith series can document the heterogeneity of the lithospheric mantle.

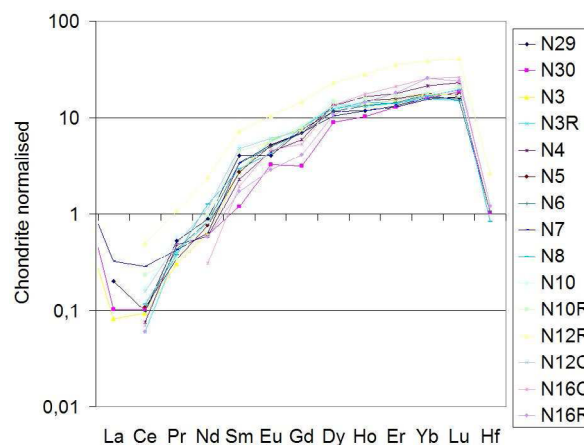


Fig. 3. REE distribution in eclogitic garnets.

Oxygen isotope garnets compositions

Oxygen isotope compositions of garnets display a large range of values, with most higher than the accepted mantle range of 5.3 ± 0.3 ‰ (Fig. 4). In fact, for the eclogite xenoliths, the garnet values for a steep-sided bell-shaped curve about 1.2 ‰ wide with a mode at ~ 6.6 ‰. This abundance of high $\delta^{18}\text{O}$ values in garnets from xenoliths of any single kimberlite pipe appears to be unique, and suggests intense modification of the lithospheric mantle beneath this kimberlite field.

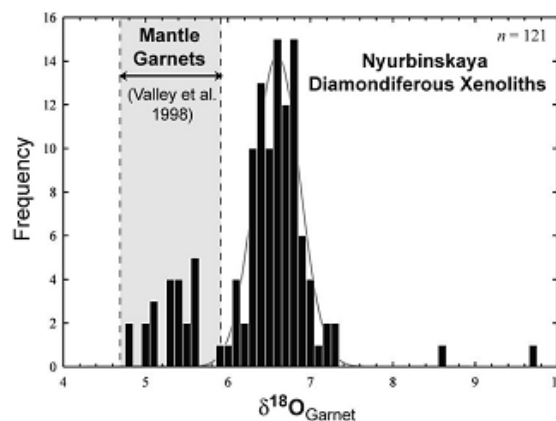


Fig. 4. Oxygen-isotope ratios of garnets in mantle xenoliths from the Nyurbinskaya pipe.



Metasomatic growth of diamonds

The unusual range of high $\delta^{18}\text{O}$ values is accompanied by evidence for strong late-stage metasomatism. We suggest that mantle metasomatic fluids may also possess crustal isotopic signatures, as a result of ancient subduction. The possible correlation of high oxygen-isotope values in many Nyurbinskaya xenolithic garnets with chemical zonations of garnets and strong metasomatic alteration might indicate that the xenoliths experienced fractionation through metasomatic influence. There is ample evidence that of the wide distribution of chemically zoned garnet in the present suite of investigated xenoliths, as well as the extensive development of phlogopite and other metasomatic minerals (Fig. 6).



Fig. 6. Octahedron (4 mm) in the Nyurbinskaya xenolith surrounded by phlogopite rim that is replaced by chlorite.

In addition, many of the xenoliths possess textures of deformation and catalysis, as well as veins of partial melt products, similar to those described from the Udachnaya pipe (Spetsius and Taylor, 2002). Based upon many of the facts and observation discussed (Spetsius, 1999; Spetsius and Taylor, 2002), it is possible to speculate on the late-stage metasomatic diamond formation in some eclogites. Proof of this process can be seen in the distribution of diamond crystals within the products of kelyphite rims around

garnet, as well as along general zones of partial melting. Such relations of diamonds in space have been found in eclogite xenoliths from the Udachnaya, and other Yakutian pipes. Close indications of the metasomatic origin of diamonds are seen in some xenoliths from the Nyurbinskaya pipe (Fig. 7).

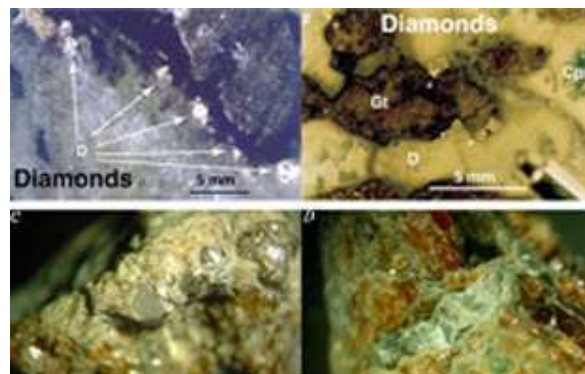


Fig. 7. Examples of metasomatic growth of diamonds. a) & b) Diamonds in kelyphite rims and partial melt (both are eclogitic xenoliths from the Udachnaya pipe); c) Linear distribution of 5 diamonds in corundum eclogite (Nyurbinskaya pipe, size of crystals 3-4 mm); d) Eclogitic xenolith cut by thr diamond vein (Nyurbinskaya pipe).

References

- Spetsius, Z.V., 1999. Two generation of diamonds in the eclogite xenoliths. In: Gurney, J.J., Gurney, J.L., Pascoe, M.D. & Richardson, S.H. (eds). Proceedings of 7th IKC, 2. Cape Town: Red Roof Design, 823-828.
- Spetsius, Z.V., 2004. Petrology of highly aluminous xenoliths from kimberlites of Yakutia. *Lithos*, **77**, 525–538.
- Spetsius, Z.V., Ivanov, A.S., Mitukhin, S.I., 2006. Associations with the diamond in kimberlites of the Nurbinskaya pipe, (Nakynsky field, Yakutia). *Dokl. Akad. Nauk*, 408, № 6, 810–814 (in Russian).
- Spetsius, Z.V., Taylor, L.A., 2002. Partial melting in mantle eclogite xenoliths: evidence from Yakutian kimberlites. *Intern. Geol. Rev.*, **11**, 983-987.
- Valley, J.W., Graham, C.M., Harte, B., Eiler, J.M., and Kinney, P.D., 1998. Ion microprobe analysis of oxygen, carbon, and hydrogen isotope ratios. *SEG Rev. Econ. Geol.*, **7**, 73-98.

Diamond-forming Fluids and Kimberlites: The Trace Element Perspective.

Y. Weiss¹, W. L. Griffin², J. W. Harris³, O. Navon¹

¹*Institute of Earth Sciences, The Hebrew University of Jerusalem, Israel*

²*ARC National Key Centre for Geochemical Evolution and Metallogeny of Continents (GEMOC), Macquarie University, NSW, Australia*

³*Department of Geographical and Earth Sciences, University of Glasgow, Glasgow, Scotland*

Major element studies of fluid inclusions in fibrous and cloudy diamonds revealed that most inclusions trapped high density fluids (HDFs) with wide range of composition. The compositions fall along two arrays between three end-members: carbonatitic to hydrous-silicic and carbonatitic to hydrous-saline. Recent studies of diamonds from Siberia and Kankan (Navon et al., 2008; Weiss et al., 2008) further subdivided the carbonatitic HDFs into: high-Mg and low-Mg groups.

Following the early neutron-activation work of Fesq et al. (1975) and Bibby (1979), Schrauder et al. (1996) measured the concentrations of 31 elements in fibrous diamonds from Jwaneng, Botswana. Akagi and Masuda (1988) burned Zairian fibrous diamonds and used isotope dilution mass-spectrometry to determine their Sr isotopic composition and REE, Sr, Rb, K and Ba concentrations.

LA-ICP-MS now allows less destructive, in-situ analysis of the trace element content of diamonds. Tomlinson et al. (2005) reported trace element ratios of diamonds from Congo. Rege et al. (2005) introduced the external cellulose standard and used ¹³C as internal standard to measure the trace element concentrations in diamonds. Comparison to earlier INAA and PIXE measurements of 23 elements in two samples yielded good correlations. Weiss et al. (in press) further tested the method and obtained good correlations between major elements/Fe concentration ratios for 28 micro-inclusion-bearing diamonds (Figure 1).

The agreement between four analytical methods, the small number of molecular interferences and the fact that the ablation pit is only ~100 µm across and 50-100 µm deep make the cellulose-calibration LA-ICP-MS the most suitable technique for the determination of trace elements concentrations in diamonds. Calibrating the LA-ICP-MS data against the K₂O of the HDFs measured by EPMA we calculate the trace element concentrations of the HDF itself.

The addition of water and carbonate concentrations estimated from FTIR, produces a comprehensive quantitative database of the HDF chemistry. Note that in Figures. 2-4, the trace elements concentrations are of the volatile free composition of the HDF. Adding volatiles will shift the whole pattern down, but by less than a factor of two.

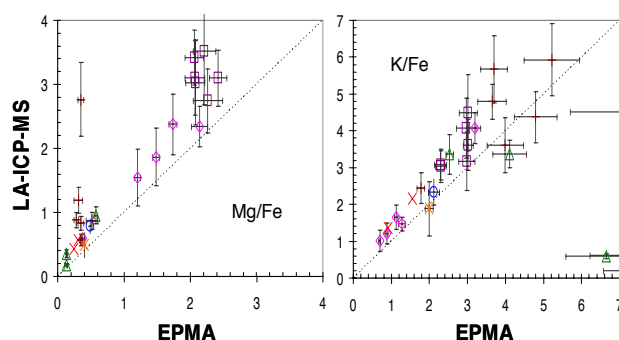


Figure 1: Comparison of K/Fe and Mg/Fe as measured by LA-ICP-MS and EPMA. The dotted lines mark the 1:1 slope, for the diamonds that deviate from this line and for original data see Weiss et al. (in press).

Samples

Twenty seven diamonds were chosen for this study: three diamonds from Kankan and six from Udachnaya carry high-Mg carbonatitic HDF; other three Kankan diamonds and single samples from Diavik, DeBeers Pool and Koingnaas carry low-Mg carbo-silicic HDFs. Five diamonds from Diavik, six from DeBeers Pool and a one from Koingnaas, carry saline fluids.

Results

The trapped HDFs in all diamonds are highly enriched with incompatible elements even in comparison to kimberlitic melts. Ba, Th, U and the light REE typically reach levels of a few thousand times the primitive mantle values.

Primitive-mantle normalized concentrations of high-Mg carbonatitic HDFs from Udachnaya and Kankan reveal patterns that are distinct in their incompatible elements and merge for the more compatible ones (Figure 2). The first have smoother pattern with somewhat lower K, Rb and Cs (we designate this flatter pattern "Bench"). The second has elevated Ba, U, Th and LREE, depleted Nb and Ta and highly depleted alkalis (we designated it "Table"). The average La/Dy ratio of high-Mg carbonatitic HDFs with "Bench" pattern is 113 while in the "Table" ones, its value reaches 225. Both patterns show negative anomalies of Sr, Hf, Zr, Ti and Y.

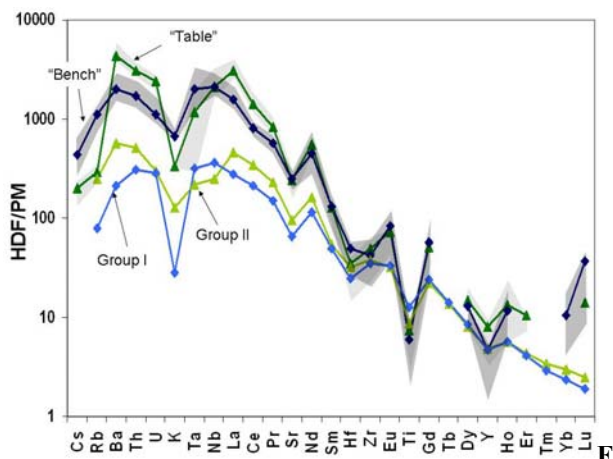


Figure 2: Trace elements of high-Mg carbonatitic HDFs in diamonds and kimberlites (normalized to primitive mantle composition). Light shaded area – the range for Kankan HDFs with "Table" pattern and their average (dark green triangles). Dark shaded area and dark blue diamonds – "Bench" patterns in Udachnaya HDFs (the darkest grey is due to overlaps). Also shown are average Group I (light blue diamonds) and Group II (light green triangles) kimberlites (Becker and le Roex, 2005).

The low-Mg carbonatitic to silicic HDFs reveal similar distinction between "Tables" and "Benches" (Figure 3). Carbo-silicic HDFs with "Table" patterns from Kankan, DeBeers Pool and Diavik are strongly depleted in Nb, Ta, Ti and usually also Sr. Their alkalis and HREE are higher than in the high-Mg carbonatitic HDFs, leading to shallower REE patterns. Their La/Dy ratio ranges from 20 to 200 and the ratio increases with increasing silica content. The La/Nb and Th/Nb also increase from 2.6 and 0.3 in the carbonatitic HDFs to 30 and 5 in the silicic ones with some values reaching up to 90 and 30, respectively (Figure 5b).

In this study we did not find low-Mg carbonatitic HDFs showing the "Bench" patterns, but carbonatitic diamonds with low-Mg content from Jwaneng, Botswana (Schrauder et al., 1996) do show "Bench" characteristics with elevated alkalis and only small depletion of Ta. "Bench" patterns in silicic HDFs in diamonds from Koingnaas and Botswana are much smoother, with Nb and Ta having similar levels to Ba, Th, U and the LREE. The alkalis are elevated as well, sometimes even higher than the other most incompatible elements.

Figure 4 indicates that "Table" and "Bench" patterns are found in the saline fluids as well. HDFs from Diavik exhibit "Table" patterns with extreme enrichment of the incompatible elements (more than 10 wt% Ba are also indicated by EPMA measurements). A sample from Koingnaas has very similar "Table" pattern but is lower in most incompatible elements. Ba, Th and the LREE are high relative to K, Rb, Cs, Ta, Nb and Sr in those diamonds. In the compatible elements, Ti, Zr and Hf are very low relative to the

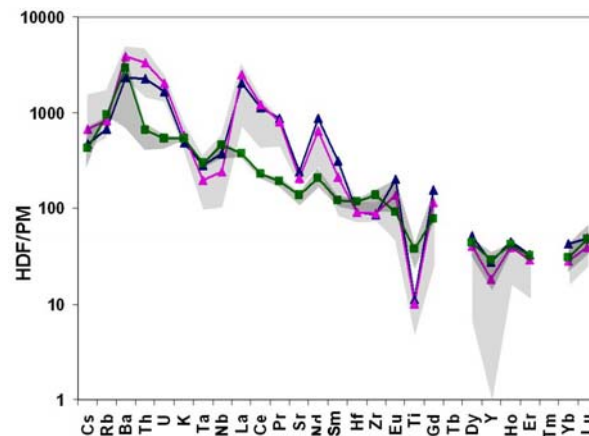


Figure 3: Trace elements in low-Mg carbo-silicic HDFs. Light shading: "Table" patterns. Blue and pink triangles: averages for more carbonatitic and more silicic HDFs respectively. Dark shading and green squares: "Bench" patterns and their average. The dotted line marks that in some diamonds, Ho falls below detection limit.

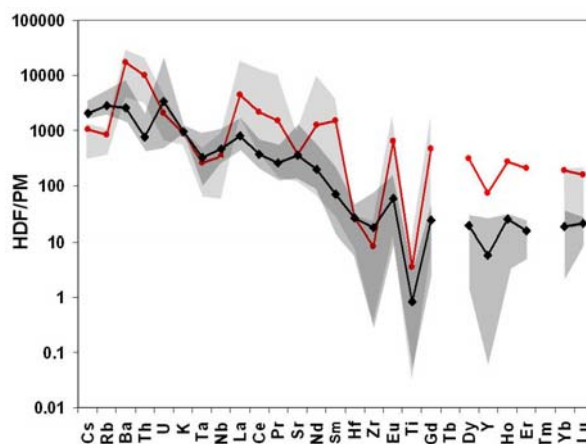


Figure 4: Trace elements in saline HDFs. Light shading and red circles – "Table" patterns and their average, dark shading and black diamonds – "Bench" patterns and average. Dotted lines as in Figure 2 for Ho and Yb.

corresponding HREE. Uranium is not as enriched as Th, perhaps reflecting the low Zr content. A smoother "Bench" pattern is exhibited by diamonds from DeBeers Pool. Nb, Ta, Zr and Hf are only slightly below the respective REEs, U is elevated to the degree that the $(Th/U)_{PM} < 1$, and Sr is higher than Ce, Pr and Nd.

Discussion

The persistence of the two trace element patterns in fluids of such diverse major element compositions is fascinating. It indicates that the two patterns are not the result of differing fractionation paths from a common source and suggest that they originate from two different sources (or from interaction between fluids originating from different sources).

The present database is still limited, but "Table" patterns were found in the coat of a Kankan diamond that carries eclogitic inclusions in its core and in a

Diavik diamond with peridotitic micro-mineral inclusions in its coat. Thus, the two patterns are probably not related to the peridotitic or eclogitic rocks that host the diamonds. The similarity in compatible elements and the difference in the incompatible ones suggest that the difference lies in the nature of the enriched sources that contribute to the very high abundance of most incompatible elements.

Figure 5a presents the similarity between the high-Mg carbonatitic HDFs and kimberlites. The "Benches" fall in the field of Group I kimberlite, while the "Tables" fall with Group II kimberlites. Figure 2 shows that the resemblance between the two patterns of the high-Mg carbonatitic HDFs and the corresponding kimberlite groups is maintained by most elements (K and Rb are exceptions with lower levels in diamonds with "Table" pattern and in type I kimberlites). The concentration of the highly incompatible elements in the HDFs are 5 times higher than in kimberlites, but all patterns share the same negative anomalies and have similar concentrations of the moderately incompatible elements. The high enrichment of the fluids in many incompatible elements and the steeper REE patterns of the HDFs relative to kimberlites requires very low HDF/rock ratio during their formation (a lower degree of melting, or higher degree of crystallization). This agrees with their major element composition that is similar to that of near-solidus melts or supercritical fluids of peridotites and eclogites.

The huge variation in Th/Nb and La/Nb ratios in carbonatitic and carbo-saline HDFs (Figure 5b), suggests Nb scavenging by rutile or similar phase. This can be achieved either by rutile addition (e.g., by dissolution during early melting) or removal (during fractionation). Similar arguments, based on major/trace elements may be made for the involvement of other phases, such as zircon, apatite mica and carbonates. Rocks rich in the above phases are known from xenoliths in kimberlites (e.g., the MARID and PIC rocks or glimmerites, Gregoire et al., 2002). As the formation of such rocks involves crystallization from kimberlitic or other enriched melts, we enter a "chicken and egg" situation,

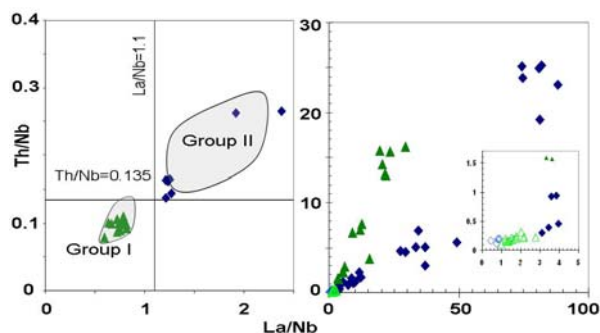


Figure 5: Th/Nb vs. La/Nb in the HDFs. (a) High-Mg carbonatitic HDFs with "Bench" patterns (green triangles) fall in the field of Group I kimberlites (shaded areas). HDFs with "Table" patterns (blue diamonds) fall in the Group II field. (b) Carbonatitic-silicic HDFs with "Bench" (full diamonds) and "Table" (open diamonds) patterns fall along a Th/La~0.3 line, Saline HDFs with Bench (full triangles) and Table (open triangles) form a steeper array with Th/La~0.65.

which may describe true cycling of many incompatible elements between melts or fluids and accessory solid phases that crystallize last and melt/dissolve first upon heating or decompression of mantle rocks.

Conclusions

Major elements defined the nature of the HDFs and their 3-4 end member compositions. Trace element added the "Table" and "Bench" patterns that represent various sources for the incompatible elements of the HDF. The "Table" patterns resemble Group II kimberlites and probably represent "re-cycling" of lithospheric material. The "Benches" resemble Group I kimberlites.

References

- Akagi T. and Masuda A. (1988) Isotopic and elemental evidence for a relationship between kimberlite and Zaire cubic diamonds. *Nature*, 336, 665-667.
- Becker, M., and le Roex A. P., 2006. Geochemistry of South African On- and Offcraton, Group I and Group II Kimberlites: Petrogenesis and Source Region Evolution. *Journal of Petrology*, 47, 673-703.
- Bibby, D.M., 1979. Zonal distribution of inclusions in diamond. *Geochimica et Cosmochimica Acta*, 43, 415-423.
- Fesq, H.W., Bibby, D.M., Erasmus, C.S., Kable, E.J.D. and Sellschop, J.P.F., 1975. A comparative trace element study of diamonds from Premier, Finch and Jagersfontein mines, South Africa. *Physics and Chemistry of the Earth*, 9, 817-836.
- Gregoire, M., Bell, D.R., Le Roex, A.P., 2002, Trace element geochemistry of phlogopite-rich mafic mantle xenoliths: their classification and their relationship to phlogopite-bearing peridotites and kimberlites revisited *Contributions to Mineralogy and Petrology*, 142, 603-625.
- Navon, O., Klein-BenDavid O., Logvinova A. M., Sobolev N. V., Schrauder M., Kaminsky F. V., Spetius Z. V., 2008. Yakutian Diamond-forming fluids and the evolution of carbonatitic high-density fluids. *9th IKC, Extended Abstracts*.
- Rege, S., Jackson, S., Griffin, W.L., Davies, M.R., Pearson, N.J. and O'Reilly, S.Y., 2005. Quantitative trace-element analysis of diamond by laser ablation inductively coupled plasma mass spectrometry. *Journal of Analytical Atomic Spectrometry*, 20, 601-611.
- Schrauder M., Koeberl C., and Navon O. (1996) Trace element analyses of fluid-bearing diamonds from Jwaneng, Botswana. *Geochimica et Cosmochimica Acta*, 60, 4711-4724.
- Tomlinson, E., De Schrijver, I., De Corte, K., et al., 2005. Trace element compositions of submicroscopic inclusions in coated diamond: A tool for understanding diamond petrogenesis. *Geochemica et Cosmochemica Acta*, 69, 4719-4732.
- Weiss Y., Griffin W. L., Elhlou S., and Navon O. (in press) Comparison between LA-ICP-MS and EPMA analysis of trace elements in diamonds. *Chemical Geology*.
- Weiss, Y., Kessel, R., Griffin, W. L., Kiflawi, I., Bell, D. R., Harris J. W., Navon, O., 2008. Diamond forming fluids from Kankan, Guinea: major and trace element study. *9th IKC, Extended Abstracts*.

Diamond forming fluids from Kankan, Guinea: major and trace element study

Y. Weiss¹, R. Kessel¹, W. L. Griffin², I. Kiflawi¹, D. R. Bell³,
J. W. Harris⁴ and O. Navon¹

¹*Institute of Earth Sciences, The Hebrew University of Jerusalem, Israel*

²*ARC National Key Centre for Geochemical Evolution and Metallogeny of Continents (GEMOC), Macquarie University, NSW, Australia*

³*School of Earth and Space Exploration, Arizona State University, Tempe, AZ, USA*

⁴*Division of Earth Sciences, University of Glasgow, Glasgow, Scotland*

The association of some diamonds with metasomatic minerals and with veins and alteration zones in xenoliths, as well as their morphology and internal symmetric textures suggest the involvement of fluids in their formation. Infrared spectroscopy and EPMA of microinclusion-bearing diamonds revealed that the microinclusions trapped high-density fluids (HDFs) with compositions varying along two arrays between three end-members: carbonatitic, hydrous-silicic and hydrous-saline. The carbonatitic end-member is further divided into high- and low-Mg members (Klein BenDavid et al., 2008). Klein-BenDavid et al. (2007, 2008) suggested evolution from the high- through the low-Mg carbonatite to silicic and saline HDFs by crystallization of silicates and carbonates and liquid immiscibility. Most diamonds sample only a small fraction of the HDF evolution and zoned diamonds with a significant radial variation in inclusion composition are exceptional. The investigation of such zoned diamonds, including their trace elements characteristics is important for constraining the source and chemical evolution of diamond-forming fluids.

The diamonds

We report here an extensive major and trace element study of seven coated diamonds from the Kankan district in Guinea. Major elements were analyzed using both EPMA and LA-ICP-MS. The good agreement between the two techniques validates the accuracy of both (Rege et al., 2005; Weiss et al., 2008). Water and CO₂ contents were determined using FTIR.

In four diamonds (ON-KAN-384, 386, 388 and 389) the inner coat hosts abundant micro-inclusions while the outer part is clear (Fig. 1a). CL imaging reveals uniformly dull luminescence throughout both zones (Fig. 1b). In ON-KAN-382 the number density of inclusions increases outwards. The coats of ON-KAN-381 and 383 are zoned with sharp boundaries that are seen optically and in CL images (Figure 1c, d). The core of ON-KAN-383 carries tens of mineral inclusions. Raman spectroscopy and EPMA document almandine garnet, omphacitic clinopyroxene, coesite, rutile and low-Ni monosulfide-solid-solution, clearly indicating that the core grew in an eclogitic host rock.

In general, the octahedral cores of the diamonds carry nitrogen in A and B centers, indicating long residence times in the mantle. The coats carry nitrogen in A centers, but in the rims of ON-KAN-381, 382 and 383 bands at 1344 and 1130 cm⁻¹ identify the presence of single nitrogen atoms in C centers (Figure 2). This sequence indicates a long time gap between the formation of the cores and coats, a shorter time gap between the inner and outer coats, and a very short mantle residence time after growth ended.

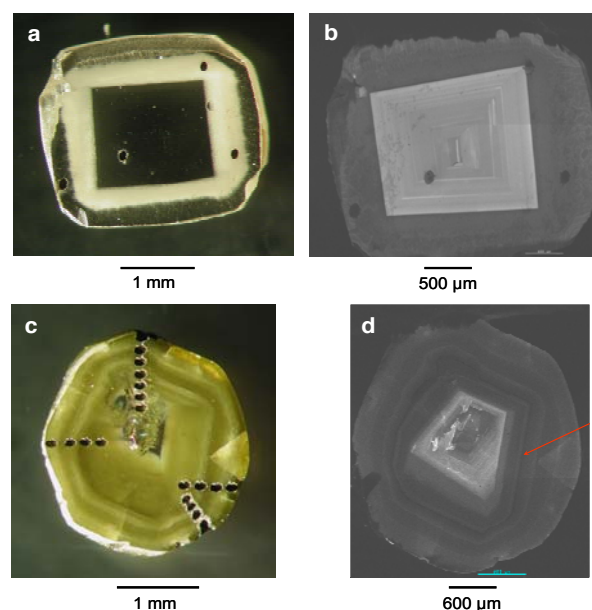


Figure 1: Photographic and CL images of diamonds ON-KAN-386 (a, b) and ON-KAN-381 (c, d). Holes are laser ablation analysis spots. The arrow points to the core-coat boundary.

The High-Density Fluids

Four of the diamonds (ON-KAN-384, 386, 388 and 389) trapped high-Mg carbonatitic HDFs. These diamonds are homogenous and the HDFs do not show a significant compositional variation from the inner coat to the rim. However, in three diamonds we found small increases in CaO and MgO towards the rim. The uniform CL suggests a single growth event. Thus, fluid evolution from silicic to carbonatitic during this growth

event contradicts the prediction of the fractionation model (Klein BenDavid et al., 2008).

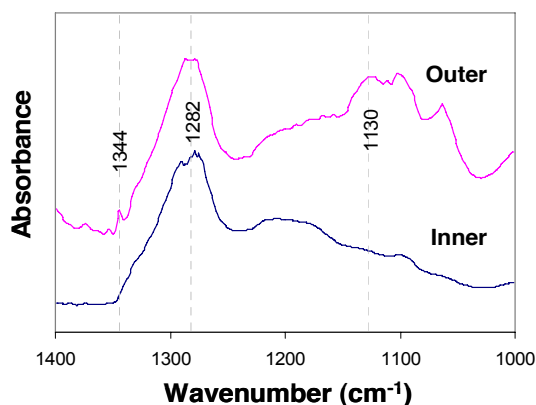


Figure 2: IR spectra of the inner and outer parts of the coat of diamond ON-KAN-381 showing the presence of A and C nitrogen centers. While in the inner coat nitrogen exist only in A centers (1282 cm⁻¹), the outer part also carries C centers (1130 and 1344 cm⁻¹).

The HDFs in the other three diamonds vary between low-Mg carbonatitic and silicic composition. Diamond ON-KAN-382 carries HDFs of silicic composition, whereas the two zoned diamonds exhibit strong chemical zoning, from silicic inner parts to a carbonatitic outer part (Fig. 3). Clear borders separate the various zones. Radial compositional variations within the zones are also clear and reveal evolution in contrasting directions. These contrasting trends together with the presence of nitrogen C centers only in the outer zones indicate multiple growth events with complex evolution of HDF chemistry. The above conclusion agrees with previous reports of two diamonds with zoning in HDF composition by Klein BenDavid et al. (2004) and Shiryaev et al. (2005). They attributed the clear zoning to diamond growth from fluids of different chemical and carbon isotopic composition.

Crystallization, melting, immiscibility and interaction with the wall-rock are all possible mechanisms for the evolution of the HDFs (Schrauder and Navon, 1994; Izraeli et al., 2001; Tomlinson et al., 2005; Klein BenDavid et al., 2007, 2008; Zedgenizov et al., 2007). The detailed information presented here, and especially the contrasting evolution from carbonatitic to silicic and vice-versa show that no single model describes all diamonds. Each of the above suggestions may play a role in diamond formation within the mantle and/or in the evolution of the various components. The contrasting trends of evolution in different diamonds and in different zones of the same diamond (Figure 3) call for diamond growth during mixing of fluids that evolved at different locations. Such mixing is not necessarily mechanical; it may occur by differing degrees of metasomatic interaction between HDF and its wall rock, including melting triggered by introduction of an HDF into a hot solid rock.

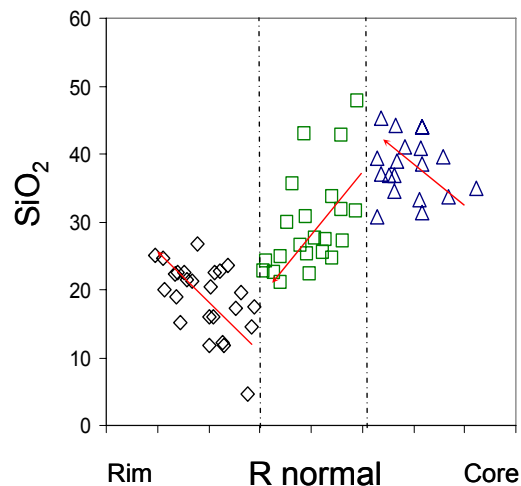


Figure 3: Chemical composition of microinclusions in diamond ON-KAN-381 along a radial profile from core to rim: triangles – inclusions in the inner coat, squares – in the middle coat, diamonds – outer coat. The dotted lines mark the borders between the three parts. The normalized radius provides the position of individual inclusions relative to these borders.

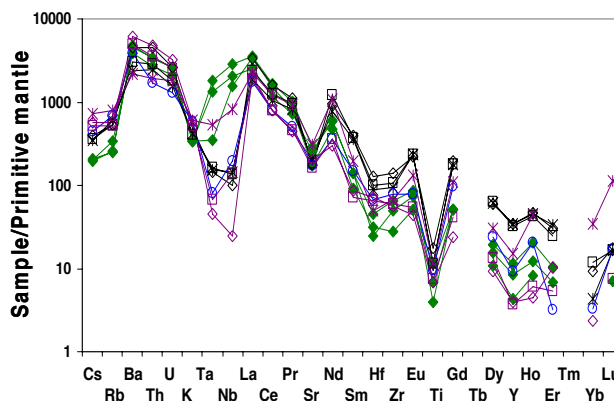


Figure 4: Trace element compositions of high-Mg carbonatitic to hydrous silicic HDF in Kankan diamonds. Solid diamonds - high-Mg carbonatitic, stars - low-Mg carbonatitic, open symbols – more silicic HDFs. The Nb anomaly deepens in the more silicic HDFs.

All diamonds, including the various parts of the two zoned diamonds, have elevated levels of incompatible elements. Relative to primitive mantle composition, the HDF are rich in Ba, Th, U and LREE compared to the alkalis (K, Cs and Rb), HFSE (Ta, Nb, Hf, Zr, Ti) and Sr and Y. (Figure 4).

Compared to the low-Mg carbo-silicic HDFs, the high-Mg carbonatitic fluids have the lowest content of alkalis, HFSE (Zr, Hf and Ti) and Y but the highest Nb and Ta concentration. They also exhibit the highest (Ba, Th, U)/alkalis and LREE/MREE and HREE (Figure 4, 5). In many plots of such concentrations and their ratios, the high-Mg carbonatitic HDFs deviate from the clear trend formed by the low-Mg carbo-silicic diamonds (Figure 5).

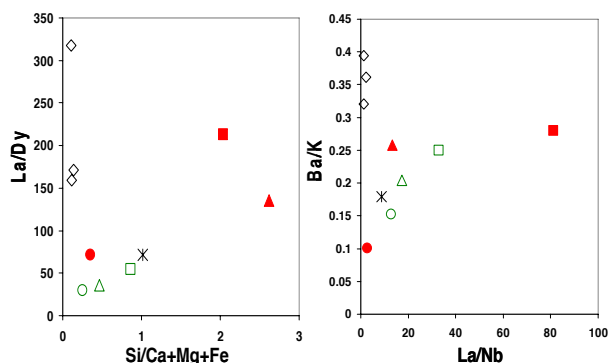


Figure 5: Trace element ratios and Si/(Ca+Mg+Fe) showing the difference between the high-Mg carbonatitic and the low-Mg carbo-silicic HDFs in Kankan diamonds. Open diamonds – high-Mg carbonatitic HDFs, star - ON-KAN-382; circles - HDFs in the outer parts; triangles – the middle parts and squares – the inner parts of ON-KAN-381 (open symbols) and ON-KAN-383 (solid symbols).

Discussion

We suggest that the differences between the HDFs reflect their different sources and mode of formation. The high-Mg carbonatitic HDF is a product of interaction between saline fluids and peridotitic source rocks (Navon et al., 2008), while the low-Mg carbo-silicic HDFs may reflect derivation from an eclogitic source. The eclogitic mineral assemblage in the core of ON-KAN-383 supports this scenario.

Melting of carbonated eclogites produces a range of silicic to Ca-rich carbonatitic melts (Yaxley and Green, 1994; Yaxley, 1999; Hammouda 2003), while carbonated peridotite produces Mg-rich carbonatitic melts (Wallace and Green, 1988; Dalton and Presnall, 1998). In principle, it is possible to explain the range of fluids by melting these two sources, and even grow the silicic inner coat before the carbonatitic rims. However, the contrasting trends in and between the parts of the two zoned diamonds, as well as the extreme enrichment in incompatible elements call for a more complex scenario that involves additional sources and mixing of HDFs.

Some garnet inclusions in Kankan octahedral diamonds exhibit a sinusoidal REE pattern, interpreted by Stachel et al. (2000) as the result of metasomatic interaction between the garnet and a fluid with extremely steep REE pattern. The very steep pattern of the high-Mg carbonatitic HDF, with $(La/Dy)_{CN}$ reaching 380, comes within the range of calculated melts in equilibrium with the Kankan garnets with the sinusoidal patterns ($La/Dy=200-650$). Saline HDF from Diavik, Canada associated with high-Mg carbonatitic HDFs, similar to those from Kankan, have even higher values ($La/Dy=440$) and could also induce such patterns in the diamonds. If the diamonds that trap the garnets were formed during such metasomatic event (Bell et al, 2005, Malkovets et al., 2007), then similar fluids may promote the growth of both fibrous and octahedral diamonds in the Earth's mantle.

References

- Bell, D.R., Gregoire, M., Grove, T.L. et al., 2005, Silica and volatile-element metasomatism of Archean mantle: A xenolith-scale example from the Kaapvaal Craton: *Contributions to Mineralogy and Petrology*, 150, 251–267.
- Hammouda, T. 2003. High-pressure melting of carbonated eclogite and experimental constraints on carbon recycling and storage in the mantle. *Earth and Planetary Science Letters*, 214, 283-297.
- Izraeli, E.S., Harris, J.W., Navon, O., 2001. Brine inclusions in diamonds: a new upper mantle fluid. *Earth and Planetary Science Letters*, 187, 323-332.
- Klein-BenDavid, O., Izraeli, E.S., Hauri, E., Navon, O., 2004. Mantle fluid evolution – a tale of one diamond. *Lithos*, 77, 243 – 253.
- Klein-BenDavid, O., Izraeli, E.S., Hauri, E., Navon, O., 2007. Fluid inclusions in diamonds from the Diavik mine, Canada and the evolution of diamond-forming fluids. *Geochemica et Cosmochemica Acta*, 71, 723-744.
- Klein-BenDavid, O., Logvinova, A. M., Sobolev, N. V., et al., 2008. Yakutian Diamond-forming fluids - the evolution of carbonatitic high density fluids. *9th IKC, Extended Abstracts*.
- Malkovets, V.G., Griffin, W.L., O'Reilly, S.Y., Wood, B.J., 2007. Diamond, subcalcic garnet and mantle metasomatism: Kimberlite sampling patterns define the link. *Geology*, 35, 339-342.
- Navon, O., Weiss, Y., Klein BenDavid, O., 2008. Diamond forming fluids: their origin and evolution. *9th IKC, extended abstracts*.
- Rege, S., Jackson, S., Griffin et al., 2005. Quantitative trace-element analysis of diamond by laser ablation inductively coupled plasma mass spectrometry. *Journal of Analytical Atomic Spectrometry*, 20, 601-611.
- Schrauder, M., Navon, O., 1994. Hydrous and carbonatitic mantle fluids in fibrous diamonds from Jwaneng, Botswana. *Geochemica et Cosmochemica Acta*, 58, 761-771.
- Shiryaev, A., Izraeli, E.S., Hauri, E., Galimov, E., and Navon, O., 2005. Chemical, optical and isotopic investigation of fibrous diamonds from Brazil. *Russian Geology and Geophysics*, 46, 1207-1222.
- Stachel, T., Brey, G.P., Harris, J.W., 2000. Kankan diamonds (Guinea) I: from the lithosphere down to the transition zone. *Contributions to Mineralogy and Petrology*, 140, 16-27.
- Tomlinson, E., De Schrijver, I., De Corte, K. et al., 2005. Trace element compositions of submicroscopic inclusions in coated diamond: A tool for understanding diamond petrogenesis. *Geochemica et Cosmochemica Acta*, 69, 4719-4732.
- Wallace, M. E., Green, D. H., 1988. An experimental determination of primary carbonatite magma composition. *Nature*, 335, 343-346.
- Weiss, Y., Griffin, W. L., Elhlou, S., Navon, O. (in press). Comparison between LA-ICP-MS and EPMA analysis of trace elements in diamonds. *Chemical Geology*.
- Yaxley, G.M., Green, D.H., 1994. Experimental demonstration of refractory carbonate-bearing eclogite and siliceous melt in the subduction regime. *Earth and Planetary Science Letters*, 128, 313-3
- Yaxley, G.M., 1999. Phase relations in carbonated eclogite under upper mantle PT conditions - implications for carbonatite petrogenesis In: Gurney, J., Gurney J, Pascoe, M., Richardson, S. (Eds.), *Proceedings 7th IKC*. Red Roof Designs, Cape Town, 933-947.

Carbonatitic to hydrous-silicic growth medium of diamonds from Internatsionalnaya kimberlite pipe (Yakutia)

D.A. Zedgenizov¹, D. Araujo², A.L. Ragozin¹, V.S. Shatsky¹, H.Kagi³, W.L. Griffin²

¹*Institute of Geology and Mineralogy, 3 Koptyuga ave., Novosibirsk, 630090, Russia*

²*GEMOC ARC National Key Centre, Macquarie University, NSW 2109, Australia*

³*Geochemical Laboratory, Graduate School of Science, University of Tokyo, Tokyo 113-0033, Japan*

Diamonds are pristine time capsules from Earth's mantle. Microinclusions in natural diamonds represent a bulk sample of high-density fluids/melts (HDFs) from which they are crystallized (e.g. Navon et al., 1988), and provide a unique opportunity to characterize diamond-forming HDFs and to understand their origin and evolution within the mantle. Here we report the compositions of micro-inclusions in 44 fibrous diamonds from the Internatsionalnaya kimberlite pipes located in the central field of the Yakutian diamond province. The compositions of HDFs from Internatsionalnaya diamonds fall on the carbonatitic to hydrous-silicic join. This compositional range is reported here for the first time in Yakutian diamonds. We also address the question of the genetic relationship between these fluids and their host kimberlite magma.

The amount of major elements in the subsurface microinclusions has been determined using EDS. All analyses are normalized to 100% on a carbon-free basis (with excess oxygen for chlorine). Major- and trace-element compositions of the bulk microinclusion populations have been quantitatively analyzed by LA-ICP-MS. The abundance of carbonates, water and silicates in the diamonds were determined by FTIR. Additionally Raman spectroscopy has been used for phase identification in individual microinclusions. The nitrogen defect abundance and aggregation state of studied diamonds were calculated from FTIR spectra. The isotopic composition of carbon of some diamonds was measured using a continuous flow isotopic ratio mass spectrometer attached to a high temperature elemental analyzer.

The diamonds studied here are opaque due to abundant microinclusions and look grey in the rough. The proportion of such diamonds in the whole diamond population from Internatsionalnaya is high (up to 5% of examined collections). Most of them have irregular roughly cubic shapes decorated by repetition of small octahedral faces (Fig.1 a). Some crystals have typical resorption features, such as the rounding of edges and etch-pits. The samples were polished into plates with a thickness of 100-200 μm . The polished plates are colorless. Most display an inner zone of high inclusion density and an outer inclusion-free rim (Fig. 1 b).

Central cubic diamonds reveal fibrous internal texture defined by trains of microinclusions. The outer transparent parts of many diamonds are not fibrous: CL patterns show layered octahedral growth (Fig. 1 c, d).

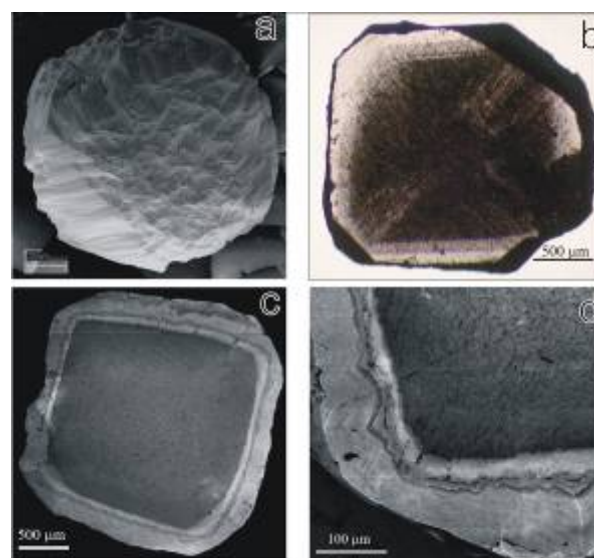


Fig. 1 Diamonds from Internatsionalnaya kimberlite pipe: (a) SEM image of diamond morphology; (b) polished plate with abundant microinclusions in the central part; (c) CL image of polished plates with zonal structure; (d) detail of (c).

The bulk nitrogen concentration in the studied diamonds ranges between 35 and 1438 ppm. The typical range for 31 diamonds is between 200 and 850 ppm and averages 450 ppm. The 20 studied diamonds are of type IaA and 21 are of type IaAB with IaB/IaA ratio from 4 to 30 %.

The carbon isotope composition has been analyzed for 12 diamonds. The total range of $\delta^{13}\text{C}$ of the studied diamonds is very narrow from -4.5 to -6.5 ‰. The average value of $\delta^{13}\text{C}$ for studied diamonds from Internatsionalnaya is exactly same as the average mantle -5.5 ‰ (Galimov, 1983). Figure 2 shows the correlation of carbon isotope composition and water/carbonate ratio of microinclusions. The carbonate-rich samples have a lighter carbon isotope



composition than is observed in diamonds with lower carbonate content.

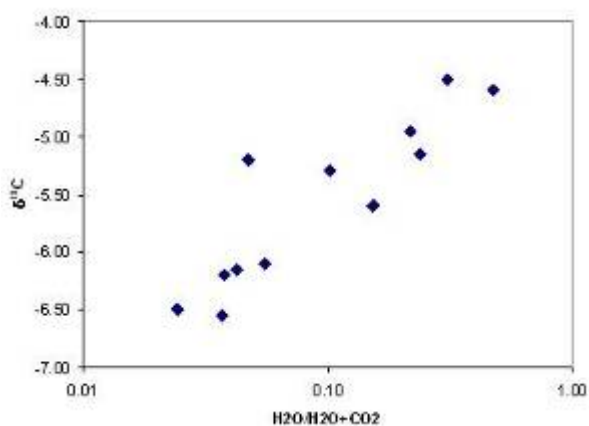


Fig. 2 Variations of water/carbonate ratio ($H_2O/(H_2O+CO_2)$) of microinclusions with carbon isotope composition of host diamonds from Internatsionalnaya kimberlite pipe.

The integrated IR and Raman spectroscopic investigations have revealed a multiphase assemblage of microinclusions in diamonds from Internatsionalnaya. The most common IR bands in the studied diamonds are those of water, carbonate and silicates. The relative amounts of these species depend on the sample. As in fibrous diamonds from other localities, some of our samples also show absorption by quartz and apatite. Rarely, weak absorption by CO_2 molecules is observed. Raman spectroscopy has revealed the presence of carbonates, olivine, apatite, rutile and graphite.

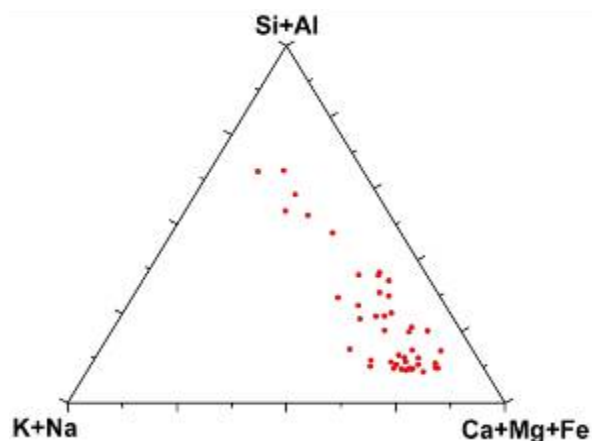


Fig. 3 Compositional variation of microinclusions in diamonds from Internatsionalnaya kimberlite pipe. Each point is the mean of data from an individual diamond.

The microinclusions in the studied diamonds have wide compositional variations. Some important correlations between silica and chlorine contents and the water/carbonate ratio of the microinclusions are observed. Water content generally correlates with the SiO_2 concentration. At relatively constant Ca/Mg (0.2-0.4), microinclusions show significant variations in Fe

content (Mg# 0.02-0.8). In comparison with the modern worldwide database most of the studied diamonds from Internatsionalnaya define a continuous range of carbonatitic to hydrous-silicic compositions and only few fall into the lower end of the carbonatitic to saline range (Fig. 3). The hydrous-silicic end-members are rich in water, SiO_2 , Al_2O_3 , K_2O and P_2O_5 . Carbonatitic microinclusions are rich in carbonate, CaO, MgO and FeO. Samples with saline component are slightly enriched in water, K_2O , Na_2O and Cl.

Figure 4 presents the trace-element abundances of micro-inclusions in diamonds from Internatsionalnaya compared to the average composition of host kimberlite (Kostrovitsky et al., 2007) and an average carbonatite (Woolley, Kempe, 1989). The bulk analyses of the microinclusions have smooth patterns for the LILE, normalized to a primitive mantle composition. Some samples show enrichment in Cs. Some samples with hydrous-silicic compositions are depleted in Sr compared to those rich in carbonates. The relative abundance of K in the fluids is significantly higher than observed in the host kimberlite and carbonatites. The pattern of HFSE in the micro-inclusions shows some depletion in Ti, Zr and Hf relative to Ta, Nb and Mo. The REE pattern reveals low abundances of the heavy REE and high light REE concentrations. The La/Dy ratio of micro-inclusions varies widely, decreasing from carbonatitic to hydrous-silicic compositions. Many samples with carbonatitic composition have a negative anomaly in Y. Diamonds from Internatsionalnaya have low contents of transition metals relative to other trace elements and most of them are significantly depleted in Ni and Co.

The trace-element compositions of the microinclusions are generally similar to those of kimberlites and carbonatites, but there are significant differences in major elements. The observed geochemical features are consistent with a genetic link between the diamond-forming fluids and ephemeral carbonatitic liquids (fluids/melts) which sometimes may be precursors of the host kimberlite. These fluids/melts may originate either from the metasomatic influx of volatile agents or from partial melting of previously carbonated eclogites and peridotites. Some elemental variations may be explained by fractional crystallization of such fluids/melts, or mixing between liquids with different compositions. Schrauder and Navon (1994) suggested fractional crystallization as an explanation for the range of carbonatitic to hydrous-silicic compositions of fluid microinclusions in Botswanian diamonds: the precipitation of Ca-Mg carbonate, apatite and titanates from this fluid will drive the residual fluid composition towards more H_2O -rich compositions. This evolution may be responsible for carbon isotope fractionation as it observed in studied diamonds (Fig. 2). These fluids seem to be important for volatile and trace-element transport between mantle reservoirs and may also affect the stability of many mantle phases and facilitate melting. These processes may result in diamond formation and kimberlite generation.

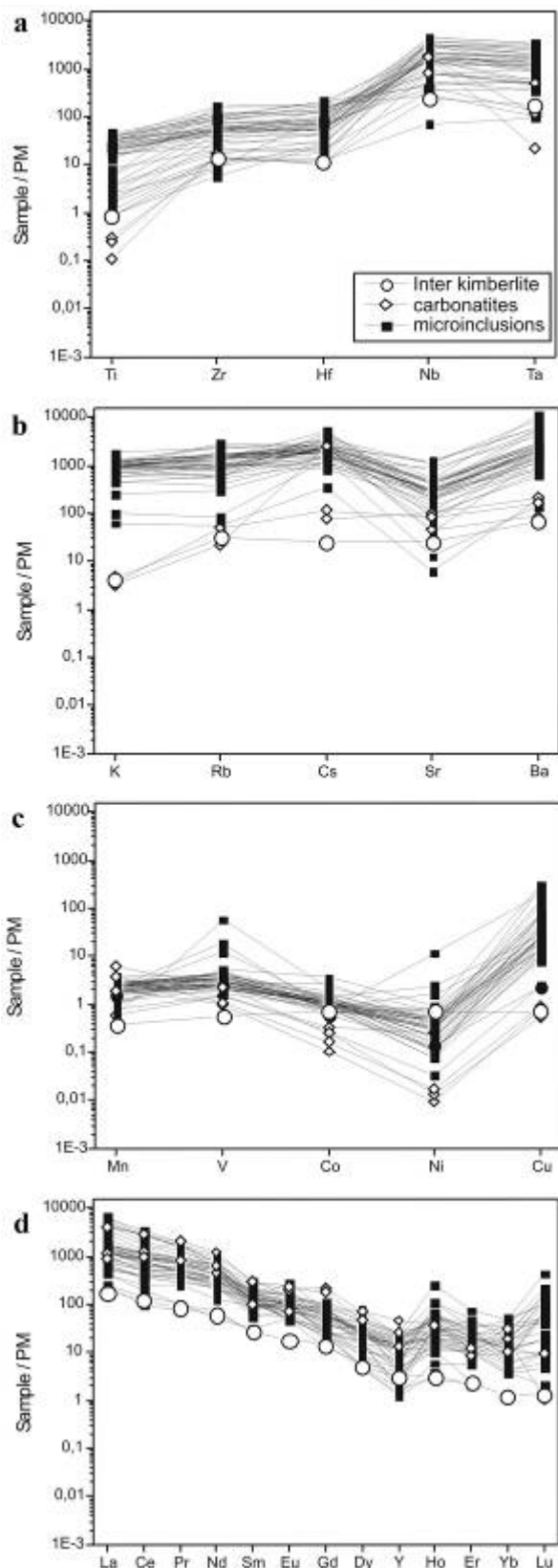


Fig. 5 Trace-element abundances of bulk microinclusions in Internatsionalnaya diamonds (black squares) normalized to Primitive Mantle values (McDonough, Sun, 1995). The abundances in the host kimberlite (open circles) and average carbonatites (open rhombs) are also shown.

This work was supported by the Council for grants of the President of Russian Federation (grant MK-1613.2007.5) and by grants from the Australian Research Council.

References:

- Navon, O., Hutcheon, I.D., Rossman, G.R., Wasserburg, G.J., 1988. Mantle-derived fluids in diamond micro-inclusions. *Nature* 335, 784-789.
- Galimov, E.M., 1991. Isotope fractionation related to kimberlite magmatism and diamond formation. *Geochimica et Cosmochimica Acta* 55, 1697-1708.
- Kostrovitsky, S.I., Morikiyo, T., Serov, I.V., Yakovlev, D.A., Amirzhanov, A.A., 2007. Isotope-geochemical systematics of kimberlites and related rocks from the Siberian Platform. *Russian Geology and Geophysics* 48, 272-290.
- Woolley, A.R., Kempe, D.R.C., 1989. Carbonatites: Nomenclature, average chemical compositions and element distribution. In: *Carbonatites - Genesis and Evolution* (ed. K.Bell), Unwin Hyman, 1-14.
- Schrauder, M., Navon, O., 1994. Hydrous and carbonatitic mantle fluids in fibrous diamonds from Jwaneng, Botswana. *Geochimica et Cosmochimica Acta* 58, 761-771.
- McDonough, W.F., Sun, S.-S., 1995. The composition of the Earth. *Chemical Geology* 120, 223-253.



**ARC National
Key Centre for the
Geochemical Evolution and
Metallogeny of Continents**